MASTER THESIS

TITLE: Joint Radar and Communication Application for Traffic Safety System

MASTER DEGREE: Master in Science in Telecommunication Engineering & Management

AUTHOR: Raúl Quijada Ferrero

DIRECTOR: Lars Kildehöj Rasmussen

DATE: February 25 th 2011

ACKNOWLEDGEMENT

First of all, I would like to thank to my supervisor Lars Kildehöj Rasmussen, who has given me the opportunity to develop the research presented in this thesis. His supervision method has allowed me to focus on the most interesting areas from my point of view and to reinforce my skills to solve problems. Furthermore, he has contributed to the thesis decisions in a constructive manner, such that my work has been always respected instead of disregarded.

It would be unfair to do not appreciate the praiseworthy work carried out by of all the teachers that I had during my entire student life. Their motivation and advices have led me to continue my studies; besides, they have instilled important values into me.

At last but not least important, I have to show my gratitude to my family and friends, who have understood and encouraged me during my student life.

“I haven't failed. I've found 10,000 ways that won't work”

-Benjamin Franklin

OVERVIEW

The concept of “smart” cars or intelligent vehicles is presented as one of the most promising solutions to reduce the high mortality rate that occurs on the world’s roads nowadays. Besides, the recent publication of standards as the *European Standard for Intelligent Transportation System* (ITS) or the international standard IEEE 802.11p confirm the importance of the future vehicle-to-vehicle or vehicle-to-infrastructure networks, which can diminish gridlocks or aid the driver with information about the road status or the weather forecast in order to prevent accidents, for instance.

The main drawbacks of such intelligent network regarding the accident prevention lie in the presence of obstructing objects on the road or cars that do not implement this V2V system. Therefore, a radar application based on the used waveform for the V2V communication can be suitable as a direct method to avoid collisions.

The aim of this thesis consists in the verification of the viability of a radar application in a V2V scenario. Thus, a thorough evaluation of the implemented V2V propagation channel has been performed so as to determine the main constraint factors, such as the power fading, Non Wide Sense Stationary Uncorrelated Scattering (NWSSUS) or the Doppler frequency, that can affect at detection and location application. From the conclusions obtained based on the characterization of a V2V channel, a radar algorithm has been designed as well as a tracking system.

The design of the proposed radar algorithm is based on power peak detection that the estimated channel impulse response presents based on the reflected power originated by possible targets. The trilateration method is used for the location of these targets in the azimuth plane; thus, a Multiple Input Multiple Output system is required.

In order to carry out this viability study, a MIMO structure 4x4 using OFDM with PSK or QAM as the modulation and over a real V2V propagation channel has been simulated. The Geometric Stochastic Channel Model (GSCM) is considered, since it contains most of the relevant channel-specific features; in particular it models the Non Wide Sense Stationary Uncorrelated Scattering (NWSSUS) behavior typical for such channels. Furthermore, the IEEE 802.11p standard has been implemented so as to simulate a scenario as close to reality as possible.

The results obtained conclude with a positive result for the implemented scenarios. It is important to highlight that the extrapolation of this algorithm to other environments can lead to improvements or deteriorations of the probability of detection. However, the most valuable part of the thesis is the conclusion obtained for a radar implementation in a V2V scenario.

The thesis is organized into 5 chapters. The first chapter provides an introduction, the second chapter explains the V2V implemented system, the third chapter contains the characterization of the V2V propagation channel, the forth chapter explains the radar and tracking system, while the fifth chapter presents the results of the proposed radar algorithm. Furthermore, at the end of the thesis some conclusions and future work are detailed.

TABLE OF CONTENTS

1. INTRODUCTION

1.1. MOTIVATION

The *World report on road traffic injury prevention* [1] presents some assessments and conclusions regarding road traffic accidents, in which they state that more than 1.2 million deaths per year occur on the world's roads and around 50 million more of injured people. The appraisal of the main responsible accident factors indicates different solutions to adopt in order to diminish the total number of crashes. The most important and efficient is to raise awareness in the society; however, they also emphasize the concept of "smart" cars or intelligent vehicles in order to improve the visibility of the driver, provide road state knowledge or just reduce the reaction time against an accident through automatic brake controls.

The *European standard for Intelligent Transportation Systems (ITS)* [2] and the international standard IEEE 802.11p [3], which is a part of the Wireless Access in Vehicular Environments (WAVE), are the reference standards in this field. Their aim is to establish an intelligent network among vehicles and the infrastructure, such that the car-to-car and car-to-infrastructure communication are possible. In addition to prevent car accidents, this network could also be useful for diminishing gridlocks, which imply fuel consumption and travel time reduction; besides, it could be used to get information to drivers, such as road status and weather forecasts.

Nonetheless, the idea of using an intelligent network to perform a traffic safety system is considered as an indirect method, since the locations of the cars can be implicitly determined by the communication among the vehicles that belong to this network. The main purpose of this network is not to avoid accidents, is to convey information such that the position of the cars could be transmitted. An obvious drawback of this indirect safety system is related with the cars that do not belong to the network or possible objects obstructing the road; in these situations the driver is still in danger. A direct method to improve the traffic safety could be designed from the utilization of the transmitted and received wave of the V2V communication application in order to implement a radar application. Thus, the radio waves used to establish the communications among the vehicles and infrastructure could be used to detect other cars or obstructing objects based on the radar operating principle. Besides, the radar and communication applications can be compatible and improve their efficiency resulting from a kind of symbiosis.

It has been demonstrated that the radar spectral efficiency can be improved regarding a bandwidth increment [4] or reusing the radar bandwidth to perform communication operations [5][6][7][8][9]. Besides, a joint radar and communications applications is feasible due to recent advances in the digital signal processing, such that the computational cost arisen from the baseband signal processing from such merged system can be easily performed. On the other hand, the proposed modulation, - Orthogonal Division Multiplexing Frequency combined with phase shift keying - to join these applications, presents a high robustness against the Doppler shift [10], which is a valuable feature concerning the radar application. Furthermore, some economical interests present the union of a radar and communication application, since both share the same hardware (HPA, antennas and other components) as well as the radio-electromagnetic spectrum; thus, the efficiency of the spectrum is improved and some frequencies do not have to be booked.

Therefore, the idea of combining a Multiple Input, Multiple Output (MIMO) radar structure with OFDM modulation in a Vehicle-to-Vehicle (V2V) communications system have been studied in different publications [6][9][10]. These investigations introduce different techniques for target ranging and Doppler estimation; however, all methods aim at determining the location and speed of the targets,

which is closely related to estimating and tracking the parameters of the V2V channel. Different campaigns have been carried out in order to obtain a reliable V2V model [11][12][13][14][15] and the peculiarities of such a channel have enhanced the importance of a reliable and exact V2V channel modeling.

1.2. PROBLEM STATEMENT

The aim of this thesis is to verify the viability of a radar application in a V2V environment. The system implemented consists of a MIMO radar structure that uses OFDM modulation over a real channel for the V2V communication and radar application. The Geometric Stochastic Channel Model (GSCM) in [13] is considered, since it contains most of the relevant channel-specific features; in particular it models the Non Wide Sense Stationary Uncorrelated Scattering (NWSSUS) behavior typical for such channels[16][17].

A significant part of the project is focused on a software implementation of a V2V channel implementation, which in turn strongly influences the design of the joint radar and communications application. The proposed ranging system is based on the trilateration method [18] from the channel impulse response estimation, which is obtained from the antennas of a 4x4 MIMO structure. The channel estimation is based on the Maximum Likelihood Estimation (MLE), which provides an optimal solution [19]. Besides the radar algorithm, a tracking system has been implemented in order to estimate the Doppler frequency.

In order to keep the simulation scenario as close to reality as possible, the IEEE 802.11p standard has been implemented. It is important to stress that the great majority of the existent investigations concerning the joint of radar and communication applications in a V2V scenario are based on WSSUS channels. Accordingly, this fact becomes one of the most interesting parts of this thesis, since the implemented channel contains the NWSSUS feature.

1.3. THESIS CONTENT

The thesis is organized as follows. The goal of Chapter two is to review the concepts of OFDM and to present the overall model system based on the IEEE 802.11p standard and implemented in Matlab. Chapter three focuses on the description and characterization of the V2V channel as it is an important component of the thesis. Furthermore, this chapter includes a review of some important concepts for channel modeling.

The basic theory of radar systems is detailed in Chapter four, where the implemented radar algorithm is presented and related to the simulated channel. Furthermore, the tracking algorithm as well as performance criteria and metrics used for performance evaluation are performed.

Chapter five is assigned to the results obtained from the implemented radar and tracking algorithm for different scenarios. Consequently, some conclusions are announced in order to determine the efficiency of such ranging method as well as to highlight some future works to improve the proposed radar system.

Finally, some conclusions are presented about the viability of a V2V join radar and communications application using a MIMO Radar structure and OFDM. The thesis is completed by a discussion of a potential future work.

2. SCENARIO DESCRIPTION

In this chapter OFDM modulation is briefly reviewed with the aim to establish the essential theory required to understand the rest of the thesis. The main advantages and disadvantages of OFDM in terms of joint radar and communication applications are emphasized.

As mentioned previously, one of the objectives of the thesis is to implement a realistic V2V joint radar-communications scenario. The overall communication system based on the IEEE 802.11p draft [3] is detailed in Section 2.1 together with relevant discussions on the Matlab implementation. Consequently, all the steps as well as the respective considerations are detailed. Furthermore, the parameters used according to the standard are presented too.

2.1. OFDM MODULATION

Orthogonal Frequency Division Multiplexing (OFDM) [20] is well-known as the multicarrier modulation format used in different important standards such as DAB/DVB, wireless LAN, xDSL, WiMAX and PLC. OFDM is basically characterized as a multiplexing technique formed by different subcarriers, which are modulated by Phase-Shift keying (PSK) or Quadrature Amplitude Modulation (QAM). Hence, each subcarrier is responsible for carrying the respective modulated symbols, e.g. by BPSK, QPSK, 16QAM and others PSK or QAM modulations.

The cleverest feature of this technique is the overlapping method of the subcarriers that does not entail Inter Carrier Interference (ICI), since the subcarriers are orthogonal among them. Thus, the spectral efficiency is improved and high data rates are easily achieved. The subcarriers are defined by the Equation **(2.1)**, and graphically illustrated in **Figure 2.1** as a result of the Fourier Transform of a rectangular pulse.

$$\gamma_n(t) = exp(j2\pi f_n t)\frac{1}{\sqrt{T}} rect\left(\frac{t}{T}\right), \quad n = 0, \dots, N-1 \tag{2.1}$$

where, N denotes the number of subcarriers, T is the pulse duration and f_n denotes the subcarrier frequency defined by the function

$$\Delta f = \frac{1}{T} = \frac{B}{N} \xrightarrow{yields} f_n = n\Delta f, \tag{2.2}$$

with Δf as the frequency distance between subcarriers and B is the total available bandwidth of the transmission.

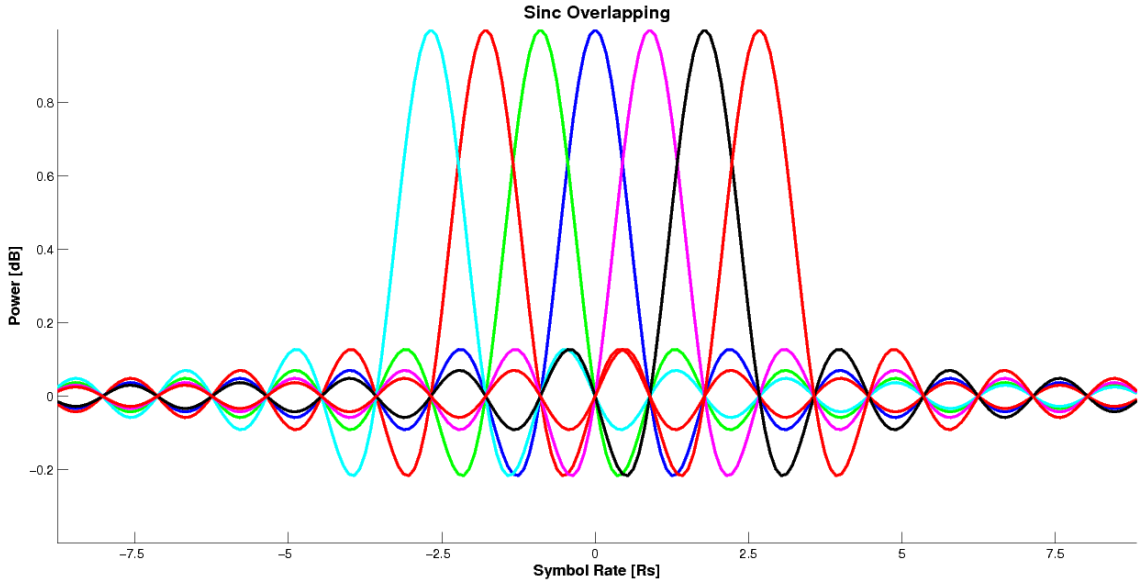

Figure 2.1 *Sinc Overlapping in the frequency domain. As can be seen, all the crests of each sinc coincide with the zeros of its neighbor sinc's. Thus, the addition is neither destructive nor constructive. It summarizes the orthogonality of the subcarriers.*

The basic aspects of an OFDM transmission can be summarized as an Inverse Discrete Time Fourier Transform (IDFT) of the information symbols from the frequency domain (known as the OFDM multiplexer), a posterior convolution of the signal with the respective channel and the OFDM de-multiplexer in the receiver by means of the Discrete Fourier Transform (DFT) from the time domain to the frequency domain. For instance, an OFDM system is composed of N subcarriers and transmitting frames of length K symbols, such that the indexes *n* and *k* are defined as *n=0,…,N-1* and *k=0,…,K-1*, and resulting in the analytical expression **(2.3).**

$$x[k] = e^{j2\pi f_c \frac{kT_{Total}}{K}} \frac{1}{\sqrt{T}} \sum_{n=0}^{N-1} s_{n+N\left\lfloor \frac{k}{N} \right\rfloor} e^{j2\pi f_n \frac{kT_{Total}}{K}} \; rect\left(\frac{\frac{kT_{Total}}{K} - lT}{T} \right)$$

$$y[p] = \sum_{m=-\infty}^{\infty} x(m)h(p-m) \qquad \textbf{(2.3)}$$

$$r[k] = e^{-j2\pi f_c \frac{kT_{Total}}{K}} \sum_{n=0}^{N-1} y_{n+N\left\lfloor \frac{k}{N} \right\rfloor} e^{-j2\pi f_n \frac{kT_{Total}}{K}}$$

where $\lfloor A \rfloor$ denotes the nearest integer less or equal to A. f_c is the central frequency, which corresponds to the frequency that the signal modulated in baseband is centered around after the conversion to pass-band. Whilst, s_n represents the resulting symbol according to the PSK or QAM modulation, whose length is equal to $N + N\left\lfloor \frac{K}{N} \right\rfloor$. Therefore, s_n is composed by *K* symbols and the rest of the coefficients (N) are set to 0 to fulfill expression **(2.3)**. The received symbol vector is represented by r, whose length is equal to the *K* symbols. The pulse duration is symbolized by T, whereas T_{Total} is used for the total time required to transmit the information sequence, s_n. In addition, x represents the signal in the time domain, while y corresponds to the convolution in the time domain of the channel h with x. It is important to stress that x and y are in the discrete time domain, whereas in the **Figure 2.2 and 2.3** are in the continuous time domain.

In **Figure 2.2 and 2.3** the basic system is illustrated, where bits are mapped to symbols and converted to time domain in the IDFT block. Then, the real and the imaginary parts of the time domain signal are converted to analog signals through Digital-to-Analog Converters (DACs), since the output of the IDFT is in discrete time as its name indicates. The baseband signal is then up-converted to pass-band carrier frequency.

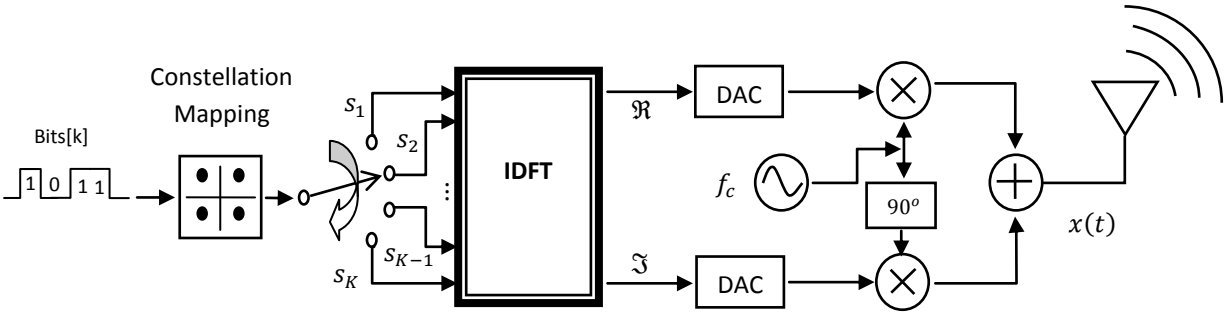

Figure 2.2 *OFDM Transmitter scheme*

The receiver obtains the baseband signal using a down-converter centered around f_c and a low-pass filter to eliminate harmonics, e.g. $2f_c$. After analog-to-digital conversion, DFT conversion of the received signal to the frequency domain and the de-mapping are conducted to obtain the binary signal.

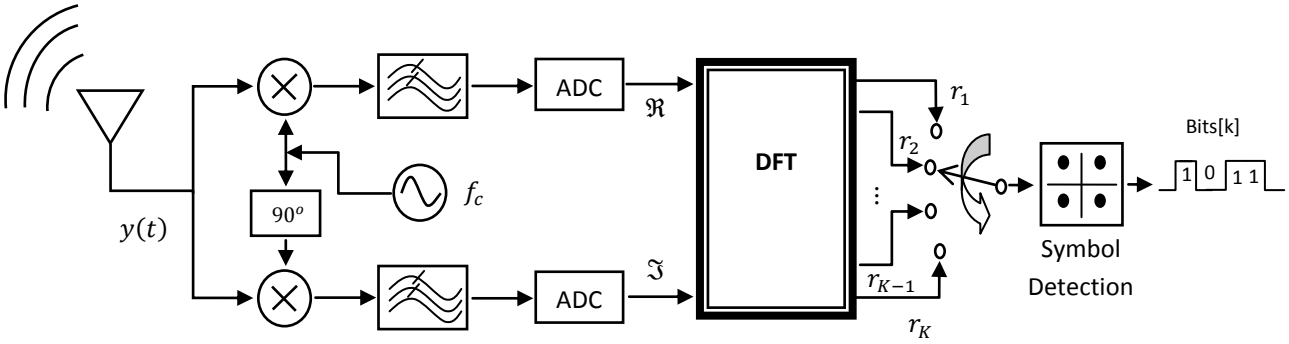

Figure 2.3 *OFDM Receiver scheme*

The advantages of modulation are:

- Robustness against Intersymbol Interference (ISI) as is depicted in the **Figure 2.1**
- Robustness against multipath fading, allowing for easy channel equalization.
- High flexibility regarding data rates configuration.
- High data rates due to parallel transmission.
- High tolerance against Doppler shift.

The orthogonality of the subcarriers allows for high data rates, while the robustness against multipath fading and easy channel equalization are basically achieved due to the bandwidth reduction of each subcarrier. As the bandwidth of the signal becomes smaller than the coherence bandwidth of the channel, each subcarrier sees the channel as a flat fading instead of a frequency selective fading channel. However, the most important feature regarding the thesis issue is the good properties that OFDM exhibits against Doppler effect, which is demonstrated in [8].

The main disadvantages of OFDM are the strict time and frequency synchronization requirement, which affect the orthogonality of the subcarriers, resulting in ICI. Furthermore, there are other drawbacks

(which are not directly relevant for the scope of this thesis) such as the Peak to Average Power Ratio (PAPR), which affects the saturation point of the High Power Amplification (HPA) and the non-ideal auto-correlation properties between OFDM signals.

2.2. COMMUNICATION SYSTEM DESCRIPTION

This Section describes the Matlab simulation setup for implementing the IEEE 802.11p standard, derives from the IEEE 802.11a [21]. The description of this scenario is limited to the Single Input Single Output (SISO) case for notational simplicity; the corresponding block diagram is depicted in **Figure 2.4**.

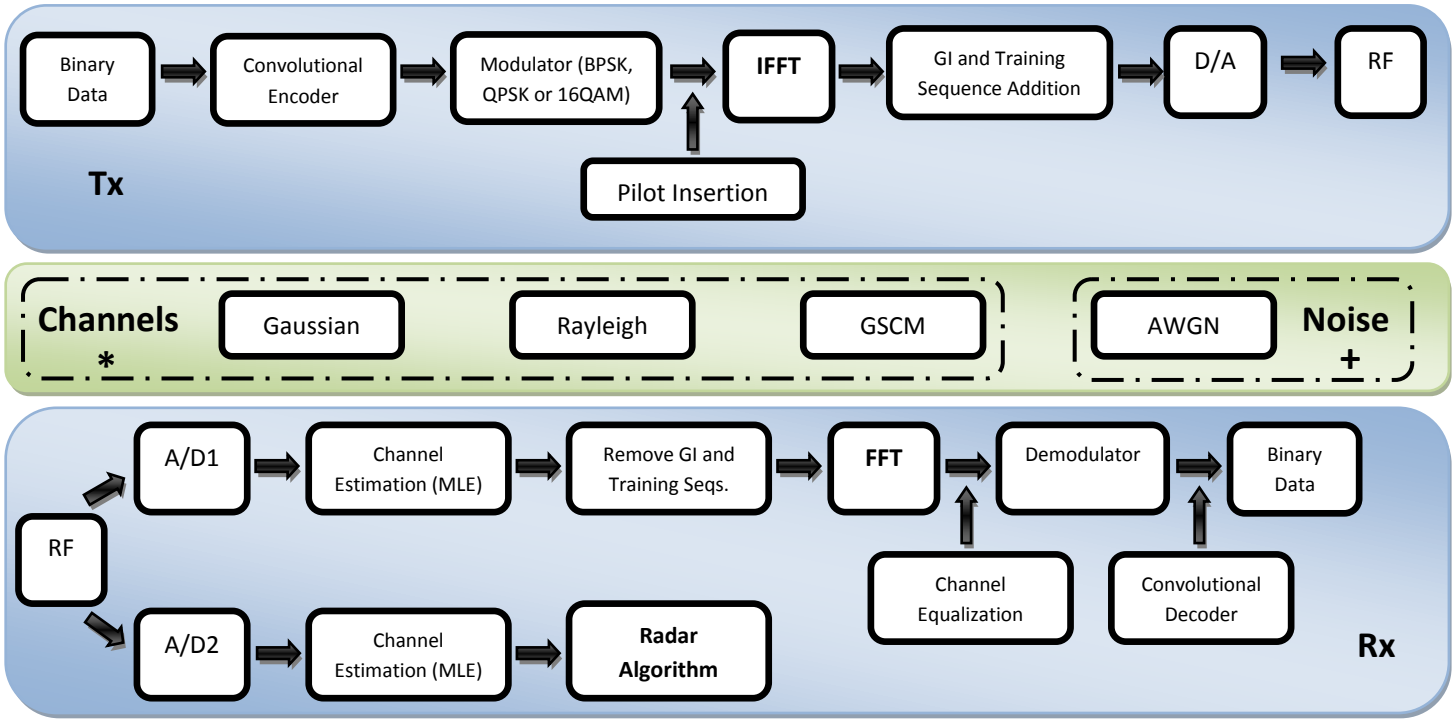

Figure 2.4 *Block Diagram. The receiver contains two different sampling times (A/D1 and A/D2). One of them is for the Radar application, while the other is for the V2V communication.*

Firstly, the data is generated randomly, independently and uniformly; such that $data \in \{0,1\}$ .Secondly, a convolutional encoder is applied [22]; the implemented model is the same as the IEEE 802.11a standard proposes for the OFDM PHY (Physical Layer) in the 5GHz band, with a rate equal to R=1/2 if puncturing is not performed. The generator polynomials are 133_8 and 171_8 in octal for the upper and lower encoding branches, respectively.

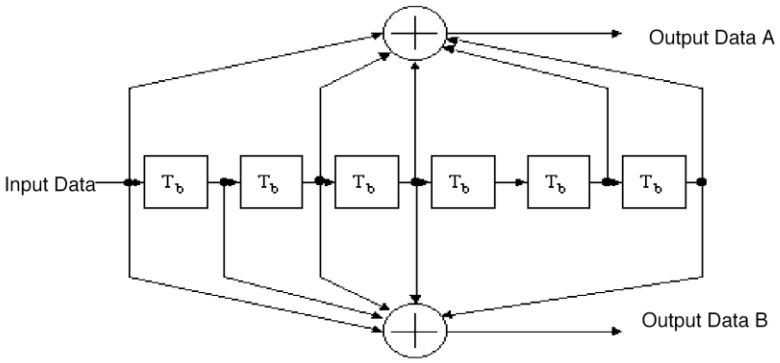

Figure 2.5 *Convolutional Encoder*

The next step is the mapping of data into symbols of a PSK or QAM constellation. The implemented modulations formats are the BPSK, QPSK and 16QAM, whose constellations are formed by 2, 4 or 16 points, respectively. It is important to highlight that the symbol-amplitudes are normalized to have unity average energy. Thus, the expectancy of the transmitted symbol power:

$$\mathbb{E}[|s_k|^2] = 1 \tag{2.4}$$

The Inverse Discrete Fourier Transform maps respective symbols to respective orthogonal subcarriers. In place of the IDFT, the IFFT (Inverse Fast Fourier Transform) has been implemented as an effective IDFT fast algorithm for the transform vectors with a length as a power of two. In the DFT case the analog algorithm has been applied, FFT (Fast Fourier Transform).

The IEEE 802.11a standard proposes a way to map the symbols in the IFFT input block, such that for a 64-point IFFT the resulting configuration is depicted in **Figure 2.6**.

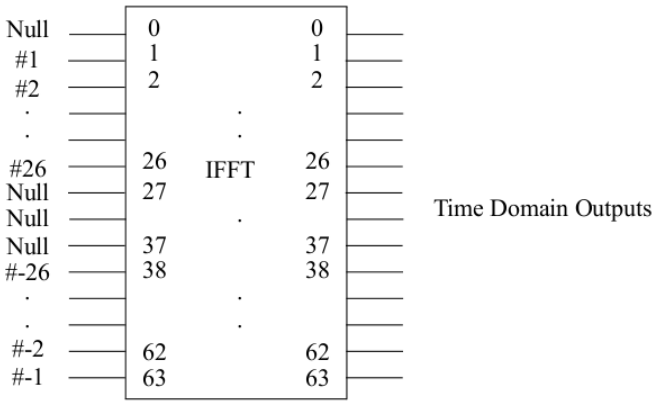

Figure 2.6 *IFFT inputs mapping according to the IEEE 802.11a standard.*

As the implemented system also uses a 64-point transform, the IFFT has been carried out in the same manner. The symbols with coefficients from 1 to 26 are mapped in the same numbered IFFT inputs, while the coefficients from -26 to -1 are introduced in the inputs from 38 to 63. The rest of inputs from 27 to 37, which are placed on the sides of the OFDM spectrum, are set to 0 and their purpose is to ensure separation from the adjacent sub-bands, as guard subcarriers. The same happens to the DC subcarrier, which is placed in the middle and set to 0.

The next step deals with the OFDM frame, which is depicted in **Figure 2.7**. It consists of the preamble, which is formed by a short and long training sequence, and the OFDM symbols. The function of the short sequence is to obtain the automatic gain control, signal detection, diversity selection, coarse frequency offset estimation and timing synchronizes. While the long sequence is formed by two long symbols and the Guard Interval (GI2) or Cyclic Prefix (CP) so as to prevent ISI caused by the multipath propagation; its aim is the channel and fine frequency estimation. It is assumed ideal time synchronization and gain equal to the unity, and therefore the short training implementation is useless. However, it is required for simulating the total OFDM frame length that affects the channel variation as explained later. Accordingly, the long training sequence, which is used for the channel estimation, has been copied in the short sequence.

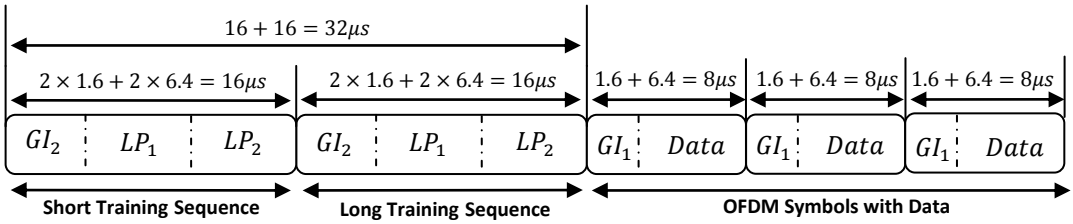

Figure 2.7 *Implemented OFDM frame.*

The long preamble coefficients used in the long training sequence is defined in the IEEE 802.11a standard. Thus, the coefficients before the IFFT are:

LP {–26, 26} = {1, 1, –1, –1, 1, 1, –1, 1, –1, 1, 1, 1, 1, 1, 1, –1, –1, 1, 1, –1, 1, –1, 1, 1, 1, 1, 0,

1, –1, –1, 1, 1, –1, 1, –1, 1, –1, –1, –1, –1, –1, 1, 1, –1, –1, 1, –1, 1, –1, 1, 1, 1, 1} **(2.5)**

The GI2 has a duration of one half of the T_{FFT} and it is generated as a copy of the time domain coefficients of the long preamble from the previous frame.

The OFDM symbols consist of the data and the GI. The data is also formed with 52 active subcarriers. Four are used as pilot subcarriers in order to make the transmission robust against frequency and phase noise; their positions are 8, 22, 44 and 58 and their values are 1, -1, 1 and 1, respectively. The 48 remaining subcarriers are carrying information. While GI1 is generated in the same manner has GI2, the difference lies in the duration that is only half of the GI2 ($\frac{T_{FFT}}{4}$). The pilot subcarriers have been defined but are not used.

Following the block diagram, the next step is the convolution with the channel. In the implemented system three different channels have been used, which are a Gaussian, Rayleigh and V2V channel that is explained in the next chapter due to its complexity and importance in this thesis. All the channel lengths, due to multi-path, are supposed to be shorter than the cyclic prefix duration. Therefore, ISI is not considered; however, this consideration for the V2V channel is not required, since it does not surpass the CP constraint.

The Gaussian channel for a SISO system is defined as

$$\boldsymbol{y}_i = \boldsymbol{x}_i + \boldsymbol{z}_i \;:\; \boldsymbol{z}_i \sim N(0,1); \quad i = 0{:}\,k. \tag{2.6}$$

where X_i is the *i*th input coefficient of the channel, Z_i is the Additive White Gaussian Noise (AWGN) with zero mean and unitary deviation, Y_i is the respective output coefficient and k is the total length of the transmission vector. As the noise is added in the next block, the discrete impulse channel response of the Gaussian channel has been implemented as a discrete Dirac delta function without delay as shown in **(2.7)**. Thus, the convolution of the channel with the signal results in the input signal without temporal displacement.

$$Gaussian(k) = \delta(k); \qquad \delta(k) = \begin{cases} 1, & k = 0 \\ 0, & k \neq 0 \end{cases} \tag{2.7}$$

As the deviation is equal to 1 as can be seen in the expression **(2.6)** and the input signal is defined as an energy signal, thus its energy is finite; the capacity of the Gaussian channel is not infinite.

Concerning the Rayleigh channel, it has been implemented as an exponential distribution to represent the multipath, while the fading has been represented as a Gaussian distribution for the real and the imaginary components. Therefore, the discrete channel impulse response expression is defined as

$$Rayleigh(k) = \mu e^{-\mu k} \frac{\left(N_k(0,1) + jN_k(0,1)\right)}{\sqrt{2}}. \tag{2.8}$$

with μ as the mean of the exponential distribution and value equal to the unity. The addition of the two Gaussian distribution in the real and the imaginary part has to be divided by the square root of two to maintain the unitary deviation.

Once the signal is convolved with the respective channel, the addition of the AWGN is the following process. A property of this kind of noise is that affect all the frequencies; hence, the addition has been performed for all the coefficients resulting of the convolution process. The power of the noise has been determined through the Signal to Noise Ratio (SNR) as the expression **(2.9)** highlights.

$$P_{signal} = \sum_{n=0}^{N-1} \frac{\|d_n\|^2}{N^2} (e^{j2\pi f_n t})^2 = \frac{52}{64^2}; \qquad SNR = \frac{P_{Signal}}{P_{Noise}}; \qquad P_{Noise} = \frac{P_{Signal}}{SNR} \tag{2.9}$$

The numerator of the signal power represents the total number of active subcarriers (52), while the numerator is the total number of subcarriers. Thus, the highest SNR occurs when all the active subcarriers are transmitting information. $\|.\|$ denotes the Euclidean Norm.

For the cannel estimation, the assumption of a SISO system has been considered for simplicity. Hence, the received discrete-time baseband signal for the long training sequence transmission can be defined as

$$\boldsymbol{y} = \begin{bmatrix} m_0 & \cdots & 0 \\ \vdots & \ddots & \vdots \\ m_{P-1} & \cdots & m_{P-L-1} \end{bmatrix} \begin{bmatrix} h_0 \\ \vdots \\ h_L \end{bmatrix} + [n_0, \cdots, n_L], \tag{2.10}$$

with $\boldsymbol{h}$ as the complex channel impulse response vector, $\boldsymbol{n}$ as the AWGN vector and $\boldsymbol{M}$ as the convolution matrix coefficients formed with the training sequence. The index L denotes the length of the channel response, while P is determined as the length of the long training sequence.

Concerning **(2.10)**, the channel estimation is performed through the Likelihood approach.

$$\widehat{\boldsymbol{h}} = arg \min_{h} \|\boldsymbol{y} - \boldsymbol{M}\boldsymbol{h}\|^2 \tag{2.11}$$

As the added noise is AWGN the expression **(2.11)** according [19][23] can be written as

$$\widehat{\boldsymbol{h}}_{\boldsymbol{LS}} = (\boldsymbol{M}^H\boldsymbol{M})^{-1}\boldsymbol{M}^H\boldsymbol{y} \tag{2.12}$$

where $\hat{h}_{LS}$ is the estimated channel, while $(\cdot)^H$ and $(\cdot)^{-1}$ define the Hermitian and inverse matrices, respectively.

Assuming that the system has a perfect OFDM symbol synchronism, it facilitates the GI removal of each OFDM symbol as well as the training sequences. Hence, the remaining samples correspond to the received data in the time domain, which are converted to the frequency domain in sets of 64 samples through the FFT. The resulting vector is also of 64 samples, and it has to be equalized by the channel estimated by element-wise division in order to counteract the noise and the multipath fading effect. It implies that the estimated channel has to be converted from the time to frequency domain by a 64-point FFT.

In reference to the equalized symbols, they have to be sorted according to the previous IFFT mapping presented in the **Figure 2.6**. The demodulator is then applied in order to convert the symbols to binary regarding the PSK or QAM modulation used in the transmitter. Finally, a hard Viterbi algorithm is used for the decoding of the binary bits [22].

The parameters used in the system simulated according to the IEEE 802.11p standard are summarized in the **Table 2.1**.

Table 2.1 *IEEE 802.11p parameters*

Parameters	Values
N_D: Data Subcarriers	48
N_P: Pilot Subcarriers	4
N_T: Total Number of Subcarriers	64 (N_D+N_P+12 null subcarriers)
FFT/IFFT Points	64 (N_T)
Δ_f: Subcarrier Bandwidth	156.25 kHz (10MHz/64)
T_{FFT}: IFFT/FFT Period	6.4 μs ($1/\Delta_f$)
T_{GI}: Guard Interval Duration	1.6 μs ($T_{FFT}/4$)
T_{OFDM}: OFDM Symbol Duration	8 μs (T_{GI}+T_{FFT})
T_{LP}: Long Preamble Duration	6.4 μs ($1/\Delta_f$)
T_{GI2}: Guard Interval Duration for TS	3.2 μs ($T_{FFT}/2$)
T_{TS}: Training Sequence Duration	16 μs (T_{GI2}+$2T_{LP}$)
T_S: Sampling Time	0.1 μs ($T_{FFT}/64$)

The basic difference between the IEEE 802.11a and the IEEE 802.11p is in the bandwidth, which has been decreased from 20 MHz to 10 MHz; accordingly, all the parameter duration in the time domain is

doubled. The main purpose is to prepare the communication for high mobility scenarios between the transmitter and the receiver.

The remaining part of the block diagram is for the radar operation, which is explained in Chapter 4. However, it basically consists of channel estimation according to a shorter sampling time and the application of the radar algorithm in order to detect the targets.

3. V2V PROPAGATION CHANNEL

In this chapter is reviewed some fundamental concepts of radio signal propagation, presented a survey of recently published V2V channels models, and provided a description of the particular V2V channel model considered in the thesis. Furthermore, a description of the implemented model and its properties are also included. Finally, the chapter is completed with a characterization of the implemented channel.

3.1. CHANNEL PROPAGATION BACKGROUND

A channel description is basically focused on the influence of the propagation environment over a communication system. The wireless transmission environment is mainly characterized by multipath components (MPC) and variations due to location and movement of transmitter and receiver. The MPC contributions can be originated as a consequence of the reflection, diffraction, refraction, absorption, waveguiding and other electromagnetic propagation effects of the wave over the components. These contributions correspond to signal copies with a determined attenuation, phase shift and delay time as a result of the propagation paths; thus, the addition can be performed in a constructive or destructive manner.

Therefore, a channel can be defined by obtaining the path loss, fading statistics, Doppler Spread and the delay spread parameters of the channel.

3.1.1. PATH LOSS

This factor indicates the power loss in a radio communication, due to the wave propagation over the media and its interaction with the MPC. The loss trends to increase exponentially with n (path loss exponent) as a function of distance

$$d^n. \tag{3.1}$$

Hence, the signal amplitude is inversely proportional to the path loss expression, such that this parameter becomes the major constraint factor in the power link budget.

3.1.2. FADING STATISTICS

One of the most important causes for the amplitude and phase fluctuation for the received signal is the obstacle presence in the communications paths. These variations are defined by the fading statistics and its purpose is to describe statistically the behavior of the received power. According to the fluctuation rate, the fading can be categorized into two types; the *small-scale fading* for the fast fluctuations and *large-scale fading* for the slow fluctuations. Therefore, a fast change can be addressed as to the antenna oscillation due to the wind effect as to the MPC displacement, multipath propagation. By contrast, a slow fading is basically originated by a large obstruction of the strongest propagation path, also known as shadowing.

3.1.3. DOPPLER SPREAD

The Doppler shift is defined as the frequency shift that the carrier frequency experiences due to the MPC and transmitter (Tx) and receiver (Rx) velocities according to the used wavelength.

$$f_D = \frac{V_{rel}}{\lambda} \tag{3.2}$$

where V_{rel} represents the speed difference between the Tx and the Rx in the Line of Sight (LOS), whereas in a single bounce, the relative velocity is determined by

$$\boldsymbol{v}(\boldsymbol{\Omega}_{\mathrm{T,p}}, \boldsymbol{\Omega}_{\mathrm{R,p}}) = \frac{1}{\lambda}\left[(v_T - \boldsymbol{v}_p)cos(\boldsymbol{\Omega}_{\mathrm{T,p}}) + (v_R - \boldsymbol{v}_p)cos(\boldsymbol{\Omega}_{\mathrm{R,p}})\right]. \tag{3.3}$$

These parameters are subsequently depicted in **Figure 3.1**. The velocities of the transmitter, receiver and the third component are assigned as v_T, v_R and $\boldsymbol{v}_p$, respectively; while the $\boldsymbol{\Omega}_{\mathrm{T,p}}$ and $\boldsymbol{\Omega}_{\mathrm{R,p}}$ are the departure and arrival angles in this order.

The Doppler spectrum is attributed to the set of Doppler shifts, which are derived from different velocities of the scenario components. The coherence time is inversely proportional to the Doppler spread and determines the time duration in which the channel phase can be predictable. The Doppler spread is the range of possible frequencies according to the Doppler shift.

3.1.4. DELAY SPREAD

The delay spread is characterized by the time dispersion of the channel, whereas the Doppler spread is related with the time varying of the channel impulse response. Therefore, the delay spread determines the widening of the channel because of the delay rays contributions, which come from the multipath. The coherence bandwidth corresponds to the delay spread factor and it is used to characterize the communication fading behavior as a flat, the channel coherence bandwidth is larger than the signal bandwidth, or as frequency-selective for the opposite case.

3.2. V2V CHANNEL FEATURES

To characterize the main features of the V2V channel, the different scenarios for this kind of radio communication (urban, suburban, rural and highway) have to be taken into account. **Table 3.1** summarizes their range of values for the previously mentioned parameters.

Table 3.1 *Parameters summary for the different V2V scenarios [11]*

Scenario	Pathloss exponent	Delay spread (mean)	Delay spread (10%–90%)	Doppler spread (mean)
Highway	n = 1.8 [7] n = 1.85 [20] n = 1.9/4 0[a] [22]	247 ns [7] 41 ns [20] 141–398 ns[b] [17] 165 ns [27] 53/127 ns[d] [8]	120–340 ns [7] 50–190 ns [15] 30–300 ns [27] 0.3/0 5–90/260 ns[d] [8]	92 Hz[f] [20] 120 Hz [14] 761–978 Hz[b] [17]
Rural	n = 1.79 [20] n = 2.3/4 0[a] [22]	52 ns [20] 22 ns [17]	20–150 ns [15]	108 Hz[f] [20] 782 Hz [17]
Suburban	n = 2.5 [4] n = 2.1/3 9[a] [4]	104 ns [27]	40–110 ns [15] 20–230 ns [27]	
Urban	n = 1.61 [20]	47 ns [20] 158–321 ns[c] [17] 373 ns [27] 126/236 ns[e] [8]	30–1100 ns [27] 3/20–250/570 ns[e] [8]	33 Hz[f] [20] 86 Hz [14] 263–341 Hz[c] [17]

[a] Breakpoint model; [b] TX-RX separations of 300–400 m; [c] TX-RX separations of 200–600 m; [d] low/high traffic density; [e] antenna outside/inside car; [f] median value

Some conclusions from the table can be drawn. The path-loss exponents from the highway, rural and urban cases show comparable values as the LOS exponent for cellular channels. The suburban exponent is closer to the NLOS (Non LOS) cellular channels.

Regarding the mean Doppler spread, its values can oscillate from 33-978 Hz; however, high values can be registered in the highway scenarios. The behavior is obvious, since in the speed of the vehicles are higher, thus the relative velocities can be also large.

As the delay spread depends on the scenario, the values reported in the table are conditioned to the locations where this parameter was measured. Nevertheless, the range of the mean values can be restricted from 22 to 398 n_s, although instantaneous peaks of 1100 n_s have been registered. This parameter is the responsible for producing ISI; however, a well-designed GI of 1.6 μ_s in the IEEE 802.11p (see **Table 3.1**) does not overcome this maximum spread.

The most peculiar and important feature of the V2V propagation channel is the assumption of Non Wide Sense Stationary Uncorrelated Scattering (NWSSUS).

3.2.1. WSSUS

The Wide Sense Stationary (WSS) concept describes channels whose statistical descriptions time variations are independent of the absolute time. The Uncorrelated Scattering (US) assumption is valid for stationary behavior of the channel frequency variables as compared to the absolute frequency. Consequently, the channels that fulfill both features, in time and frequency, are classified as WSSUS[16][17].

Concerning the definition, WSSUS channels only depend on the increment of time and frequency and the influence of the absolute time or frequency positioning of the channel is not significant. Nonetheless, the fast motion of the V2V channels implies that the vehicles do not remain in a constant location during the wave propagation time between the Tx and Rx. It thus affects the time dispersion and time variation, which change inside this time period. For example, two vehicles that are moving in opposite directions will show different Doppler shift and delay as they are approaching or moving away from each other, according to a tracking over the absolute time.

3.3. V2V CHANNEL MODELS SURVEY

There are different modeling approaches to describe a channel, such as the narrowband and wideband stochastic channel models, tapped-delay-line, ray tracing, Geometry-based stochastic channels models (GSCM. However, they can be basically classified into three different model approaches: the deterministic, stochastic and the geometry-based stochastic.

The deterministic method can be identified by modeling approaches as the ray tracing, for instance. The fundamental concept of this group relies on the generation of an accurate scenario, where the wave behavior is thoroughly determined according to the wave equations (e.g. Maxwell's equations) conditioned to the scenario characteristics. This approach offers good performance, but the detailed environment results in a difficult method to vary parameters; besides, the high computational cost to carry out the calculations becomes other drawback.

Stochastic methods can be represented by a tapped-delay-line channel model where the essential idea is to describe statistically all the interactions occurring in a given scenario. It is computationally cheapest method for modeling a channel; however, it does not allow for the NWSSUS condition of the V2V channels.

As a last method, the GSCM is presented. Its theoretical principle is based on the appraisal of the objects interactions that constitutes a simulated scenario, where the components are placed randomly according some statistics distributions; the contributions are carried out by basic ray tracing. The main advantages of this model are the computational cost, which is between the both methods previously mentioned, and the automatic fulfillment of the NWSSUS condition. The fact of working with geometrical scenarios entails the NWSSUS assumption, since the channel components displacements and their contributions are easily achieved.

3.4. DESCRIPTION OF THE GSCM MODEL

The implemented model [13] is based on a measurements campaign performed for V2V communication with a MIMO system 4x4 (four transmit antennas and four receiver antennas) at frequency 5.2 GHz, which is close to 5.9 GHz used in the IEEE 802.11p standard. And the locations of the measurements have been carried out in a highway and rural environment in Lund, Sweden.

The main advantages of this model are the facility to fulfill the NWSSUS criterion of the V2V channels, the modeling of the delay and Doppler spectra, the inherently modeling of the MIMO properties and the ability to change easily different parameters, e.g., the radiation pattern of the antennas as well as the environment.

The main concept of this GSCM model is to first build the scenario. Then, the channel properties of the different components of the environment are set, their interactions among them concerning the signal distortion are calculated and finally, the sum of all the contributions is performed to obtain the channel impulse response (see 2.15).

$$h(t,\tau) = \sum_{i=1}^{N} a_i e^{jkd_i(t)} \delta(\tau - \tau_i) g_R\left(\Omega_{\mathrm{R,i}}\right) g_T(\Omega_{\mathrm{T,i}}) \tag{3.4}$$

where N is the total number of contributions or different path regarding the amount of scatterer points, a_i is their respective complex amplitude, the radiation patterns are represented by g_R and g_T for the transmitter and receiver antenna, $\Omega_{\mathrm{R,i}}$ and $\Omega_{\mathrm{T,i}}$ are the angles of departure (AOD) and arrival (AOA) of each ray, respectively. The distance for each path is d_i and k is the number of wavelengths ($k = {}^{2\pi}/_{\lambda}$).

In order to reproduce the NWSSUS feature, the transmitted signal has to be convolved with different channels regarding the time evolution. The ideal case is to generate the same number of channels as coefficients have the transmitted signal in the discrete time domain; thus, each sample is convolved with its respective channel that is calculated from the real state of the scenario according to the specific time of this coefficient.

$$y[k] = \sum_{m=-\infty}^{\infty} x[m] H[k, k-m] \tag{3.5}$$

where H is a matrix, whose rows are the channels simulated for different time instants and its columns represent the coefficients of the channel due to multipath. As a consequence of the computational cost that it supposes and the little displacement of the vehicles for the sampling time (duration of each coefficient), the total number of channels can be reduced. It is important to highlight that although the scenario does not significantly change concerning the geometry, the fading is always present.

3.4.1. SCENARIO

The first step is to establish the scenario, which can be composed by three different types of components or scatterer points. They are sorted as the mobile discrete (MD), static discrete (SD) and diffuse (DI) according to their channel properties, which represent vehicles, traffic signals and trees, respectively. Their placement in the two dimensional geometry is performed regarding some statistical distribution (see **Table 3.2**) obtained from the highway and rural statistical analysis. Furthermore, this traffic analysis defines the densities of the scatterer points, χ_{MD}, χ_{SD} and χ_{DI} for knowing the total number of components to represent in the scenario board.

The scenario example proposed in [13] is depicted in **Figure 3.1**. As can be seen, the scenario illustration is practically divided in three zones: the lanes (W_{Road}), ditches (W_{SD}) and outside road areas (W_{DI}). In the proposed model from the paper, the width of the static discrete scatterers is not defined; however, it has been assumed to be the half of the W_{DI}. Furthermore, it is important to note that this last width overlaps the other two areas, since a road signal can be inside the road or diffuse areas. Hence, W_{SD} is only used to determine the number of static discrete scatterers, their placement is not dependent on its width as explained below.

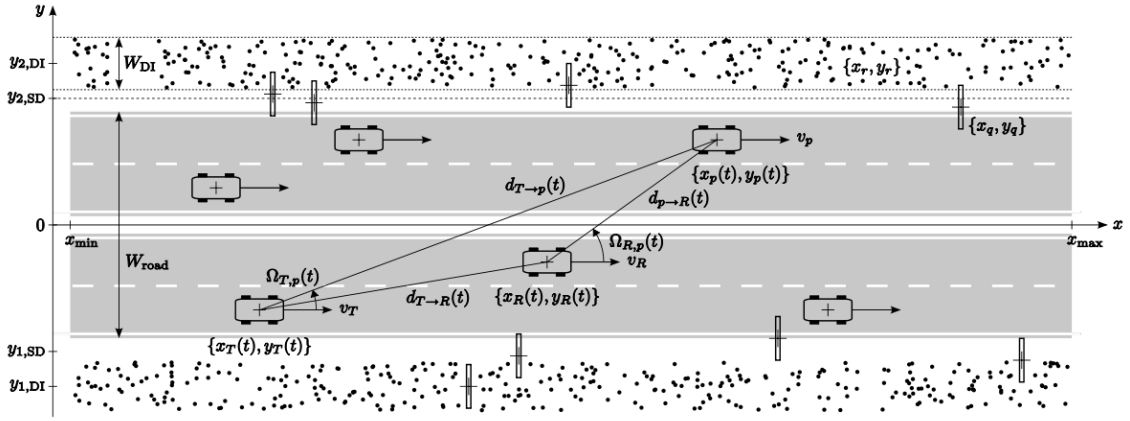

Figure 3.1. *Example of a possible scenario designed by [13], where the communication through the reflection effect in a third car is performed. The angles of departure and arrival are $\Omega_{T,p}$ and $\Omega_{R,p}$, respectively. The location of the transmitter, receiver and passive car are $\{x_T, y_T\}$, $\{x_R, y_R\}$ and $\{x_p, y_p\}$, whilst the distances of the travelling wave are represented by the sum of $d_{T\to p}$ and $d_{p\to R}$.*

Table 3.2. *Summary of the statistical distributions placement and speeds for different scatterer types.*

	COORDINATES			VELOCITY
	X ~	Y ~		
MD	$\mathcal{U}[x_{min}, x_{max}]$	$\mathcal{U}[\frac{-W_{Road}}{2}, \frac{W_{Road}}{2}]$		$\mathcal{N}(v, {\sigma_{v,MD}}^2)$ $-\mathcal{N}(v, {\sigma_{v,MD}}^2)$
SD	$\mathcal{U}[x_{min}, x_{max}]$	$\mathcal{N}(y_{1,SD}, {\sigma_{y,SD}}^2)$	$\mathcal{N}(y_{2,SD}, {\sigma_{y,SD}}^2)$	-
DI	$\mathcal{U}[x_{min}, x_{max}]$	$\mathcal{U}[y_{1,DI} - \frac{W_{DI}}{2}, y_{1,DI} + \frac{W_{DI}}{2}]$	$\mathcal{U}[y_{2,DI} - \frac{W_{DI}}{2}, y_{2,DI} + \frac{W_{DI}}{2}]$	-

In **Table 3.2** $\mathcal{U}[\cdot]$ and $\mathcal{N}(\cdot)$ denotes the uniform and Gaussian or normal distributions, respectively. The velocity statistics are defined by a normal distribution centered in the average speed of the car route with a certain variance ${\sigma_{v,MD}}^2$, due to the difference speeds of the cars. Another important detail to note is the ensemble of velocities that are negatives. The sign is used to distinguish the two possible directions of the cars, same and opposite direction according to their placement (lane). The variance is supposed to be smaller than the half of the centered speed, thus a sample coming from a normal distribution centered in a positive speed cannot be negative or zero. The common speeds used have been 80 and $100\ km/h$ for the rural and highway environment, respectively.

With the aim to account for the different heights of vehicles, a normal distribution is also used. It is centered in 1.5 meters as the average height car and its standard deviation is assumed to be of 0.5 meters for all the scenarios, such as the highway or rural environment.

$$Height \sim \mathcal{N}(1.5, 0.5^2) \tag{3.6}$$

3.4.2. Complex Amplitude

The contributions of the multipath components to the transmitted signal are defined by the expressions **(3.7)** and **(3.8)**. These equations reproduce the attenuation of the signal according to the distance increment, the fading effect as well as the Doppler shift. The delay spread is determined by the time delay between different signal paths, which is related by the geometry of the scenario. Therefore, the amplitudes can be classified in two ensembles: the diffuse scatterer amplitude ensemble and the discrete scatterer amplitude ensemble, formed by the LOS and the NLOS of the MD and SD scatterers. In fact, the only difference between the LOS and NLOS lies in the used parameters, since the complex amplitude expression is shared. The authors of this GSCM model attribute the ground reflection as one likely cause of the fading experienced in the LOS path.

3.4.2.1. Diffuse scatterer

The complex amplitude from the diffuse scatterer paths is defined by

$$a_{DI,p} = G_{0,DI}^{1/2} c_{DI,p} \left(\frac{d_{ref}}{d_{T\to p} + d_{p\to R}} \right)^{n_{DI}/2}. \tag{3.7}$$

where $c_{DI,p}$ is the observation of the zero-mean complex Gaussian distribution for the p path, d_{ref} is a reference distance equal to 1 meter used for the reference power definition $G_{0,DI}$. The path-loss exponent is n_{DI}, while the total distance is formed by the sum of the distances from the transmitter to the component ($d_{T\to p}$) and from the component to the receiver ($d_{p\to R}$). It is important to highlight that all the parameters are constant for all the diffuse scatterers, except the total distance and $c_{DI,p}$ that are related with the different paths.

3.4.2.2. Discrete scatterer

The expression for the discrete scatterer complex amplitude is such that

$$a_p = g_{S,p} e^{j\theta_p} G_{0,p}^{1/2} \left(\frac{d_{ref}}{d_{T\to p} + d_{p\to R}} \right)^{n_p/2}. \tag{3.8}$$

The distances, path-loss exponent and reference power gain are defined as before and they represent the deterministic part of the complex amplitude. By contrast, the stochastic part is represented by the phase θ_p of the scatterers, which is uniformly distributed over $[0,2\pi)$ as the classical GSCM approach, and the real-valued $g_{S,p}$, which identifies the complex amplitude of the respective scatterer and whose behavior is slow varying. Therefore, it represents slow fading, while the fast fading is not included in the model proposed by its creators for different reasons that are justified in [13].

It is important to highlight the difference between the LOS and the NLOS of expression **(3.8)**. The path-loss exponent for the LOS remains constant, while the NLOS is uniformly distributed. The reference power $G_{0,p}$ leads the second dissimilarity being constant for the LOS, while for the NLOS it is linearly related with the path-loss exponent (see **Table 3.4**).

The complexity of the discrete scatterer complex amplitude modeling lies in the calculation of the amplitude for the stochastic part, $g_{S,p}$. The authors defined a method to generate it, which is based on the correlation of uncorrelated data from a $\mathcal{N}(0,1)$ using the autocorrelation function defined below.

$$r_d(\Delta d) = \sigma_S^2 e^{-\frac{ln2}{d_c^2}(\Delta d)^2} \tag{3.9}$$

where σ_S^2 is the variance of the stochastic amplitude gain and follows an exponential distribution.

$$\sigma_S^2 \sim \frac{1}{\mu_\sigma}\, e^{\frac{-1}{\mu_\sigma}\sigma_S^2}. \tag{3.10}$$

The coherence distance d_c of the stochastic amplitude gain is determined as the distance that fulfills $\rho_d(d_c) = 0.5$ and its behavior is defined by

$$d_c = d_c^{min} + d_c^{rand} : \; d_c^{rand} \sim \frac{1}{\mu_c} e^{\frac{-1}{\mu_c} d_c^{rand}}. \tag{3.11}$$

Where d_c^{min} is a minimum distance that depends on the scenario, while Δd represents the distance increment of this autocorrelation function. It is important to highlight that the set of values of $\sigma_{S,p}^2$ and $d_{c,p}$ are assigned according to the different paths.

The correlation required to compute $g_{S,p}$ can be performed by either using a discrete linear filter, the covariance matrix, or an auto-regressive process. In this thesis, the channel model has been implemented through a discrete linear filter, whose impulse response is defined by expression **(2.9)**. Therefore, the convolution of the r_d filter by the samples generated according to a normal distribution, $\mathcal{N}(0,1)$, establishes the ensemble of possible values for $g_{S,p}$, which is randomly chosen from this set of values. The behavior of r_d is characterized in Subsection 3.5.1.

$$g_{S,p} \sim y[n] = \sum_{m=-\infty}^{\infty} N(m) r_d(n-m) \tag{3.12}$$

where *N* denotes the samples of the Gaussian distribution, r_d is interpreted as the filter and *y* entails all the possible values of this convolution.

3.4.3. PARAMETERS AND RADIATION PATTERN

The model parameters defined in [13] for the rural and highway environments placed in Lund are illustrated in **Table 3.3**.

Table 3.3 *Empirical parameters for the rural and highway scenarios in Lund.*

	Parameter	Unit	LOS	MD	SD	DI
Hi	G_0	dB	-5	$-89+24n$		104
	n		1.8	$\mathcal{U}[0,3.5]$		5.4
	μ_σ		6.8	9.4	6.3	–
	μ_c	m	7.2	5.4	4.9	–
	$d_c^{\min}$	m	4.4	1.1	1.0	–
	χ	m^{-1}	–	0.005	0.005	1
	y_1	m	–	–	-13.5	-13.5
	y_2	m	–	–	13.5	13.5
	W_{DI}	m	–	–	–	5
	W_{road}	m		18		
	N_{lanes}			4		
Ru	G_0	dB	-9	$-89+24n$		23
	n		1.6	$\mathcal{U}[0,3.5]$		3.0
	μ_σ		11.7	15.1	14.8	–
	μ_c	m	8.0	8.3	2.5	–
	$d_c^{\min}$	m	5.4	2.5	1.4	–
	χ	m^{-1}	–	0.001	0.05	1
	y_1	m	–	–	-9.5	-9.5
	y_2	m	–	–	9.5	9.5
	W_{DI}	m	–	–	–	5
	W_{road}	m		8		
	N_{lanes}			2		

From **Table 3.3** the uniform distribution between 0 and 3.5 for the MD and SD path-loss exponent can be observed, as their reference gain that is proportional to the path-loss exponent. An important detail is the length of the scenario or the x axis, which is obviously not defined. This parameter affects the computational cost, because the longer the x axis is, the longer the time dispersion of the channel impulse response will be. This leads to more rays to track due to more components in the scenarios, as a result of the product of the densities with a higher scenario area.

The definition of the x axis is based on a trade-off between the x parameter and the amplitude of the rays that decay exponentially with the distance. Therefore, the length of the scenario is defined based on the power contribution of the rays to generate the channel impulse response. It will be as long as the amplitude of the rays is not significant or the delay spread is equal to the time duration of the GI and not larger, since non ISI is supposed. This parameter is characterized in Subsection 3.5.2.

Finally, the radiation pattern of the used antennas is presented in **Figure 3.2**.

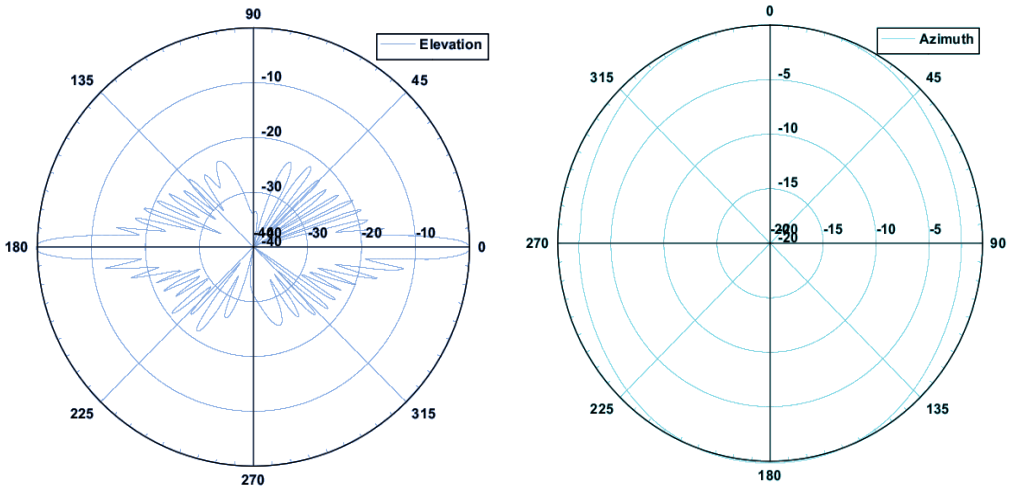

Figure 3.2 Elevation and azimuth radiation pattern of the Omni-Directional antennas at 5.8 GHz [24].

Only a few researches for antennas patterns and locations for the V2V communications are available in the literature; however, an interesting investigation has been performed in [25]. They have carried out some experiments with the location of the antennas for the in-vehicle as for the external (car's roof) communication. Their conclusions state that the radiation pattern is remarkably affected by the antennas placement, although it can be slightly corrected by means of antenna diversity. However, it is out of scope of this thesis and the only parameters of interest are the positioning of the antennas, which affects the ranging in the Radar application, and the type of radiation pattern for a 5.9 GHz frequency. As a consequence of the trilateration technique used in the Radar algorithm, an omni-directional antenna has been chosen. By contrast, the gains of the antennas have not been considered and no distortion of the radiation pattern has been simulated. It is important to stress that this antenna is not feasible aerodynamically, whereas a microstrip model fits better with this feature.

3.4.4. INTEGRATOR

At the end of the model an integrator is required to sum the contributions of all the rays according to their delays. This process is required in order to work with the channel impulse response in the discrete time domain. Thus, the channel in the continuous time is divided by time intervals called integrator time; then, the rays inside each interval are added to obtain the equivalent amplitude and phase of the respective sample for the channel in the discrete time domain.

This process is the most problematic for the radar algorithm because of the loss of information, as it is explained later. However, some of the reasons are the summation that can be constructive or destructive, which affects in the amplitude and phase, and the integrator time that offers a channel with more or less detail.

$$y[k] = \sum_{k=0}^{K-1} \int_{kT_{int}^{+}}^{(k+1)T_{int}} x(t)\delta(t)dt \tag{3.13}$$

where T_{int} is the integrator time, T_{int}^{+} is the right part of T_{int} in order to avoid values repetition. K represents the total number of samples of the channel in the discrete time domain as the quotient between the total time duration of the input signal $x(t)$ and the integrator time. While, δ is the Dirac delta and y is the result of the integrator.

The integrator is required to carry out the convolution with the transmitted signal in the discrete time domain. Thus, the integrator time must be equal to the sampling time; it implies that each coefficient of the discrete channel impulse response must have a duration equal to the sampling time.

3.5. CHARACTERIZATION OF THE GSCM MODEL

The parameters to characterize the GSCM channel can be sorted into two groups. Those required for the channel simulation - the autocorrelation function r_d and the length of the *x* axis of the scenarios -, and the variables that affect the channel response: the SNR, the rate variation of the channel according to its NWSSUS feature and the length of the OFDM frame that intervenes in the channel variability during the transmission time.

As the proposed GSCM model contains the model parameters for two different scenarios, highway and rural, the characterization proofs have been duplicated. As a consequence of the big number of cases to study, the most important curves are explained.

3.5.1. AUTOCORRELATION FUNCTION

The expression of r_d presented in equation **(3.9)** is composed by an exponential function that decay according to the coherence distance, such that the higher is d_c^2, the slower is the decreasing curve. Whilst, σ_S^2 indicates the variance of this process.

The purpose of r_d is to simulate the slow fading that the signal experiences, but before is necessary to characterize the different curves for the different paths and scenarios so as to use a suitable correlation distance. The only common criterion of r_d for the different paths of the same scenario is the number of discrete samples for the autocorrelation function (r_d length), thus the total distance and the distance increment are related.

In order to obtain a reliable curve due to the parameter variation of r_d, an average of 1000 curves have been performed.

3.5.1.1. LINE OF SIGHT (LOS) MOBILE DISCRETE (MD) SCATTERER

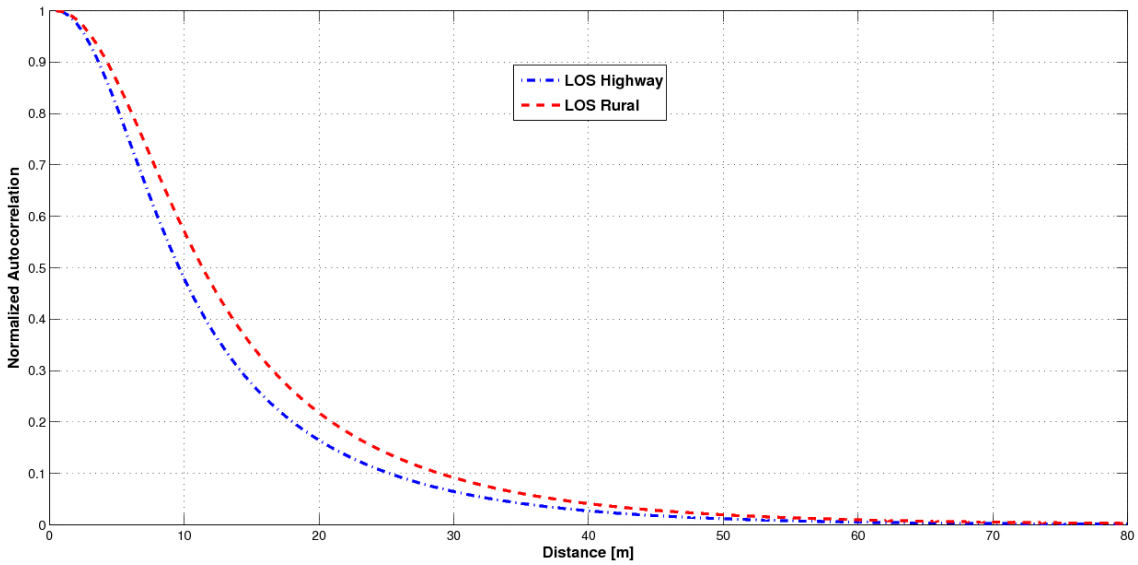

Figure 3.3 Normalized autocorrelation function r_d for the MD LOS.

The autocorrelation function for the LOS in the highway as in the rural scenarios shows a similar behavior. It is because the coherence distances in both environments according to their parameters presented in the **Table 3.3** are very similar. The d_c^{rand} factor tends to converge to the mean value of its distribution due to the average. Thus, the mean coherence distance results in a sum of the converged d_c^{rand} and d_c^{min}. If these parameters are added in both scenarios the result is very similar. It is important to stress that the LOS scatterers present the longest coherence distance in all the discrete scatterer types.

The total distance of the decaying functions can roughly reach until 60 meters, but the mean distances are more or less close to 11 meters for the highway and around 13 meters for the rural. The increment distance (Δd) used for the representation has been of 0.5 in both environments.

3.5.1.2. NOT-LOS (NLOS)MOBILE DISCRETE (MD) SCATTERER

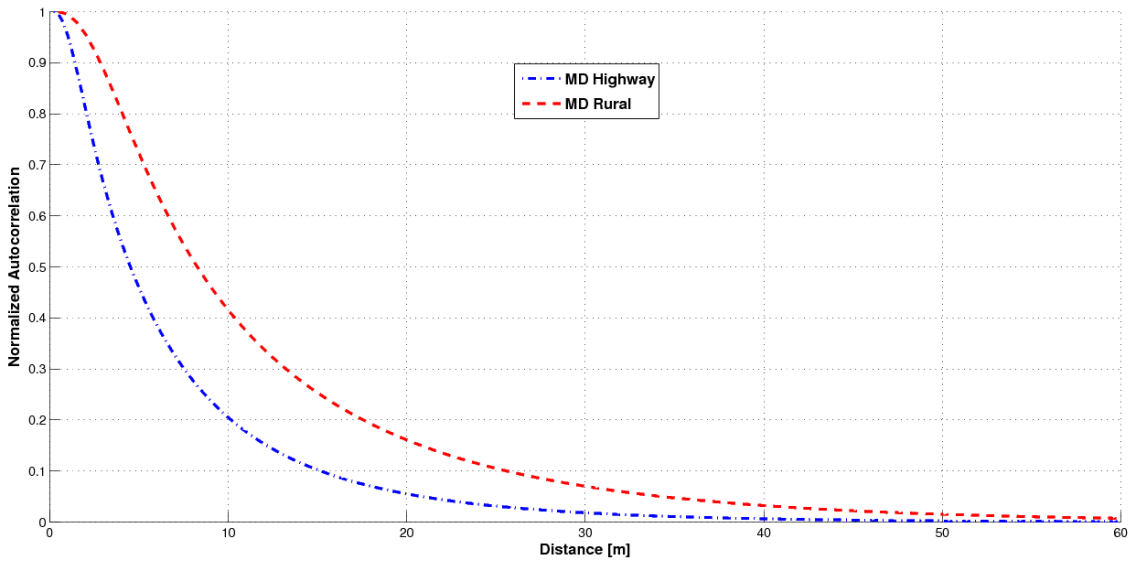

Figure 3.4 Normalized autocorrelation function r_d for the MD NLOS.

The MD is the kind of discrete scatterer with the highest difference in the coherence distance regarding the rural and highway scenarios. Therefore, their curves are very dissimilar concerning the decaying brusqueness.

In **Figure 3.4**, the MD Rural curve is wider than the highway case and its coherence distance is around 11 meters. Its total distance is close to 60 meters and the increment distance is half a meter as in the LOS case (0.25). On the other hand, the MD curve for the highway reaches until 50 meters with an Δd equals to 0.25 meters and a coherence distance close to 6 meters.

3.5.1.3. STATIC DISCRETE (SD) SCATTERER

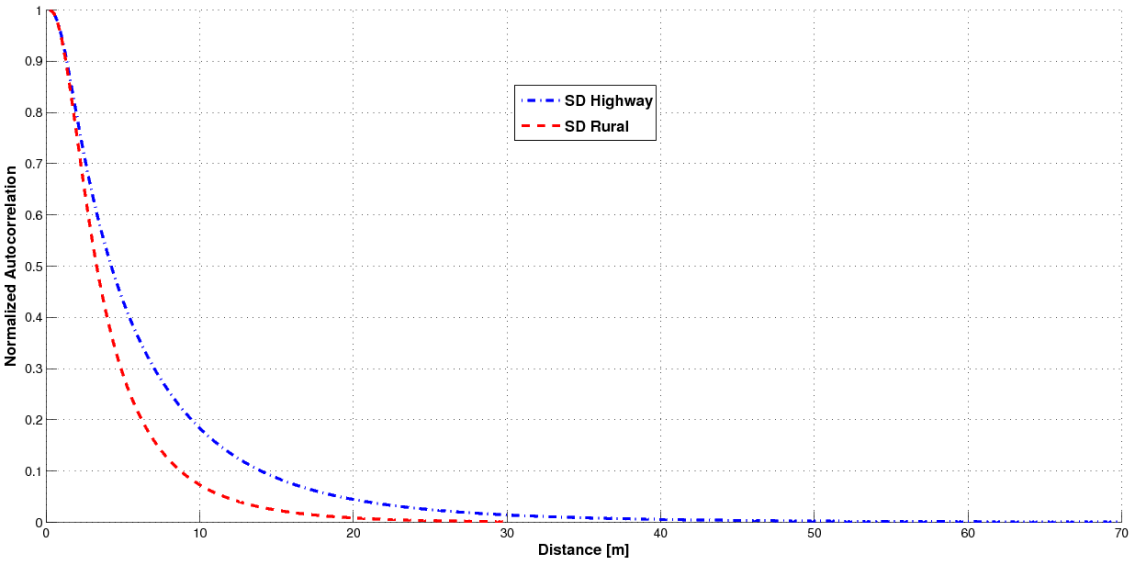

Figure 3.5 Normalized autocorrelation function r_d for the SD.

Figure 3.5 presents the SD Rural curve with the smallest coherence distance (around 5 m) of all the different scatterer types and scenarios. Therefore, the decaying trend of this function is the most abrupt of all. Besides, it decays completely close to 25 meters for a distance increment equal to 0.25 meter.

The highway SD also uses the same Δd as the rural and it roughly reaches a distance up to 50 meters.

A conclusion from all these autocorrelation functions is that the highway scenario has the curves with a more rapid decaying trend for the MD NLOS and LOS. It implies that the slow fading for this scenario has a stronger influence than the rural environment. An explanation can be attributed to the predominant high speeds of the highways in reference to the rural roads. However, in the SD scatteres, which are characterized with the lowest coherence distance, the rural curve decays faster than in the highway situation. The reason can be related with the scenario dimensions, which are wider in the highway concerning the rural roads; thus, the SD contributions can influence lower in the channel impulse response since their placement are in the sides of the scenario.

3.5.2. SCENARIO

For the characterization of the rural and highways scenario, the only parameter to determine is the length of the x axis, since the rest of parameters are detailed in **Table 3.3**. It affects the time dispersion of the channel, since some scatterers can be placed too far from the transmitter and receiver; it can entail a ray with a long propagation time that can provoke ISI. Therefore, the criterion to determine the maximum value of the x axis is based on the duration of the cyclic prefix in order to avoid the ISI that is disregarded.

The worst case condition of the time dispersion occurs when the duration of the channel impulse response is as long as the GI. It implies that the maximum distance that the wave can travel is determined by

$$d_{MAX} = c_0 T_{GI}/2 = 240\ m. \tag{3.14}$$

where c_0 is the speed of the light. The distance is divided by two for the worst case condition in which the Tx and the Rx are placed in the same point. Thus, the wave has to travel the going and coming paths with time duration equals to the cyclic prefix.

Figure 3.6 is a possible rural scenario. The cars are represented with triangles that point at the direction of the vehicles; the squares indicate the road signals and the circles are the diffuse scatterers. This scenario is composed by two lanes delimited by the solid dark line placed in the middle of the road. It is important to stress that blue triangle is for the Tx-Car, while the red one is for the Rx-Car.

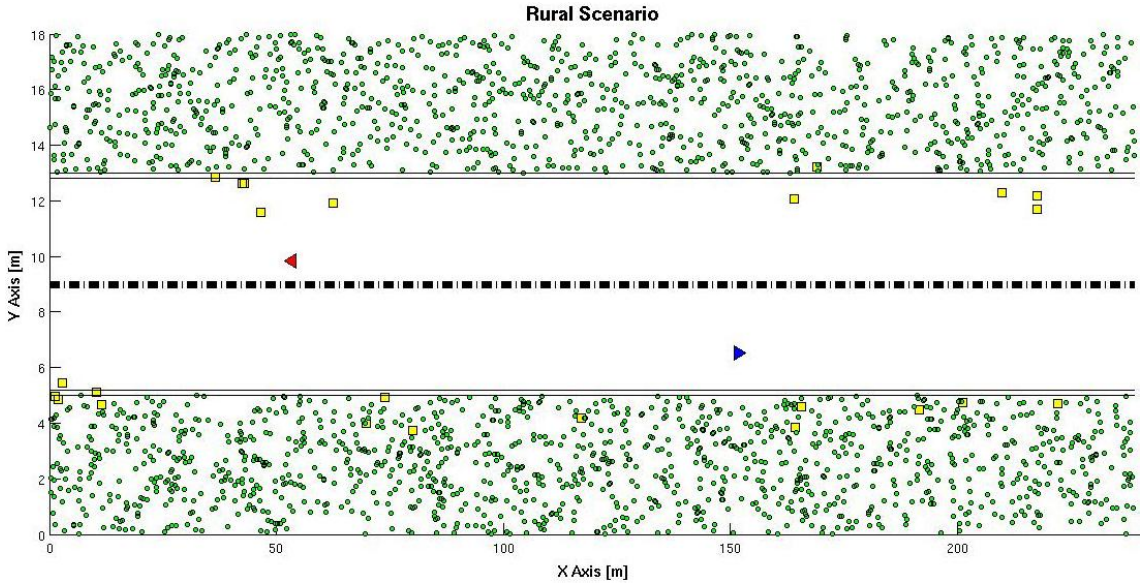

Figure 3.6 *A possible rural scenario.*

The system of symbols for the highway scenarios is the same; nonetheless, in **Figure 3.7** cyan triangles appear. They represent third cars that do not intervene in the radio communication, only as MPC. In the rural scenario they are also included, but the low density for the MD scatterers is the responsible of its absence. Other feature of the highway scenario is the number of lanes: in this case it consists of 4 lanes, 2 for each direction.

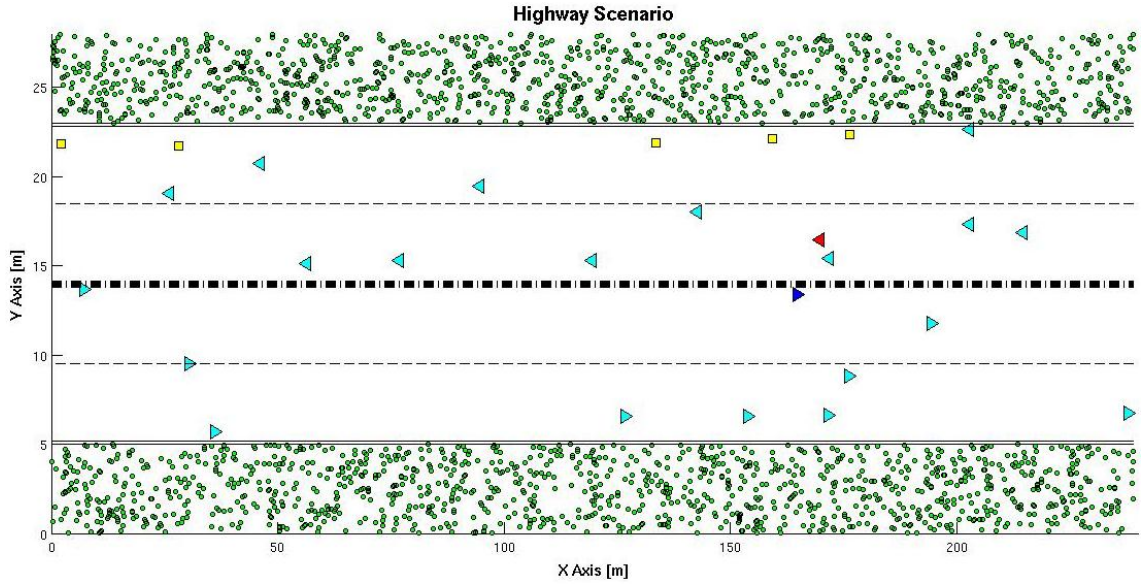

Figure 3.7 *A possible highway scenario.*

3.5.3. Channel Impulse Response

Once all the parameters required for the channel simulation have been detailed, the channel impulse response can be assessed according to its features, as for instance the NWSSUS.

In **Figure 3.8** the channel impulse response from the highway scenario depicted in **Figure 3.7** is presented. It has been highlighted for its peculiarities owing to the placement of the Tx and Rx-Car,

which are relatively close as well as a third vehicle. Besides, it is important to stress that this impulse response corresponds to the transmitter antenna 1 with the receiver antenna 1.

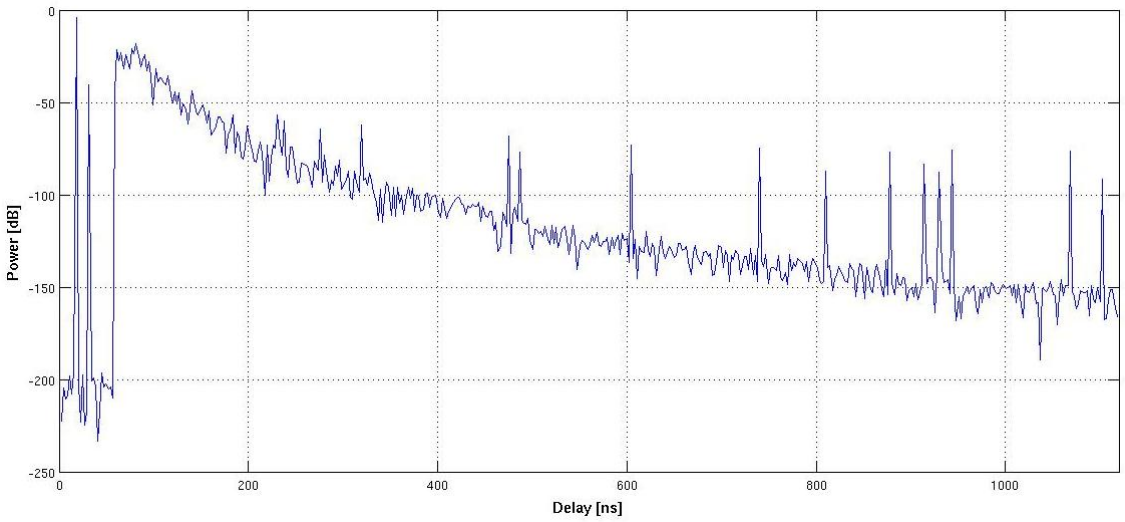

Figure 3.8 *Channel Impulse Response module for the highway scenario represented in* ***Figure 3.7.***

The behavior of the channel impulse response is characterized by an exponential decaying function, despite of the existence of two rays at the beginning. The first one of them comes from the LOS with the highest power and the minimum delay, whilst the second ray belongs to the third car as mentioned before. On the other hand, the rays that differ from the instantaneous mean power stem from the rest of the cars or road signals, whose reflection power is higher than the diffuse scatterer. Indeed, they are closer.

This disintegration of these two rays arises from the time delay and the integration time used in the integrator block (see Subsection 3.4.4). The propagation time is related with the placement of the cars, while the integration time sorts the rays by temporal cells for summing them later. Hence, the integrator acts more or less as smoother according to the duration of the cells. The time used for **Figure 3.8** representation has been in the range of nanoseconds.

The channel impulse response power takes values from around 0 dB, for the LOS, until -150 dB more or less. The samples with a power close to -200 dB are neglected, since they are only noise. Concerning the time dispersion, this scenario presents a maximum delay around 1.4 μs, which is under the GI duration.

The NWSSUS behavior is demonstrated in **Figure 3.10**, where the time delay for the LOS ray firstly decreases due to approaching cars, but subsequently it increases again since the cars are moving away in the opposite directions. Concerning the power, it presents a valley due to the radiation pattern of the omni-directional antennas for the channel in 0.2 seconds. The elevation pattern is the main responsible of this attenuation, since the elevation angle increases when the distance between transmitter and receiver is shorter. Besides, the azimuth pattern presents the highest losses when the antennas are parallel focused (see **Figure 3.9**). The NWSSUS can also be highlighted by the fusion of the LOS ray with the ray from the third car since the 0.2 seconds. It is important to emphasize that the delay spread of **Figure 3.10** has been truncated to 600 ns in order to interpret easily the results.

Figure 3.9 represents the respective tracking of the scenario for the channel impulse responses presented below. It has been sampled for three different moments, thus the displacement of each mobile discrete scatterers is represented with three triangles. In the case of the receiver and transmitter the colors are also decreasing.

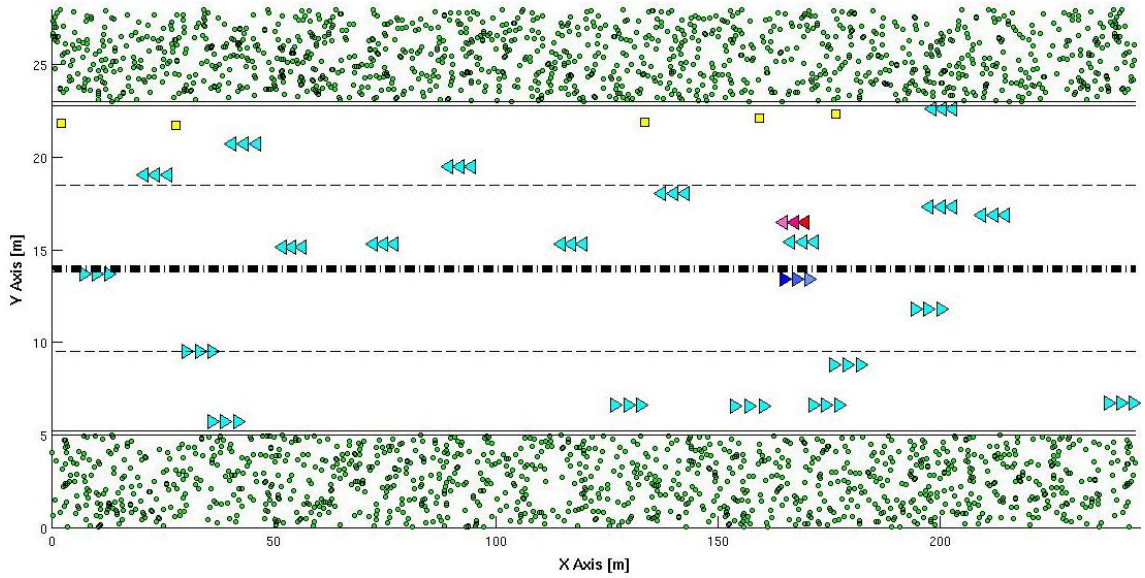

Figure 3.9 *Tracking of the given scenario for time increments of 0.2 seconds.*

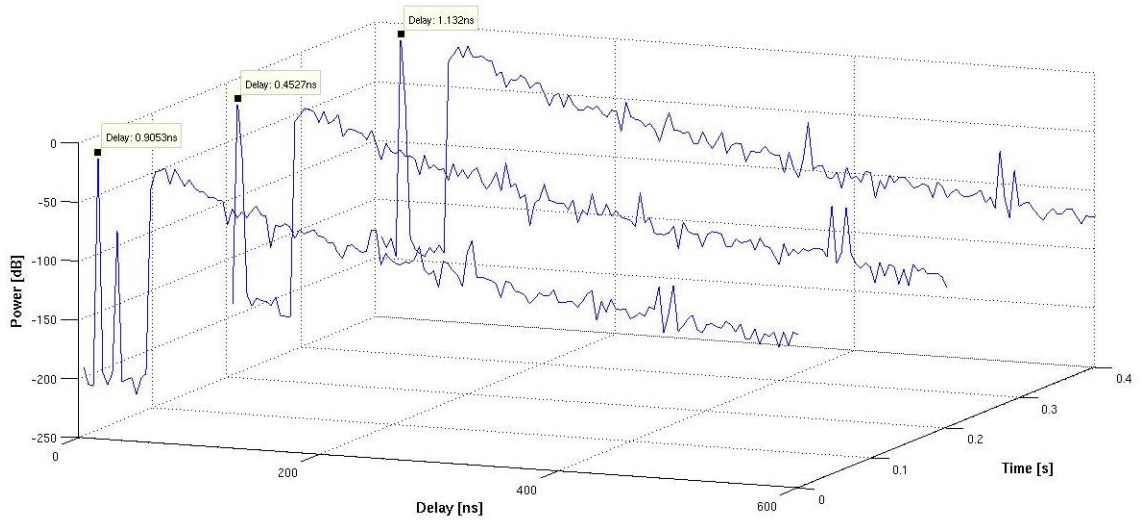

Figure 3.10 *Channel impulse responses for different time instants to show the NWSSUS behavior.*

The previous cannel impulse response depicted are performed for an integrator time in the range of nanoseconds; nevertheless, the required integrator time, according to the implemented system, has to be equal to the sampling time to carry out the convolution in the discrete time domain. Consequently, the V2V channels used for the communication application have an aspect as **Figure 3.11** shows.

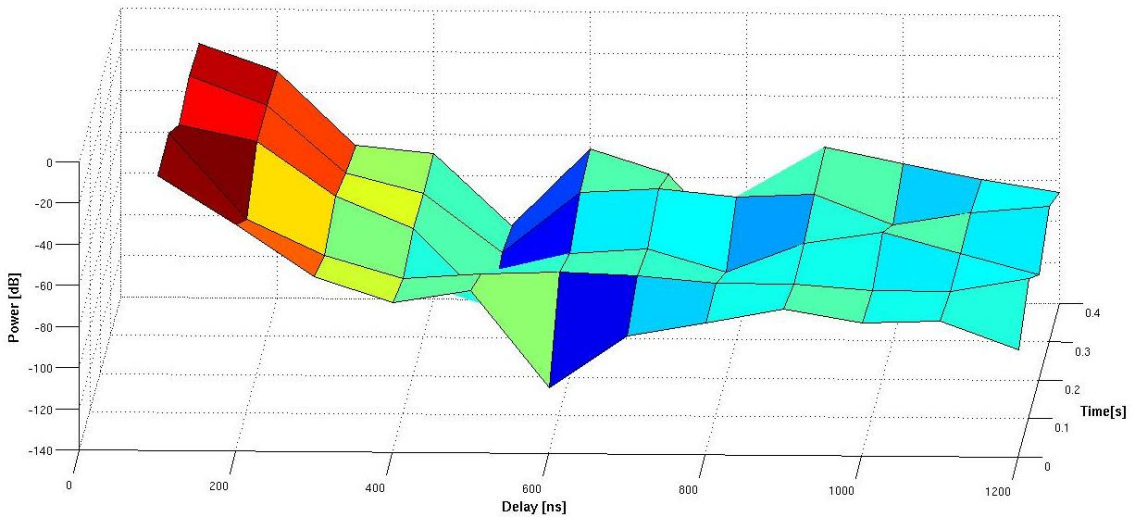

Figure 3.11 *Module of a channel impulse response for an integrator time equal to 0.1 µs*

The losses due to the radiation pattern are clearly represented by a power valley for the LOS (the first column of the curve) in **Figure 3.11**, where the power decays up to 0.2 seconds and it increases later. However, the power trend is to decrease as the transmitter and receiver cars increments their distance, since they are in opposite directions. This behavior can be extracted from the power difference of the LOS for the first and last channel.

The Power Delay Profile according to the time evolution is illustrated in **Figure 3.12**, which is characterized with a time delay decrease for the LOS on account of the approaching transmitter and receiver, and a later increment owing to the opposite direction of the Tx and Rx. There are traces that remain constants, while others are represented by positive and negatives slopes. The lines that maintain their delays are composed by whatever component that preserve the distance between the transmitter and receiver. As the speeds have been considered constant during the entire time frame, some cars can also be included in this set. By contrast, the negative slopes represent a distance increment, whereas the positive traces are assigned to a distance decrease. As a curiosity is the trajectory of the LOS, which is firstly separated from the bundle of rays; however, it converges later due to the distance increment.

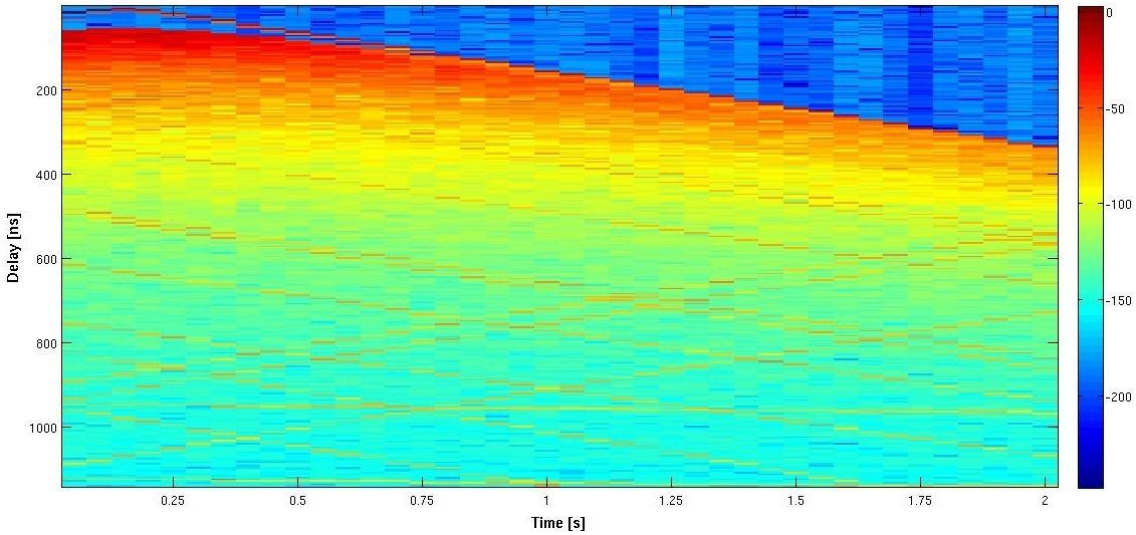

Figure 3.12 *Power Delay Profile regarding the time evolution*

3.5.4. DOPPLER FREQUENCY

The respective Doppler shift for the given scenario, where the transmitter and receiver cars are in opposite direction (ODir.), is depicted in **Figure 3.13**. By contrast, **Figure 3.14** represents the same example, but in this case the receiver direction has been changed, thus transmitter and receiver are in the same direction (SDir.).

The conclusions that can be drawn from these pictures are the frequency range, which is around $\pm 1100\ Hz$ for the ODir. and $\pm 2000\ Hz$ for the SDir., and the Doppler shift conduct for the mobile, static and diffuse scatterers that are strictly related with the relative velocity of each path.

In both cases, the paths are composed by two trajectories except the LOS, owing to the single bounce assumption. Therefore, there are four possible combinations for these trajectories concerning the MPCs: Tx and Rx approaching, moving away from each other, Tx approaching and Rx moving away and vice-versa. On account of the placement of the transmitter and receiver cars for the given scenario, which are quite close, the kind of predominant trajectory for the ODir. and SDir. cases are affected. Thus, the most common situation in the ODir. is where the transmitter or receiver are approaching or going away, whereas the SDir. is mainly composed by trajectories in which transmitter and receiver are approaching or moving away. Accordingly, the relative velocity for the Doppler Shift in the ODir. case is generally obtained as a difference of the trajectory speeds, while in the SDdir. situation the V_{rel} results in addition.

The details for **Figure 3.13** are the small Doppler Shift of the static and diffuse scatterers, since they are static and their relative velocities yield in the speeds difference of the transmitter and receiver. On the other hand, the first ray from the LOS experiences a Doppler shift around -600 Hz. Despite of the resultant speed is the sum of both velocities that is around 50m/s, the radial relative velocity is lower owing to the transmitter and receiver cars placement, whose Angle of Departure (AOD) is close to $\pi/2$. The rest of mobile scatterers are in the extremes of the Doppler frequency range, since one trajectory has a high speed while the other is low. Thus, the subtraction remains being a considerable velocity value, which produces an elevated Doppler frequency.

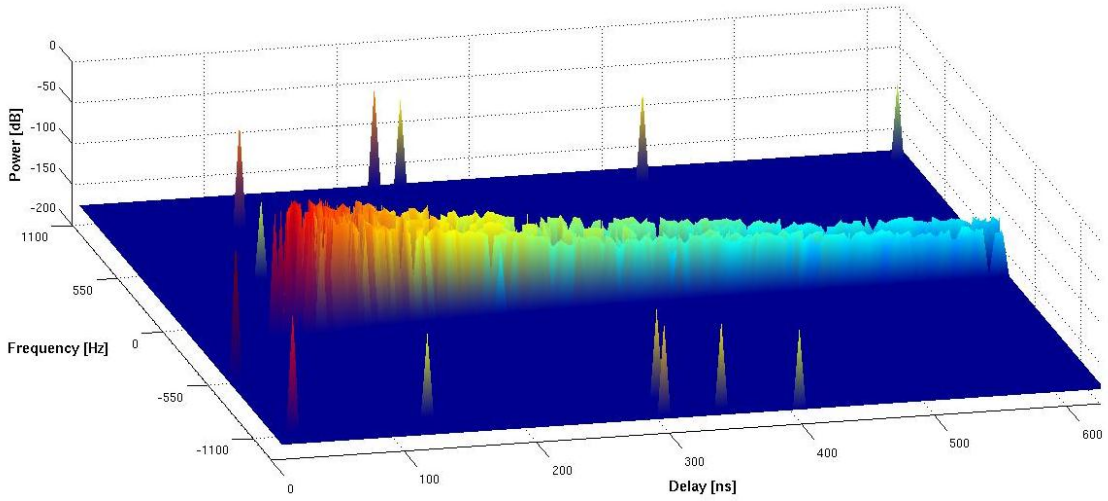

Figure 3.13 *Doppler Shift with Opposite Directions.*

By contrast, the Doppler frequency for the LOS in **Figure 3.14** is lower as a consequence of the same direction. While the static and diffuse scatterers experience a higher Doppler frequency concerning the

ODir. case, since the relative speeds entails the addition of the transmitter and receiver speeds. In reference to the Doppler frequency for the rest of mobile scatterers, they are duplicated regarding **Figure 3.13** or close to 0 Hz. The cars that are in the opposite direction experience the higher Doppler shift, since both trajectories of the path implies the addition of the speeds from scatterer car and the transmitter or receiver concerning the trajectory. By contrast, the cars in the same direction have a low Doppler frequency, because of the speed subtraction in both trajectories.

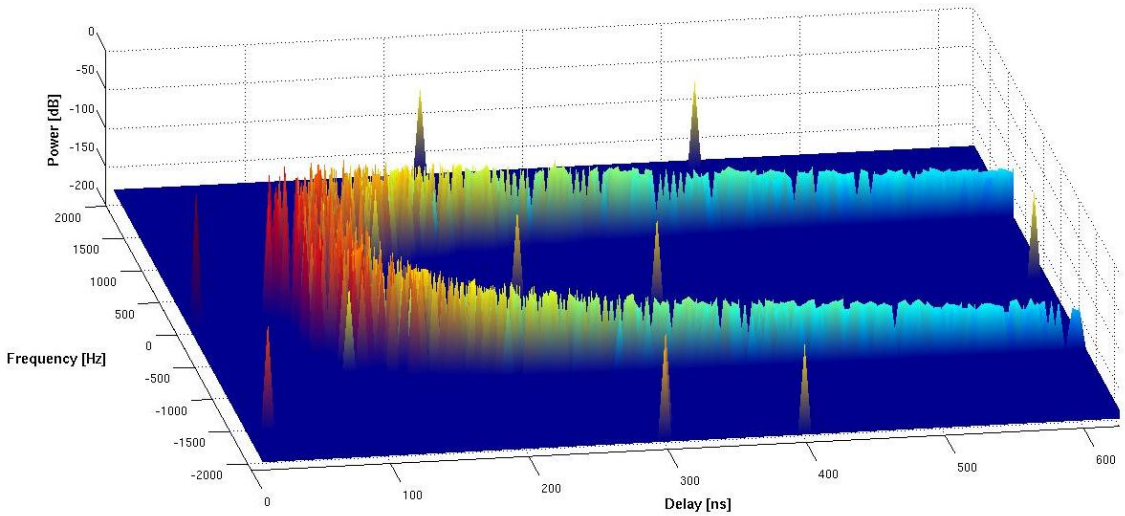

Figure 3.14 *Doppler Shift with the Same Direction.*

3.5.5. BIT ERROR RATE (BER)

In order to characterize the NWSSUS feature of the V2V channel, different simulations concerning the rate variation of the channel and the OFDM frame length have been developed for the implemented system. The SNR vector used for all the simulations consists of fives values from 0 to 20dB with steps of 5dB, and the BER has been averaged for each set of 1000 observations so as to reduce the variance of the results. Hence, each curve implies a generation of 5000 independent V2V channels. It is important to note that QPSK is the modulation used for all the results presented below.

The V2V channel is supposed to be a continuous function that changes with time. However, the method proposed to simulate the NWSSUS, which has been commented previously (see expression **3.5**), requires different channels for different time instants. These channels are generated from the current state of the scenario for the specific observation time. Therefore, the rate variation is understood as the number of observations of the V2V channel per second, which are shifted in time. Accordingly, the inverse of the rate variation is the time distance between observations.

On the other hand, the performance of the implemented V2V channel has been carried out through the comparison of its BER in the implemented system against the results obtained from a Gaussian and Rayleigh channel, instead. In addition, the improvements provided by convolutional encoding have been verified. These simulations are presented in the Appendix B for the thesis extension issue.

In reference to the simulations, the used parameters are summarized in **Table 3.4**. It is significant to highlight that each of the next curves have been averaged by the 16 BERs obtained from the different channels, since the implemented system follows a 4x4 MIMO structure.

Table 3.4 *Parameters for the performed simulations*

Simulation Parameters	
Number of simulations	1000
SNR (dB)	[0, 5, 10, 15, 20]
ODFM Frame Length (OFDM Symbols)	[500, 1000]
Variation Rate (channels/second)	[125, 128, 133, 142, 166, 200]

The variation rates have been determined empirically in order to characterize the behavior of the NWSSUS feature of the V2V channel. Thus, the most significant rates have been chosen.

In **Figure 3.15**, the BER for an OFDM frame length equals to 500 OFDM symbols is depicted. Whilst, **Figure 3.16** represents the same curves but for 1000 OFDM symbols. These curves are obtained using the implemented convolutional encoder and decoder.

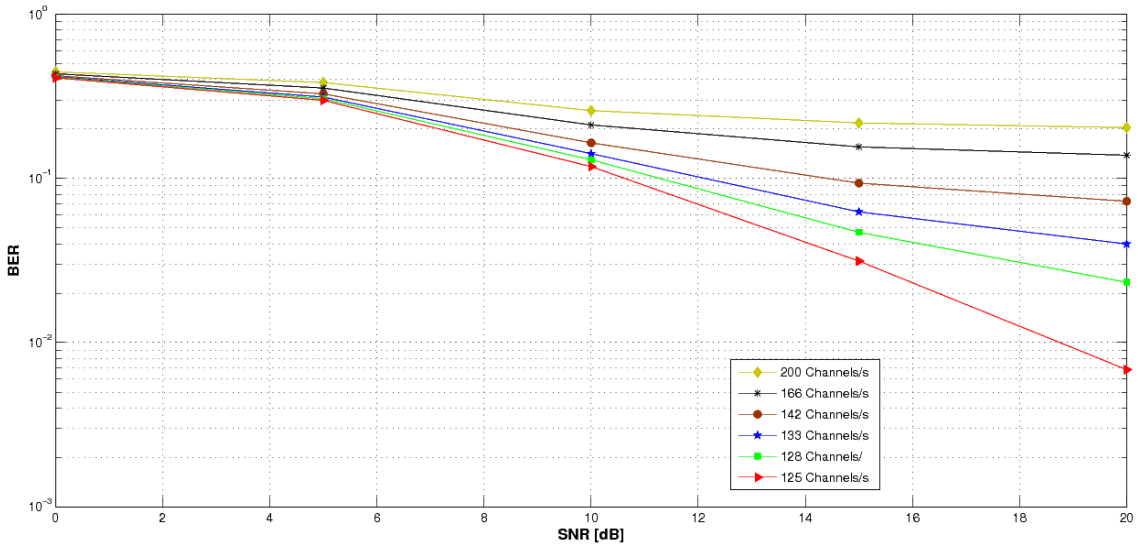

Figure 3.15 *BER for an OFDM frame of 500 OFDM symbols using coding.*

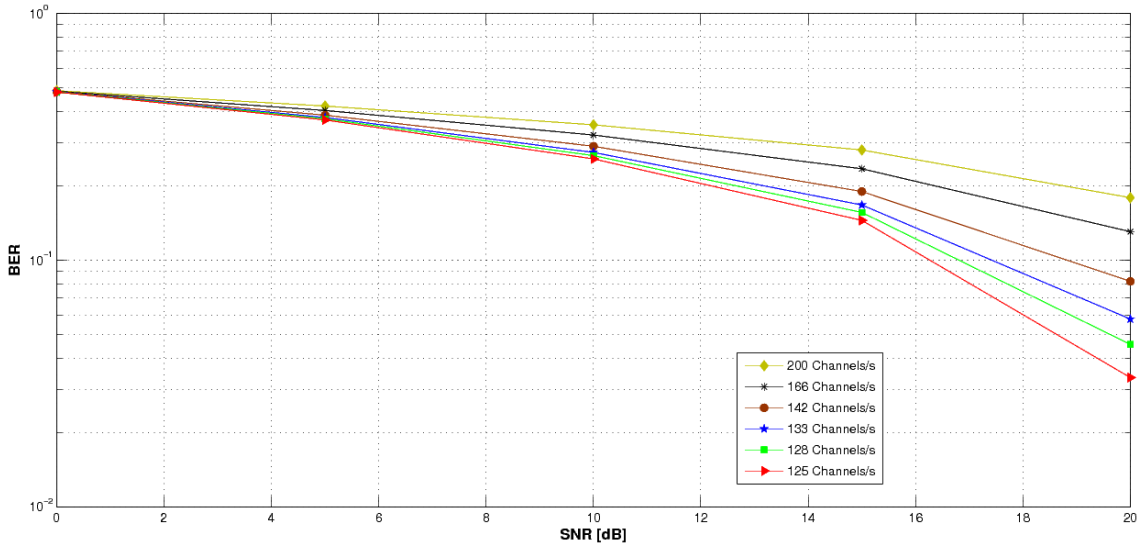

Figure 3.16 *BER for an OFDM frame of 1000 OFDM symbols using coding.*

The most important conclusion that can be drawn from these pictures is that the implemented MLE approach for the estimation of a NWSSUS channel is not suitable. As a reminder, the proposed estimation method for the implemented system is based on the long training sequence that each OFDM contains (see **Figure 2.7**). Thus, even though the estimation is well performed, it is only valid for the beginning of the frame up to a significant change in the channel occurs and the rest of the frame is convolved by other different channel regarding the initial estimated channel. Therefore, the ideal equalization of the received symbols is to estimate all the channels that intervene in the whole OFDM frame and equalize the different coefficients with their respective channels.

In the research presented in [26], they mainly study estimation techniques for NWSSUS channels based on the pilots subcarriers, long training sequence and combination of both. They call the implemented estimation technique as “Block-comb-type channel estimators” and conclude that this method is appropriate for low SNRs. However, it is out of the scope of this thesis and the only importance of this channel is concerning the Radar algorithm, which has to detect and locate the targets from the estimated channel. Thus, the detection and placement of the targets will be only valid for the beginning of the OFDM frame. It suggests the use of short frames for an accurate tracking of the targets.

In reference to the rates, the BER presents worse results for higher rates as a consequence of the NWSSUS feature; although the channel estimation method is also connected with the obtained BER. Indeed, in **Figure 3.15** the BER seems to converge for the highest rate and for a SNR of 15 dB and 20 dB. It enhances the problematic of the channel estimation technique.

Finally, the length of the OFDM frames also affects the BER; the longer is it, the worse BER is obtained. It makes sense, since the coefficients of the frame are convolved with a greater number of channels. Thus, shorter frames will help to diminish the error rate and at the same time the tracking algorithm refresh rate.

4. RADAR SYSTEM IN A V2V ENVIRONMENT

As the purpose of this chapter is the Radar parametrization based on the implemented system according to the 802.11p standard and the description of Radar algorithm, the fundamental theory of the Radar systems is explained. Furthermore, the scenario designed so as to fulfill the requirements of the Radar algorithm is also defined. Finally, the tracking algorithm and methodology used in the results representation are described.

4.1. RADAR PARAMETRIZATION

4.1.1. RADAR THEORY

The operation principle of a RADAR (Radio Detection And Ranging) systems consist in the transmission of an electromagnetic wave for its posterior detection at the receiver [27]. Its main goal is to detect the scatterers responsible of the wave reflection. In terms of the positioning of the transmitter and receiver, Radars systems can be classified in two classes as monostatic transmitter and receiver sharing the same position, or multistatic (e.g. bistatic), transmitters are placed in different locations from the receivers. By contrast, the same systems detections can be extrapolated for the cases in which transmitters and/or receivers are in motion. **Figure 3.1** illustrates a monostatic and a bistatic example, where the plane is the target to detect.

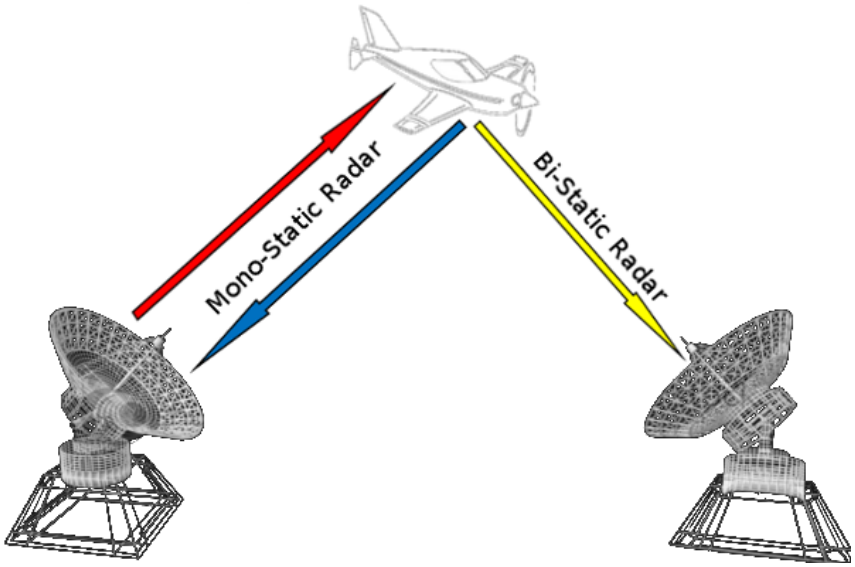

Figure 4.1 *Monostatic and bistatic Radar system.*

The possible parameters that can be detected by classical Radars are: the range, height, direction and the speed. The first one of them is determined by means of the correlation function between the transmitted and received electromagnetic energy pulse over time; thus, the location of the maximum value for the correlation response determines the propagation delay between both signals.

$$R_{xy}(\tau) = \int_{-\infty}^{\infty} x(\tau) y(t-\tau) d\tau \tag{4.1}$$

where $R_{xy}(\tau)$ represents the correlation value for the τ delay, while x and y are the transmitted and received signals, respectively. Accordingly, the range arises from the expression **(4.2)**.

$$range = \frac{\tau c_0}{2} \tag{4.2}$$

Where c_0 is the light speed in the vacuum for the electromagnetic wave propagation. The range is divided by 2, since in a monostatic situation the wave has to travel twice so as to collide with the target and reach the receiver.

The height is determined through the appraisal of the link budget, which is defined by the respective Radar equation (see **4.3**). Hence, the attenuation extracted from the radiation pattern indicates the elevation and azimuth angle. The accuracy and veracity of this procedure depends on how detailed is the Radar equation.

$$P_R = \frac{P_T G_T G_R \sigma_{target} \lambda^2}{(4\pi)^3 R^4 L_{ges}} \tag{4.3}$$

where P_T and P_R are the transmitted and receiver power in watts, λ represents the wavelengths, R is the range, σ_{target} is the coefficient that indicates the percentage of power reflected by the target. L_{ges} is the loss factor that includes atmospheric losses, fluctuation losses during the reflection and the respective losses according to the transmitting and receiving path. Finally, G_{Tx} and G_{Rx} are the gains of the transmitter and receiver antenna, which are related with its respective radiation pattern.

The direction and the speed are determined by the Doppler effect, whose magnitude entails the speed and its phase corresponds to the direction (approaching or moving away).

There are different parameters to characterize a Radar system as the Radar range resolution and range ambiguity. The first concept determines the minimum separation distance between two targets such that the Radar is capable of detecting them. The expression is defined by

$$\Delta r = \frac{c_0}{2B} = \frac{c_0 \, T_{pulse}}{2}. \tag{4.4}$$

The bandwidth of the pulse is determined by B and its inverse represents the time duration of this pulse denoted by T_{pulse}. The Δr is the range resolution of the Radar in meters. Thus, if the bandwidth of the transmitted signal used for detecting the target is high, the accuracy of the Radar is improved. In **Figure 4.2** an example to highlight the importance of the range resolution is presented. In the first case, the cars maintain a distance higher than the range resolution and the Radar is able to detect both targets. Nevertheless, the other pair of vehicles is close enough such that the time difference between them is shorter than the half of the pulse duration. It implies that the reflected waveform is interpreted as a single pulse for the second pair of vehicles.

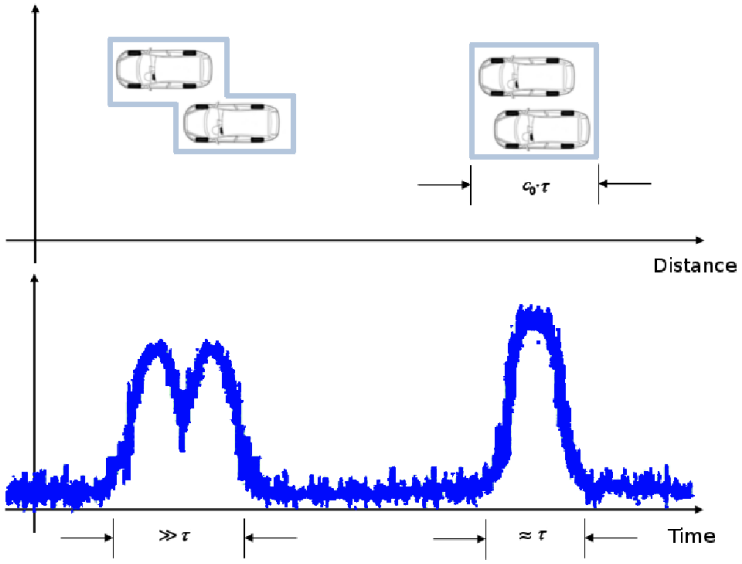

Figure 4.2 *Picture of the range resolution. T_{pulse} is represented by τ.*

The range ambiguity specifies the maximum distance that a target can be placed from the Radar system to be detected without ambiguity error (see **4.5**). This kind of error occurs when the response of different subsequent pulses are misunderstood by the Radar. For instance, if the pulse rate generation (PRF) is equal to 1 second and the time distance of the target is about 1.2 seconds, there will be an error due to the ambiguity. The explanation is that the Radar system will decide that a first pulse transmitted in the initial time equal to 0 seconds has been lost, since this pulse requires 1.2 seconds to reach the target and go back. However, the waiting time for this Radar is only one second due to the PRF; it implies that no response from the first pulse has been detected. Therefore, a second pulse is transmitted in the time equal to 1 second, but in 1.2 seconds the response of the first pulse arrives to the Radar, which does not know that this response is from the first pulse. Consequently, it deems that a target is placed at a time distance of 0.2 seconds instead of 1.2 seconds.

$$d_{Amb.} = \frac{c_0}{2\Delta f} \tag{4.5}$$

4.1.2. V2V Radar Parametrization

The analytical characterization of the V2V Radar system implemented based on the 802.11p standard is detailed below.

In order not to destroy the orthogonality of the OFDM system due to the Doppler frequency, the subcarrier bandwidth has to be 10 times higher than the maximum Doppler frequency.

$$\Delta f \gg 10 f_{D_{MAx}} \tag{4.6}$$

where Δf is the subcarrier bandwidth equal to 156.25 kHz according to **Table 2.1** and the maximum Doppler frequency $f_{D_{MAx}}$ reaches 2.18 KHz for a carrier frequency equal to 5.9 GHz and a maximum speed of 200 km/h, which results from the transmitter and receiver in opposite directions with a velocity of 100 km/h for each one of them. Accordingly, the expression **(4.5)** is fulfilled and the orthogonality can be asserted.

In reference to the range ambiguity, it results in 960 meters, which is higher than the maximum distance regarding the GI duration that has been calculated in **(3.14)** (240 meters). Therefore, the allowed multipath effect to carry out a V2V communication is the main restriction for the maximum distance of the targets that could be detected.

Finally, the range resolution is determined, whose value is equal to 15 meters for a bandwidth of 10MHz. It is not a feasible result in a V2V environment, since cars can have minimum distances of units of meters instead of tens. Consequently, this bandwidth must be increased, thus the proposed Radar algorithm must have a different sampling time that the used in the V2V communication system.

Table 4.1. *Radar Parameters according to the implemented system.*

Radar Parameters	
f_c	5.9 GHz
$f_{D.Max}$	2.18 KHz ($V_{Max} = 200\ km/h$)
Δf	156.25 KHz
Bandwidth	10 MHz
Range Resolution	15 meters

4.2. SCENARIO

The simulated system contains two different environments: the highway and rural. However, the designed scenario for implementing the Radar algorithm has not been introduced yet. It consists of a MIMO system 4x4, hence each vehicle has mounted 4 antennas. The placement of the antennas has been performed on the four corners of the roof instead of inside the car; although any special consideration concerning the electromagnetic propagation effects for being located inside or outside the car has been taken into account. The only important parameter is the distance among antennas, which affects the delays of the reflected rays. Consequently, the longer is the distance between antennas, the higher is their delay difference. This property is essential for the placement method, thus the antenna with the lowest delay will be closer to the scatterer and a preference concerning the antennas and their distance from the targets can be established. Nonetheless, the case of two or more received rays with the same delay provokes some uncertainty; this is thoroughly explained in the Radar algorithm.

The proposed vehicle model to determine the real distances among antennas has been the Volvo V50 as can be observed in **Figure 4.3**; its generous dimensions are the reason for this choice. The main idea is to use a touring or sportwagon model instead of a van or a lorry, otherwise it would be unfair for their favorable sizes, as for the height and antennas distance. It is important to highlight that the great majority of V2V channels measurements have been performed with vans or lorries.

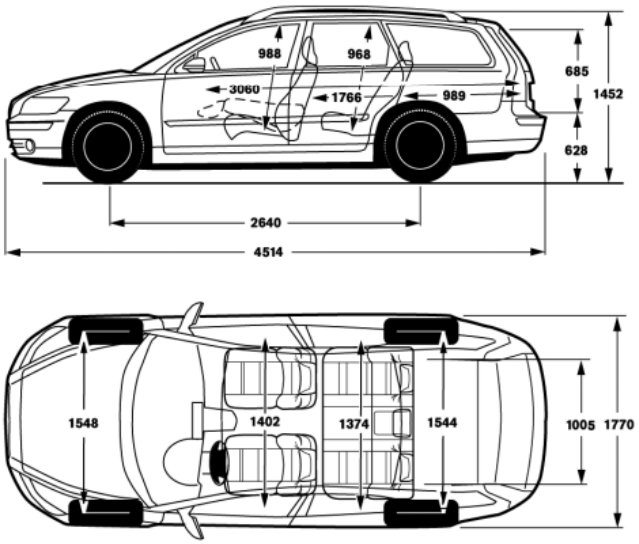

Figure 4.3 *Measurements of a Volvo V50 [28].*

From **Figure 4.3**, the transversal distance of the antennas is around 1.4 meters for the front part of the roof and 1.374 meters for the rear part. While the longitudinal distance is not defined; however, it is supposed to be roughly 2 meters. The height of the car is 1.5 meters, which coincides with the mean of the normal distribution used to determine the heights of the mobile scatterers. The four antennas have been orientated to point at 45, 135, 225 and 315 degrees, respectively. The 0 degrees is assigned for the direction of the vehicle. **Figure 4.4** represents the positioning of the antennas array and their coverage area depicted with circles on account of their radiation pattern.

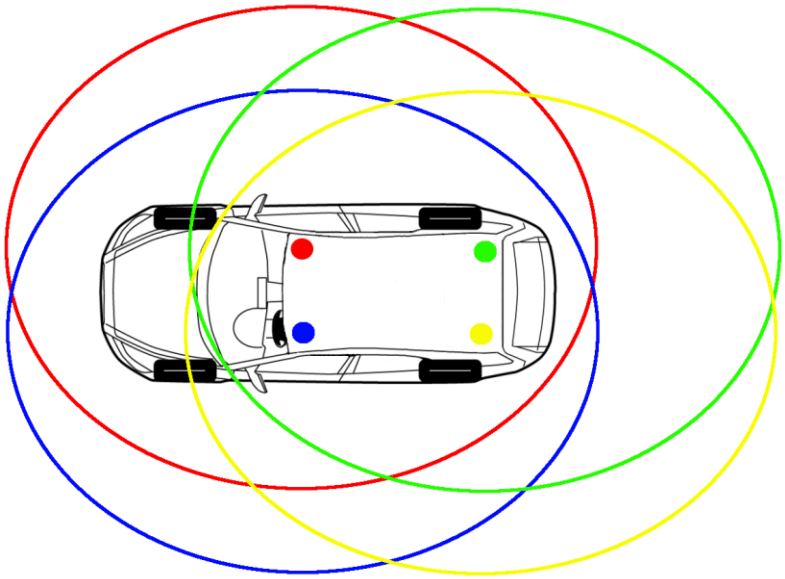

Figure 4.4 *Positioning of the antennas array and their coverage area.*

4.3. RADIO DETECTION AND RANGING ALGORITHM

4.3.1. BACKGROUND

Innovative techniques have been developed along the time with the purpose of joining radar and communication applications in a unique platform. It mainly supposes a radio spectral efficiency and cost reduction concerning the hardware reuse.

One of the oldest methods is presented in [6]. It is based on spread spectrum techniques for the ranging method over a wireless optical link. The operation principle basically consists in the delay computation that the transmitted signal experiences in order to reach the target and come back. The criterion used for matching the transmitted with the received information lies in the correlation function, thus the maximum correspondence determines the delay. It implies to use a pseudo noise signal as the transmission information so as to improve the correlation performance. Despite of the good results presented of this method, the investigation is only focused on the ranging and not in the azimuth placement of the scatterers; besides, they use optical links, which does not fits with the proposed V2V standard.

A practical method to implement Radar system through a communication application is detailed in [7]. The aim of that investigation is to directly apply the classical Radar operation principle over a multi-carrier communication system (Ultra Wideband waveforms in conjunction with OFDM). Therefore, the correlation for the ranging is used as defined in the expression **(4.1)**. The main drawback lies in the auto-correlation properties of the used waveform. In the case of the OFDM signal, this problem entails the appearance of high side lobes in the processed radar image, which affect the correct ranging in multiple scattering scenarios. This inconvenient can be solved using special fixed codes, but it violates the arbitrary nature of the desired transmitted information.

A smart method to overcome the previous problem statement is presented in [5] and thoroughly developed in [9]. It is basically focused on the element wise division of the symbols from $r[k]$ and s_k (see **2.3**), whose result after the conversion to the time domain indicates the ranging of the scatterers.

$$H[k] = \frac{r[k]}{s_k}; \qquad h(t) = T\sum_{k=0}^{K-1} H[k]e^{-j\frac{2\pi}{T}kt} \tag{4.7}$$

This method mainly tries to reproduce the channel impulse response in order to detect and locate the scatterers. Where the power peaks represents a significant quantity of reflected power concerning the possible targets, while their respective time shifts determine implicitly the ranging.

It is important to highlight that the desired Radar application must be able to detect and locate the targets using arbitrary information, which would not suppose a constraint for the communication application. Other feature is that the transmitter and receiver share the same position and thus the transmission information is known for the receiver. It suggests that the channel estimation method could not belong to the blind branch of estimation techniques.

4.3.2. RADAR ALGORITHM

As a conclusion from the background, the resulting channel coefficient affecting the transmitted signal contains essential information for detecting and locating the targets. Therefore, a radar algorithm can be designed based on the estimated V2V channel.

The limitations of the simulated channel regarding a Radar application can be easily noted, since all the steps of the entire channel have been implemented. The main drawback lies in the integrator block, whose function is to sum the rays in temporal cells according to their delays. The duration of these cells is named as the integrator time and the shorter is it, the more accurate is the channel impulse response. In **Figure 4.5** the importance of the integrator time is highlighted, where a longer integrator time provokes higher information lost.

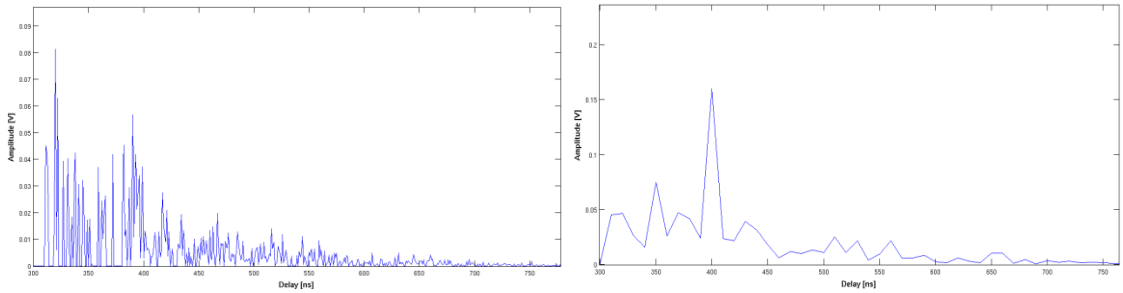

Figure 4.5 *Modules of the channel impulse responses for an integrator time within the range of hundreds of picoseconds for the left image and nanoseconds for the right response.*

Therefore, as a consequence of the constructive or destructive behavior of the rays' addition, their amplitudes and phases change considerably. It implies that the Radar algorithm cannot be strictly based on these parameters. Hence, the proposed method to detect the possible targets lies in the envolvent of the channel, since it is conditioned by the MD and SD scatterers that usually present a higher reflected power than the diffuse scatterers. Nonetheless, these power peaks can represent a MD, SD or DI scatterer; thus, their differentiation is carried out by its speed calculation or their placement. The previous knowledge of the map is supposed to be known by the receiver; it is considered that the Radar algorithm is provided by a GPS system to identify the V2V scenario (highways, roads or other kind of car routes).

In reference to the target azimuth placement in a Radar application, there are different methods as the rotating antenna system or Digital Beam Forming (DBF). The first one is not suitable for a V2V environment, since it is hard to implement and constraints the data rates in the communication application. By contrast, the DBF seems to be a promising solution, even though it also affects the data rates and coverage areas. However, the proposed technique to place the objects in a 2D scenario is based on the trilateration method as the Global Positioning System (GPS) [18]. Its purpose is to determine the location of points through the intersection of at least three different geometry figures (e.g., circles in a 2D case), whose dimensions are related according to the distance measurement from the figure center until the target.

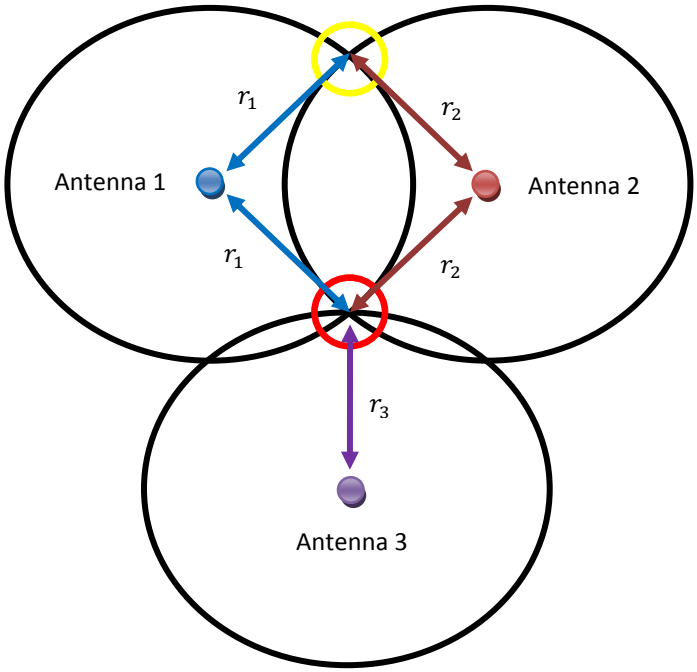

Figure 4.6 *Trilateration representation for three antennas. The antenna 1 and 2 produces two possible solutions, but one is discarded thanks to the third antenna.*

In the implemented system the used geometric figures are circles and this is the main reason of the omni-directional antennas selection, whose azimuth radiation pattern is similar to this geometric shape. Consequently, the target location according to **Figure 4.6** is determined by solving the equation systems of **(4.8)**.

$$r_1{}^2 = \left(x - p_{x,1}\right)^2 + \left(y - p_{y,1}\right)^2$$

$$r_2{}^2 = \left(x - p_{x,2}\right)^2 + \left(y - p_{y,2}\right)^2$$

$$r_3{}^2 = \left(x - p_{x,3}\right)^2 + \left(y - p_{y,3}\right)^2 \qquad \textbf{(4.8)}$$

where $p_{x,1}$ and $p_{y,1}$ are the x and y coordinates of the center point for the circle number one, while the other p coordinates belong to the other two remaining circles. The position of the target in the 2D scenario is indicated by x and y, which are the variables to be solved simultaneously in all the equations. At last, r_1, r_2 and r_3 are the radius of the different circles, which are calculated by the ranging process according to **(4.2).** The delays (τ) to apply in **(4.2)** are assigned to the temporal location of the power peaks from the channel impulse response. It is important to highlight that these peaks are locally distinguished through a threshold, which means that the peaks are determined where the derivative of the estimated channel presents the maximum values. This threshold presents a trade-off between the computational cost and the number of scatterers to detect. Therefore, the lower is the threshold, the higher is the number of peaks, which means that more targets can be detected through a computational cost sacrifice. In contrast, the probability of false detection increases proportionally to the number of peaks.

This is the essential idea of the proposed algorithm; nevertheless, in order to achieve a better performance a diversity technique based on "phantom" antennas is implemented as in [29]. The basic interpretation of this concept is to place imaginary TRx antennas (Tx and Rx antenna) between the real transmitter and receiver antennas, such that the propagation time is not modified (see **Figure 4.7**). The considerations to implement this technique are to suppose far-fields targets and intelligent receivers capable to distinguish the beam from the different transmitter antennas through coding, for example.

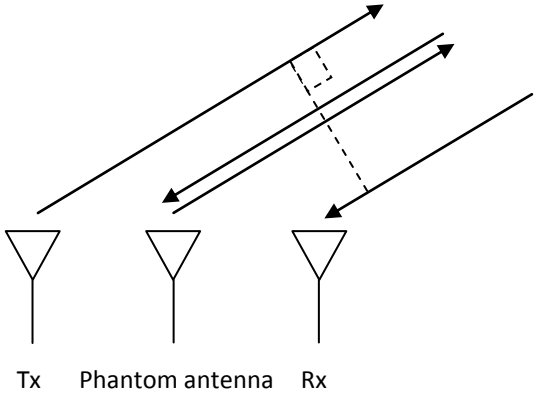

Figure 4.7 *Phantom antenna illustration.*

As the implemented system is a MIMO 4x4, it implies that the total number of possible channels is equal to 16 as the expression **(4.9)** represents.

$$\boldsymbol{H} = \begin{pmatrix} \boldsymbol{h_{11}} & \cdots & \boldsymbol{h_{14}} \\ \vdots & \ddots & \vdots \\ \boldsymbol{h_{41}} & \cdots & \boldsymbol{h_{44}} \end{pmatrix} \tag{4.9}$$

Where **H** symbolizes the matrix with all the possible channels, while $\boldsymbol{h_{41}}$ corresponds to the channel generated by the transmitter antenna 4 with the receiver antenna 1 and so on. The position of the virtual elements has been performed in the middle distance between the transmitter and receiver antenna, except for the cases in which the same antenna is used for the transmission and reception. In these situations, the virtual element location coincides with the Tx and Rx antennas position. **Figure 4.8** illustrates the resulting scheme.

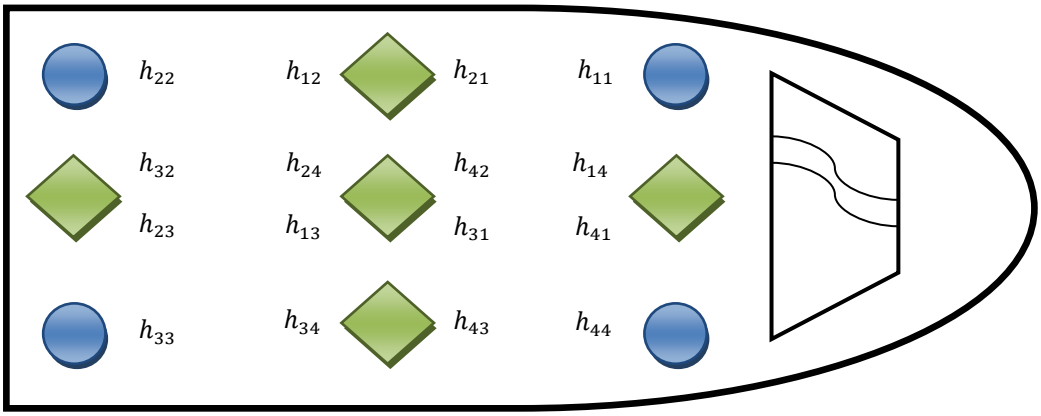

Figure 4.8 *Antenna placement scheme with the "phantom" antennas. The matrix* ***H*** *can be interpreted as symmetric, where the circles are the real antennas, whereas the rhombuses are the phantom antennas.*

This placement criterion for the virtual antennas introduces some errors in the formulation of the trilateration equations, due to the non-fulfillment of the far-field consideration. A possible example is represented in **Figure 4.9**, where the circle radius for the virtual antenna is obtained through the ranging procedure according to the channel estimated ($\boldsymbol{h_{12}}$ or $\boldsymbol{h_{21}}$). In this case the delay of the power peak is the same for the estimated channels $\boldsymbol{h_{11}}$, $\boldsymbol{h_{22}}$, $\boldsymbol{h_{12}}$ or $\boldsymbol{h_{21}}$, since the distances of the antennas to the target are equal. Thus, the criterion to place the antenna between the transmitter and receiver antennas position is not appropriate for this situation. The convenient solution is to move backward the virtual element location to counteract the distances, but it implies the supposition that the representations of the other circles are correct. Subsequently, this criterion is maintained, even though the error that it entails.

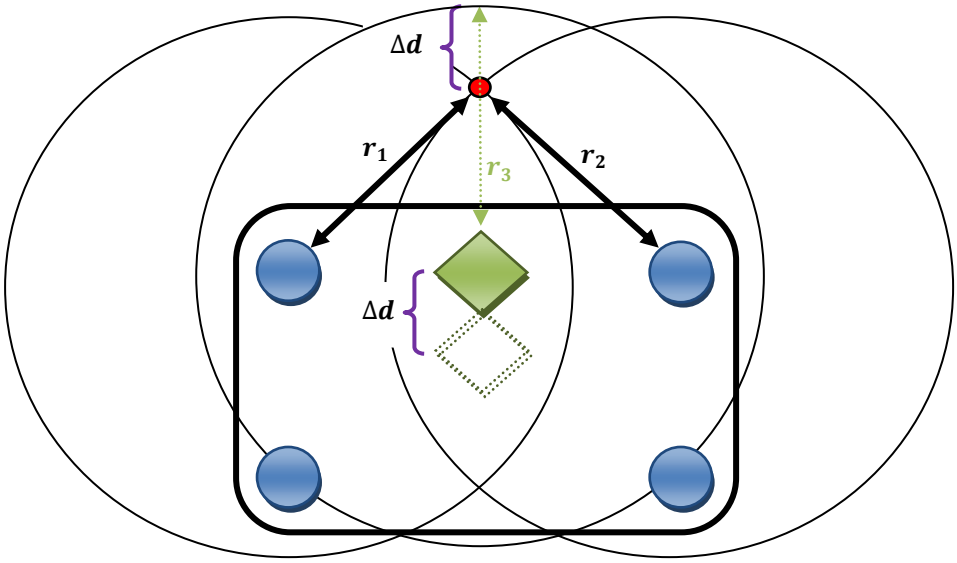

Figure 4.9 *An error example according to the "Phantom" antenna concept. The time delays of the targets determined by the channels are the same; then, the geometries of the figures are equal (r1=r2=r3). However, the positions of the antennas are different and it affects the placement of the circles in the 2D scenario, which entails an error.*

A method to overcome this drawback is to use diversity by means of the 16 estimated channels, with the aim of dismissing the wrong virtual placements or channel estimations. The diversity method performed is based on the first four channels -three required plus one more as security margin- that have the shortest delay times regarding the respective peaks of the evaluated target. Thus, the system equations **(4.8)** are solved for the four possible combinations of these channels and the solutions with the highest proximity are averaged to reduce the error. In order to group the outcomes with the maximum similarity from all the possible combinations in order to avoid false detections, a threshold is established in the more restrictive axis, y. The reason to select the y axis instead of the x is owing to the cars displacement, which is larger in the x axis rather than the y concerning the scenario design defined as a rectangle (**Figure 3.6** and **Figure 3.7**). Hence, different sets according to the y coordinate are established and the ensemble with more samples is averaged in order to obtain the final approach of the target position and reduces the error and false detections.

Other important aspect to take into account is the distinction of the rays, since the estimated channels experience dissimilar time delays and attenuations for the different scatterers. It implies that the number of targets or power peaks change from one channel to other as the time delays. Hence, a

matching method for the power peaks is required as well as to distinguish them. The proposed method is through temporal cells such that the clusters of rays are divided according to this margin. If all the rays of a cluster are inside the cell boundaries, they represent the same target. Otherwise, the existence of two or more nearby targets could be a possible explanation. The duration of these cells are determined by the maximum distance of the mounted antenna on the car ceil. According to **Figure 4.3** this temporal duration is equal to

$$T_{CELL} = \frac{d_{max}}{C_0} = \frac{\sqrt{2^2 + 1{,}4^2}}{C_0} = 8.1\ ns, \tag{4.10}$$

where C_0 is the light speed, d_{max} represents the maximum distance that corresponds to the diagonal of the rectangle formed by the antennas location. Whilst, T_{CELL} is the time duration of the cell and it is defined as the maximum time delay difference that a ray can experiences to reach the closest antenna concerning the furthest one. Thus, the maximum temporal variance for the distinction of the power peaks lies in this cell duration.

The following figures illustrate with examples how the algorithm should distinguish the peaks and select the first four rays to determine the location of each target. These pictures have been obtained from the scenario depicted in **Figure 4.10** that represents one of the most problematic scenarios, since all the MD targets are placed from the Radar car with the same distance. It implies that the reflected rays provoke a high uncertainty in order to identify the rays with the targets.

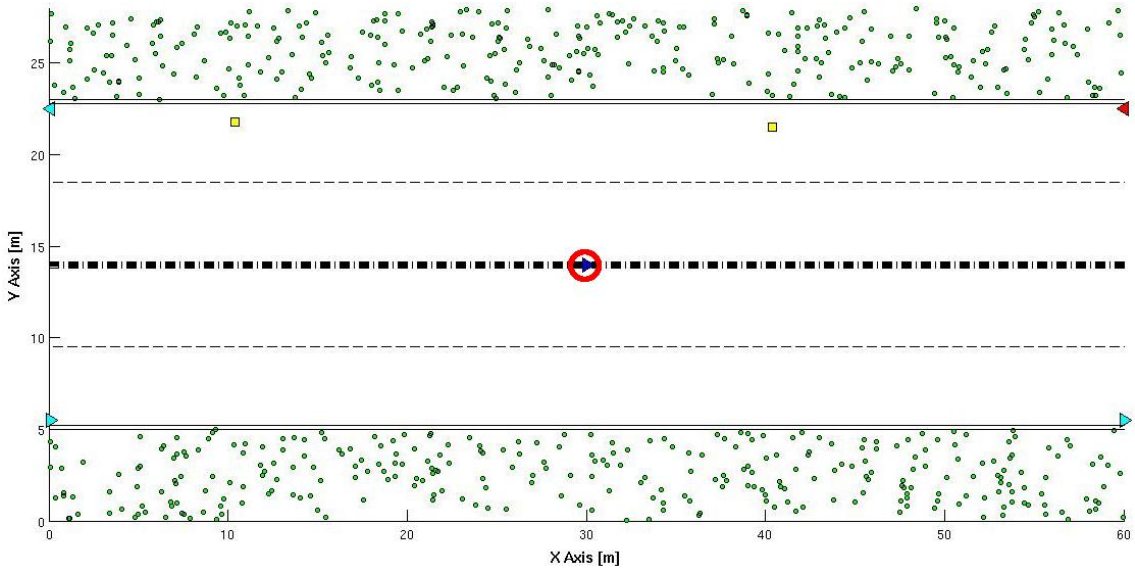

Figure 4.10 Problematic scenario in which the Radar car is placed in the middle of the map, while the targets are located in the corners of the road. This situation cannot occur, since the vehicles are forbidden to drive by the center of this via; besides, some highways separate the opposite directions lanes by a security wall.

In **Figure 4.11**, the respective V2V channel impulse response of the Radar application for an integrator time within the range of nanoseconds is depicted. It is composed by the overlapping of the 16 responses according to the MIMO structure. The significant features that can be observed are the three bundles of rays surrounded by the rectangles. The first and second ensemble corresponds to the SD scatterers, while the remaining set belongs to the four MD targets. It is important to note that the temporal width of the bundle of rays from the MD is approximately equal to the duration of a single SD scatterer; this fact affects the range resolution in a similar manner as **Figure 4.2** represents.

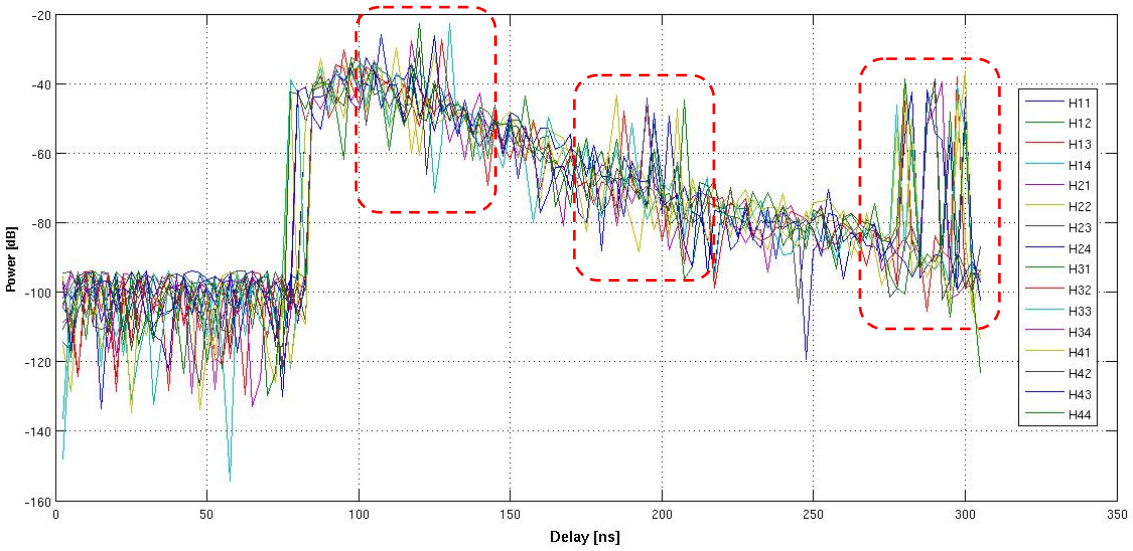

Figure 4.11 *The 16 channel responses for the scenario depicted in the* ***Figure 4.10****.*

The respective estimated channels from **Figure 4.11** is presented in **Figure 4.12**, where the furthest road signal is practically impossible to differentiate as a consequence of the cannel estimation and noise addition; the used SNR for these simulations have been of 15 dB. This picture illustrates a suitable method for the peaks searching, which has to be local instead of global.

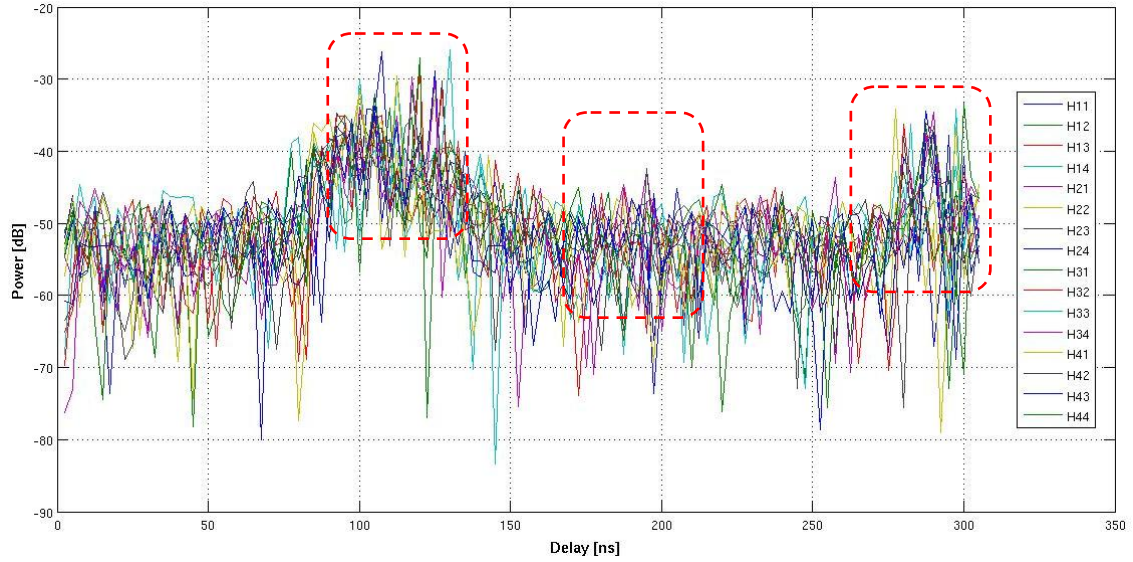

Figure 4.12 *The 16 estimated channel responses according to the used channel of* ***Figure 4.11.***

A close look at the bundle of rays corresponding to the MD scatterers is depicted in **Figure 4.13**, where the curves from the same transmitted and received antennas (h_{11}, h_{22}, h_{33}, h_{44}) are enhanced concerning the rest of channels. They are characterized by two differentiated peaks at the beginning and end of this set of rays, even though some phantom antennas present a similar behavior. The responses with only one power peak, which are wider than the others, belong to the rest of phantom elements.

Therefore, the proposed Radar algorithm would start selecting the rays to detect the first target, which must be inside a temporal window initialized from the first peak and with a duration equal to T_{CELL}. Thus, the channels that the first window contains are: h_{33}, h_{22}, h_{44}, h_{41}, h_{32} and h_{11}. As the delays must be different among them, the number of possible combinations is reduced and at the same time this

condition assures a solution for the trilateriation equations. For this first ensemble, almost all the combinations will derive in a wrong solution or high error, except for the phantom antennas contributions that can reduce the error. In the second round, the temporal window is shifted in time and the same procedure is carried out again. In this case, the total number of possible targets to be detected is equal to three, since no more windows can be placed on account of the temporal width of this bundle of rays.

This situation is one of the most difficult cases to be solved and the importance of the phantom antennas is clearly justified for being the key to solve this type of problems.

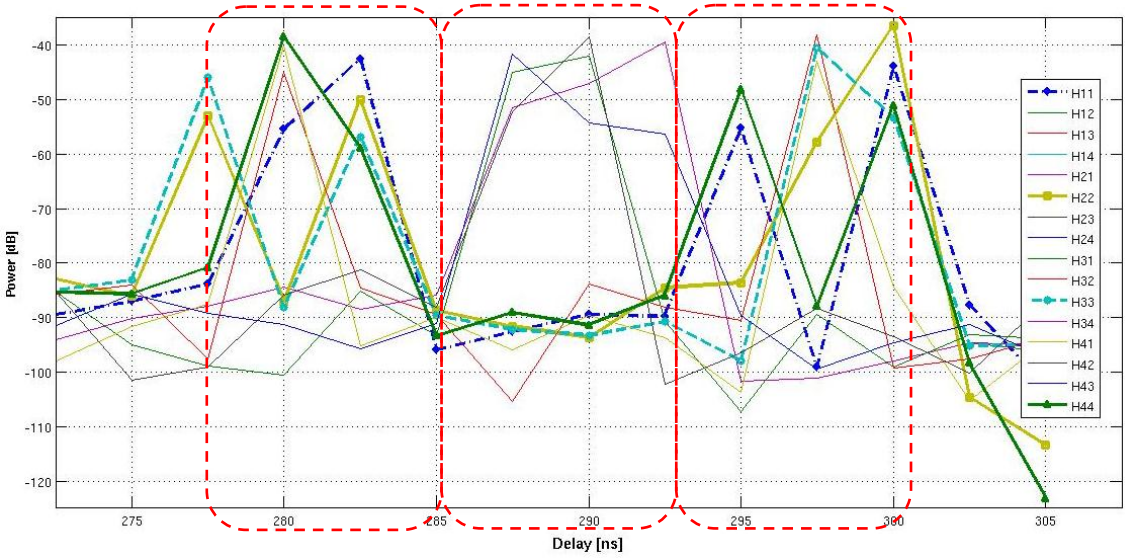

Figure 4.13 *Zoom in the bundle of rays for the MD scatteres.*

In spite of the appraisal of the proposed Radar algorithm is developed in the results chapter, some considerations for the correct functioning of this detection and location system can be noted. As the operating principle is based on the envolvent of the channel estimated, a significant reflective power from the MD has to be ensured to distinguish them from the DI. Concerning the integrator time, it has to be short enough so as to obtain reliable targets detection and positioning. Nonetheless, the sampling time has been fixed according to the 2V2 bandwidth, thus two sampling times are required to carry out the V2V communication and Radar applications. Therefore, the proposed receiver consists of two samplers (A/D devices), as can be seen in the block diagram of ***Figure 2.4.***

At last, a consideration according to the MLE criterion must be highlighted. From the conclusions obtained in the Subsection 3.5.5, the MLE for the implemented system is not a suitable criterion to estimate a NWSSUS channel. As a consequence of the fact that the MLE uses the long training sequence to determine a channel that not remains constant during the OFDM frame. Therefore, the consideration lies in the supposition that the channel during the training sequence is unvarying; the estimation of the channel can then be easily performed. Nevertheless, it is important to stress that this channel estimated is only valid for a certain time interval until the channel experiences significant changes. It means that the results obtained from the Radar algorithm through the estimated channel are only valid for that precise moment. In the case of using shorter OFDM frame, the duty cycle of the Radar system would be higher; therefore, the update rate of the targets detection and position is higher.

4.3.3. TRACKING METHOD

With the purpose to determine the Doppler Frequency as to assess in an efficient manner the Radar algorithm, a tracking has been proposed.

The tracking method is basically focused on the detection and positioning algorithm described previously, which is applied in different observations of the modeled channel along the time. In other words, the tracking method can be defined as the Radar algorithm for different time instants. It entails some advantages in reference to the error avoidance, since the known information of the past scatterers locations and speeds can be used to predict the future targets. Nonetheless, if the past samples are incorrect, the future solutions will be too; for this reason, some initial computations are required to ensure certain reliable level and discard the less common solutions.

As a consequence of the information lost due to the integrator block, where the constructive or destructive summation of the different rays changes significantly the amplitude and phase of the target to detect, a window mechanism is employed to determine the Doppler frequency. Therefore, the maximum minus the minimum displacement of a given target divided by the duration time of the window represents the speed of the vehicle and implicitly the Doppler frequency. It is convenient to fix the observation time proportional to the OFDM frame length, since the Radar algorithm has to be applied once the OFDM frame is completely received.

$$Speed = \frac{\Delta disp.}{T_{obs.}}; \qquad T_{obs.} = kT_{OFDM};\ \ k\epsilon\mathbb{N} \tag{4.11}$$

Where $\Delta disp.$ is the increment of distance that the target travels inside the window duration represented by the observation time, $T_{obs.}$. The observation time has to be a multiple of the time duration of the OFDM frame, T_{OFDM}; thus, in this case, k is a constant variable no null.

The sampling time used for the Radar application is the main parameter that affect in the tracking system, it defines how the circles used in the trilateration grow or decrease. In other words, the minimum increment or decrease of these circles is specified by the sampling time. For example, a target in front of the radar car is detected in t_0 in the samples 10, 11 and 12 of the channels h_{11}, h_{22} and h_{33}, respectively. Subsequently, this mobile scatterer is moving away from the Radar car and experiences a displacement for t_1 regarding t_0, such that the samples of the channels has to be increased 1 sample to indicate this distance increment; however, the channel h_{33} is detecting the target in the sample. Thus, there is an uncertainty in the placement of the car, since two circles have increased their radius yet the third is maintained. This situation takes place because the displacement for the channel h_{33} has not been long enough as to shift one sample the coefficient that symbolizes the target. The channel is detecting the target in the same sample, which implies that the target is maintaining the distance from the Radar.

Actually, the propagation channel before the integrator block has detected this displacement, but after the integrator this information is lost. The ideal case is to have a sampling time as low as the minimum time distance between the rays from the scatterers that constitutes the propagation channel before the integrator block. This solution is not feasible, since the sampling time is within the range of picoseconds and no such sampling frequency have been developed nowadays. Other method to overcome this problem is to assume these uncertainties and try to reduce their influence in the final result through a higher number of detections; it means a high update rate of the Radar application, which is constraint by the duration of the OFDM frames. Thus, for shorter frame lengths more detections of the targets can be performed and the previous error can be diminished.

The block diagram of the proposed algorithm is presented in the **Figure 4.14**, which starts with an estimation of the channels. Subsequently, all the peaks are determined locally and classified by cells according to the matching process, which is based on temporal windows whose durations are equal to T_{CELL}. A loop to evaluate all the cells is the next step, where the trilateration is firstly applied and an average of the result with more samples is performed as a consequence of the diversity method implemented. The outcome from this average is the solution of the Radar algorithm; however, the tracking method continues recording samples until it reaches a counter. The aim of this counter is to obtain a certain number of samples so as to compute the reliable solutions; it is considered as a warm up for the tracking algorithm. This operation to estimate the correct solutions is only executed one time for the iteration that surpasses the warm up counter.

Once, a reference set of possible solutions is built, the future samples can be compared and removed if there is not coherence with the data base. If there is some relation, the next step is to filter the obtained solutions according to a filter based on the knowledge of the map and the speed of the scatterers. Besides, an average to compress the outcomes and reduce the error is also implemented. Then the Doppler frequency estimation and the representation are performed. Finally, the data base is upgraded with the new solutions but without being averaged, since a cumulative average process would modify the results obtained from the Radar algorithm.

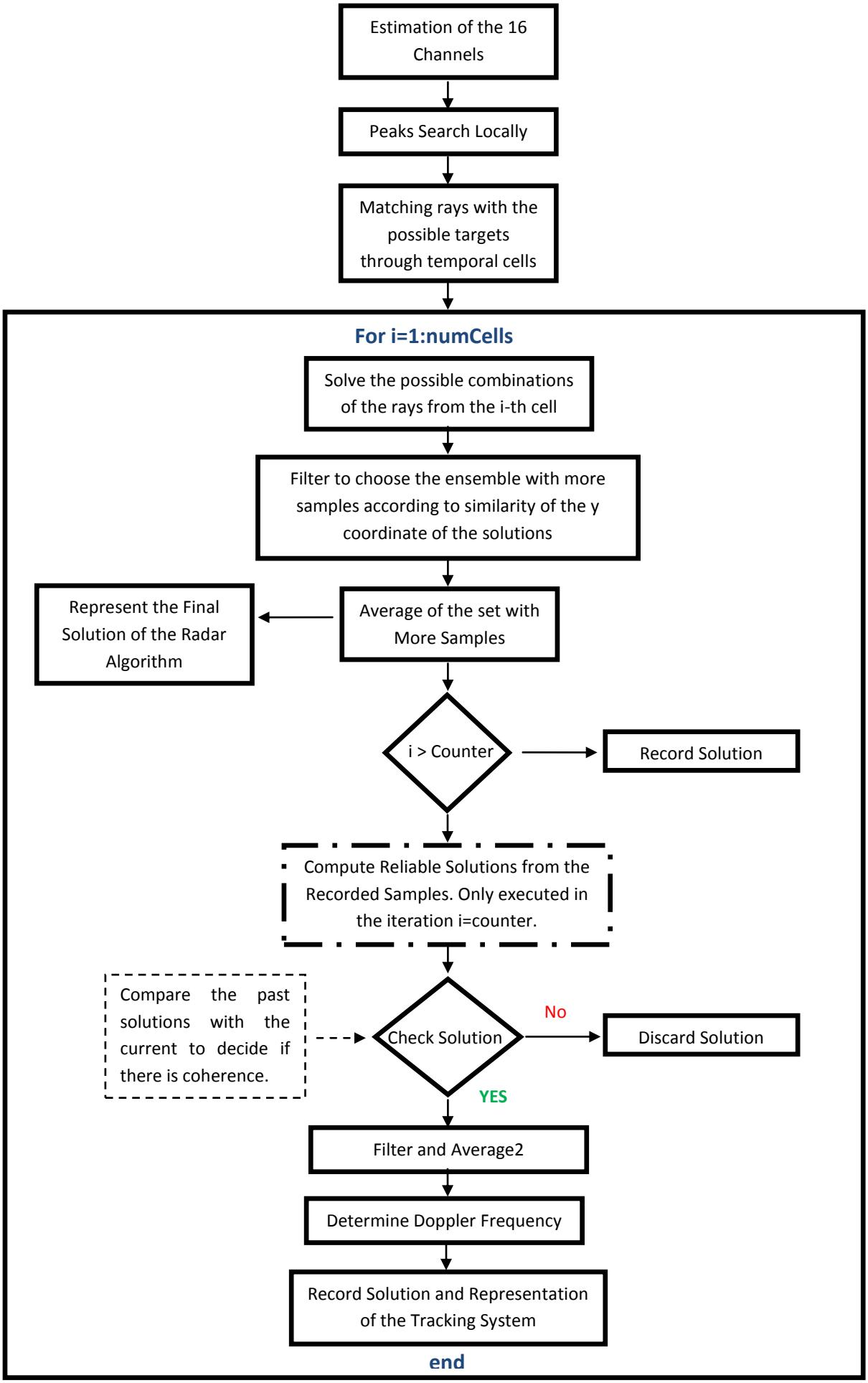

Figure 4.14 *Block diagram of the radar algorithm and the tracking system*

5. RESULTS

Once the implemented system has been defined and characterized as well as the proposed Radar algorithm, the next stage is to verify the viability of the ranging method. Subsequently, this chapter has been assigned to cover this matter.

In order to assess the functioning of this Radar mechanism some criterions need to determined, as for instance the coverage area of the Radar or the allowed error to distinguish a true from a false detection. They depend on the features of the V2V application; however, they are unknown by the author, who proposes some preliminary parameters. On the other hand, the results obtained cannot be extrapolated to all the different car routes, since the scatterers gains changes according to the environment. Therefore, in other scenarios the Radar performance could be improved or worsening.

In reference to the content of the chapter, it has been divided in two blocks. The first one of them contains the simulations regarding the Radar algorithm, while the remaining part is assigned for the tracking system based on the same ranging principle.

It is important to highlight that in the Radar applications there are not LOS and that a single bounce is only considered. On the other hand, in other to ensure a certain reflectivity of the MD and SD regarding the DI scatterers, their gain has been increased 15 dB in the highway scenario for all the simulations presented below. Thus, the used constant part of the gain for the simulations has been of -69 instead of -89 dB. This last consideration is justified by an inconvenient that the authors of the implemented GSCM [13] had in the channel measurement process, where they use a different attenuator as they commented in their work: "*In the post-processing, it was discovered that the LOS component of the SM highway measurements was approximately 20 dB lower than that of the other scenarios, likely due to the unintentional use of an additional attenuator during those measurements.*".

5.1. RADAR ALGORITHM

With the merely goal to characterize the functioning of the Radar algorithm, different test have been performed regarding the number of targets to locate. The results are expressed as detection probabilities of the targets according to a certain distance error. The SNR and the placement of the scatterers, as well as the Radar car, are the main influent factors for the outcomes of the ranging algorithm.

5.1.1. SINGLE DETECTION

A pair of scenarios composed by only one MD and SD scatterer is evaluated in this subchapter; they are represented in the **Figure 5.1**. Their difference lies in the y axis with the aim to highlight the influence of the diffuse scatterers and SNR. In the first figure the Radar car is placed in a favorable position since it is further from the diffuse area than the second picture. Hence, the power reflected in the first scenario is lower as a consequence of a longer distance regarding the DI.

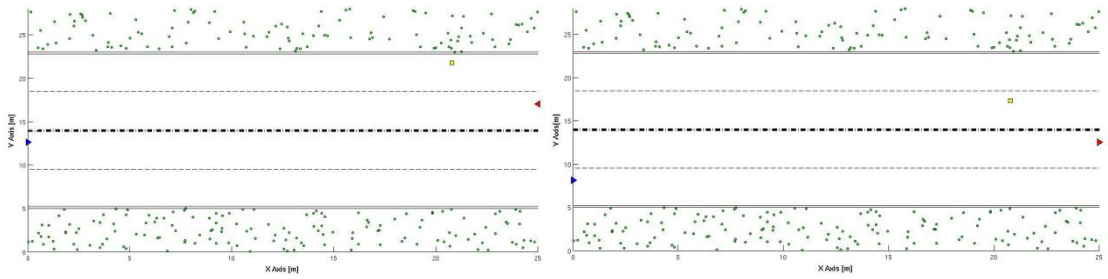

Figure 5.1 *From left to right the furthest and closest scenarios concerning the diffuse scatterers are represented, respectively. The blue triangle represents the Radar car, while the red is the car to detect.*

The length of the scenarios has been determined according to the MD densities, such that 25 meters are required to assure two vehicles in this type of highway. Besides, one SD results from these dimensions. On the hand, the Radar car and the scatterers have been placed for the worst case condition, which presents the longest distance taking into account the lanes. It is important to highlight that the distances from the Radar vehicle to the scatterers have been respected in both scenarios, the only difference is the displacement of the y axis for the MD and SD.

The result obtained from the example illustrated in the **Figure 5.1**, which have been averaged over 500 simulations and for different SNRs, is represented in the **Figure 5.2** (MD detection). The threshold used to distinguish the false and true detection has been of 1 and 4 meters. Thus, if the proposed target location by the Radar is inside a virtual circle, whose radius is the threshold and its center is the real target position, the solution will be valid.

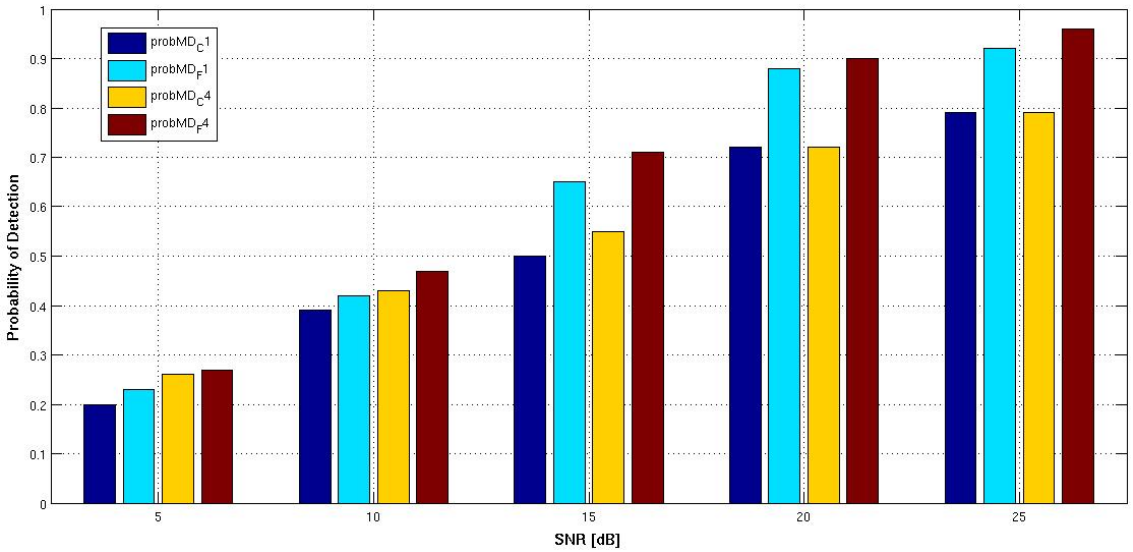

Figure 5.2 *Probability of detection of the MD scatterer for an error threshold of 1 and 4 meters.*

The conclusion that can be drawn from the previous picture is the proportional increment of the probability of detection with the SNR, since the noise does not mask the power peaks corresponding to the scatterers for high SNR. On the other hand, the interference of the diffuse scatterers is visibly enhanced in the probability of detection difference that both cases present, where the furthest situation has the highest number of good decisions. Concerning the error thresholds, the higher is it, the higher is the probability, although in this example the difference is not so much elevated. It is important to stress that the probability of detection trends to converge for a SNR better than 20 dB.

Other significant reasons that also affect the quality of the Radar decisions are the slow fading effect and the non-constant value of the MD path loss exponent. These entail some situations where the MD targets present a low power, such that they are interpreted as noise.

The previous simulations have been performed for two fixed scenarios, in which the SNR and DI influence have been assessed. The next results are for the same scenario dimensions, but in this case the positioning of the scatterers change for each simulation regarding the **Table 3.2**. The only parameter that is maintained is the y coordinate of the Radar car; its purpose is to determine in other context the importance of the DI presence for the ranging process.

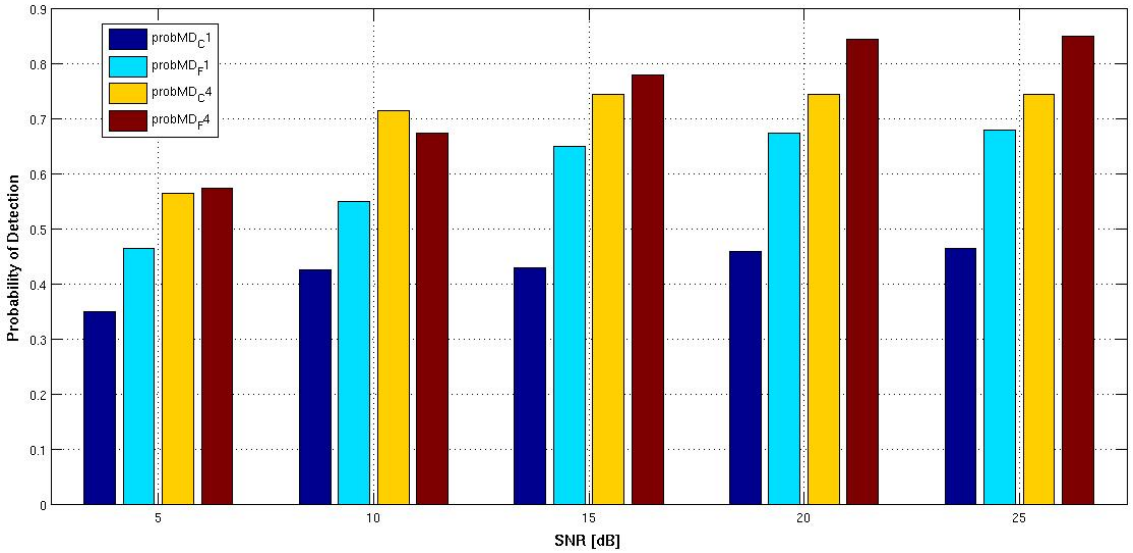

Figure 5.3 *Probability of detection of the MD scatterer for an error threshold of 1 and 4 meters in a non static scenario.*

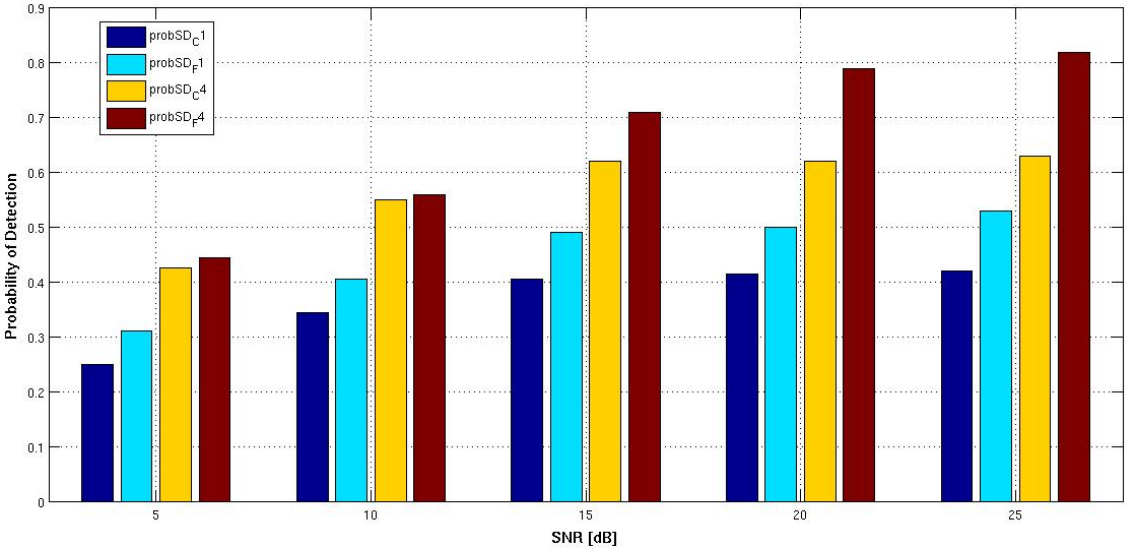

Figure 5.4 *Probability of detection of the SD scatterer for an error threshold of 1 and 4 meters in a non static scenario.*

The maximum probabilities of detection for these simulations are lower than the results obtained from the static scenario as a consequence of the randomly placement of the targets. It implies that worse scenarios than the depicted in the **Figure 5.1** exist. It could be the case in which the target to detect is

placed in the channel impulse response where the diffuse scatterers present the greatest reflected power. For instance, from the **Figure 4.12** the first rectangle placed around 100 ns corresponds to the crest for the strongest reflected energy of the DI. Then, if the target delay coincides with this temporal zone and its power is not enough to highlight from the rest of rays, it will not be detected.

On the other hand, an interesting behavior of the probability detection in reference to the SNR is observed. Its influence is also significant, but for lower distances the values of non-static simulations are characterized by greater probabilities rather than the static case. These correct detections mainly corresponds to the scenarios where the target to detect is close enough such that the reflected power overcomes a noise generated from low SNRs. Therefore, these favorable situations joined with the worst scenarios defined in the previous paragraph produce a reduction of the brusqueness that the probability of detection increases regarding the SNR experience.

Other important feature to enhance is the importance of the threshold used, in these simulations there is a noticeable difference between the probability for 1 and 4 meters. The reason is attributable to the wider variance concerning to the static simulations that the location error presents, it is due to a higher number of cases regarding the different simulated scenarios.

5.1.2. Multiple Detections

In these simulations the scenario used is depicted in the **Figure 5.5**, which consists of five vehicles and two road signals. It corresponds to a possible example of a highway stretch with a length of 70 meters, with the aim of having the commented number of MD scatterers regarding its density.

The simulations that have been performed in this scenario are similar than in the previous subchapter; although no furthest and closest cases have been implemented. Thus, the purpose of such scenario is to assess the functioning of the Radar algorithm in a multiple detection situation.

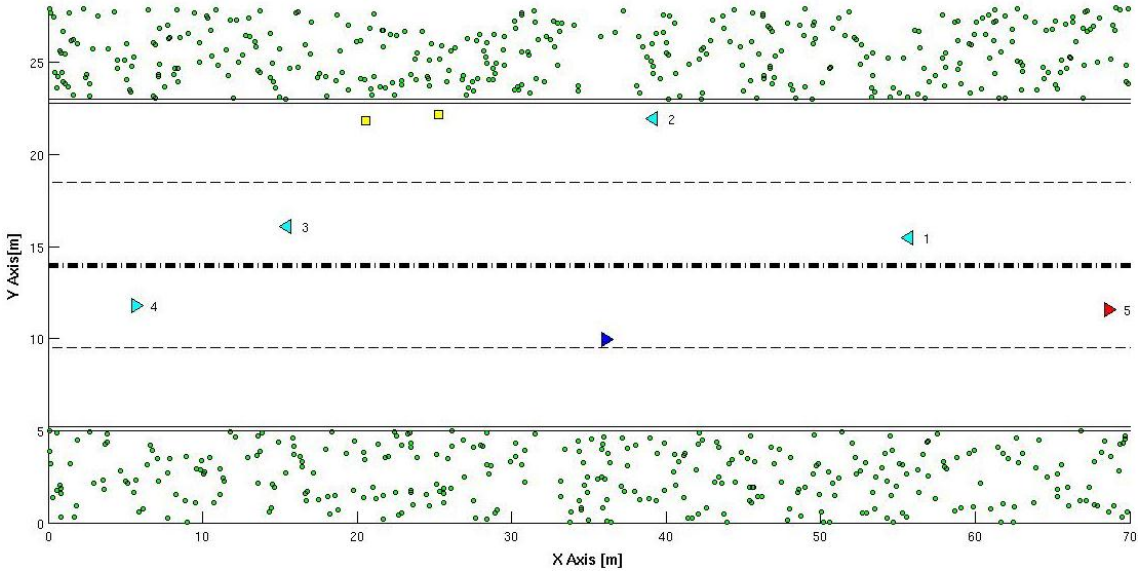

Figure 5.5 *Scenario formed by five vehicles and two road signals. The blue triangle is the Radar car.*

The first simulation has been executed over the static scenario of the **Figure 5.5**, where the positions of the scatterers are maintained during the 500 simulations. The results are presented in the **Figure 5.6**, where the probabilities of detection of each target for a threshold of 4 meters are illustrated.

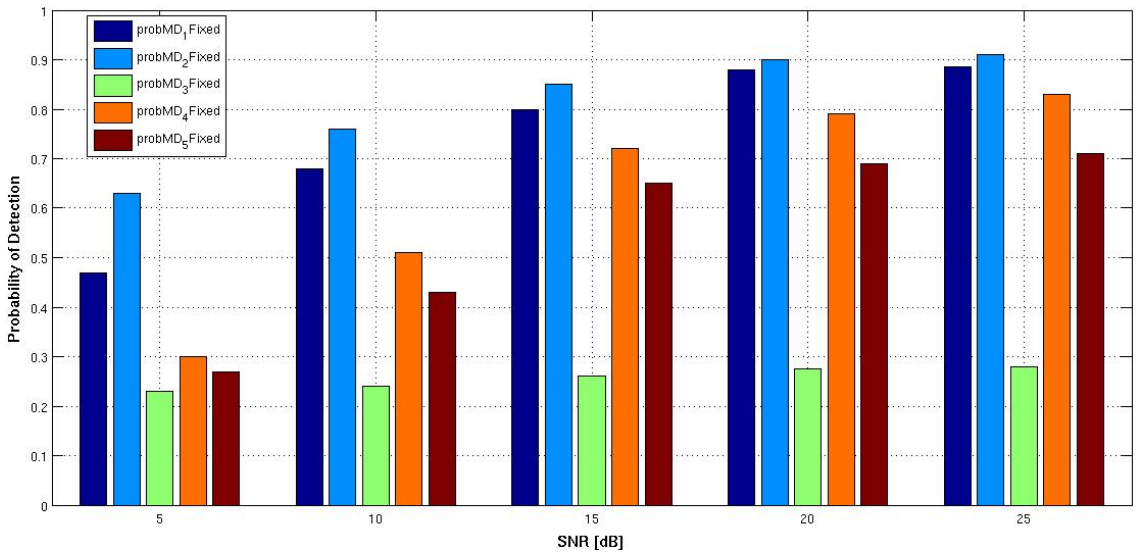

Figure 5.6 *Probability of detection of the 5 MD for an error threshold of 4 meters in a static scenario.*

The target that experiences the poorest detection probability for the given scenario is the car number 3, which is placed between the road signals and the car number 5. Thus, the rays reflected from the vehicle number 3 are mixed with the rays coming from the neighbor scatterers. This fact entails some confusion in the Radar algorithm that is represented as a low probability of detection.

The second hardest target to locate is the number 5, which is placed almost in front of the Radar car. This situation can be interpreted similar as the depicted in the **Figure 4.9**, where the phantom antennas introduce some uncertainty in the results and the real antennas detect the target placed at the same distance, since the sampling time of the Radar receiver is not small enough to establish a difference in the channel impulse responses obtained from antennas located in dissimilar positions. It means that the target is detected in the same channel coefficient, which supposes the same distance for different antennas. A possible solution to overcome this drawback is to place more antennas in the car's roof or to decrease the sampling time.

Something similar occurs to the target number 4, but its probability is higher. It could be explained as the confusion of some wrong detections from the vehicle number 3 that are attributed as solutions of the car number 4. The rest of cars that are located diagonally concerning to the Radar car present the highest values of the probability of detection, where the phantom antennas presents the best efficiency.

The next simulations have been performed over a non static scenario except for the Radar car, whose location has been maintained for the 500 iterations. The threshold used has been of 4 meters again.

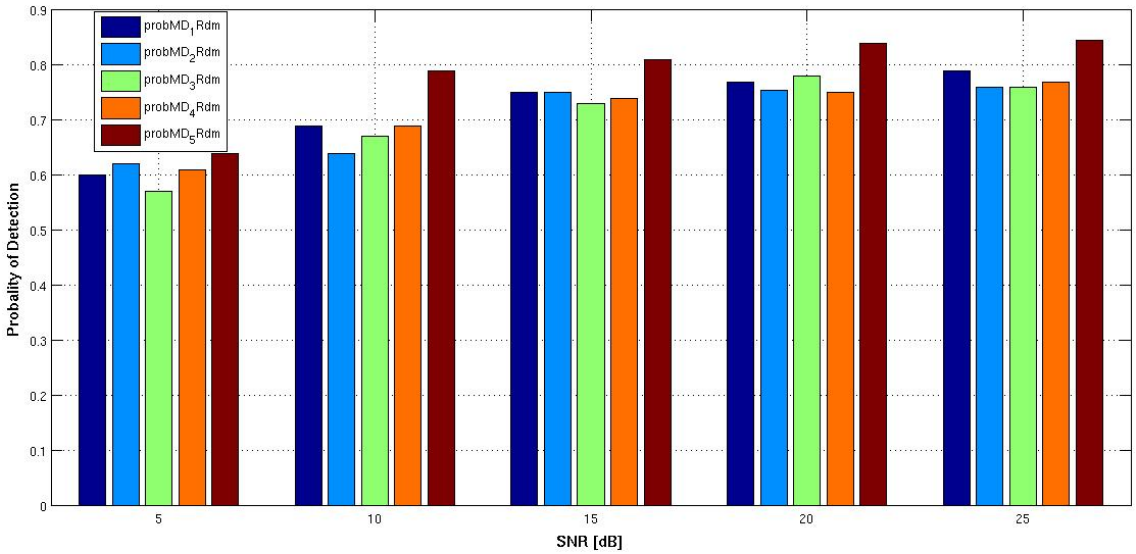

Figure 5.7 *Probabilities of detection of the 5 MD for an error threshold of 4 meters in a non static scenario.*

In reference to the **Figure 5.6**, the conclusions are similar to the single MD detection. The values of probability of detection are lower than the static scenario and the brusqueness of the bar graph is diminished. An interesting feature is the similarity of the probabilities according to the different targets, thus, the previous example of the **Figure 5.5** can be considered as a worse scenario for at least the location of the targets number 3 and 5.

5.2. TRACKING ALGORITHM

For the evaluation of the target tracking method, different scenarios have been performed for different length of the OFDM frames. These lengths can be of 250, 500 and 1000 OFDM symbols, which entail a time duration of 2, 4 and 8 milliseconds, respectively.

The tracking has been performed during the same time interval for the different OFDM frames that is around 800 milliseconds. Thus, the numbers of simulations are 400, 200 and 100 for the frames of 250, 500 and 1000 OFDM symbols, respectively. The SNR has been maintained to 20 dB for all the scenarios and the tracking results illustrated in the next pictures are before and some of them after the filter. The filtering is based on the map dimensions and speed of the determined targets; thus, if the detections are outside the maps, they are removed as well as if their speeds are higher than a certain threshold, 150 Km/h.

The results have been averaged each 2, 4 or 8 samples according to the number of simulations 100, 200 or 400. On the other hand, to determine the Doppler frequency the used temporal window has been fixed to the total time duration of the simulations, 800 milliseconds, so as to obtain an accurate result. For example, the green rectangle with discontinuous lines from **Figure 5.8** represents the observation window used to determine the Doppler frequency as well as the target speed.

The tracking has been performed for 4 different scenarios: 1MD&1SD (furthest case), 3MD&2SD, 4MD&1SD and 5MD&2SD. For the 1MD&1SD and 3MD&2SD the tracking using OFDM frames of 1000, 500 and 250 OFDM symbols are illustrated. Besides, the tracking before the filter for OFDM frames of 250 are also depicted. On the hand, the results from the 4MD&1SD and 5MD&2SD are only represented for frames formed by 250 OFDM symbols as a consequence of the extension of the thesis. Finally, a bar graph shows the probability of detection of each target according to the tracked scenarios (**Figure 5.18**).

In order to interpret the results, it is important to define what the employed geometric figures symbolize. The Radar car is represented by a blue triangle and its displacement along the time is described by a set of triangles plotted for the different time instants. By contrast, the MD scatterers are depicted by red or cyan triangles and their displacement is represented in the same manner as the Radar car. The red triangle is supposed to be the receiver for the V2V communication but in the Radar application it has not any influence. The real position of the SD is determined by a yellow square, while the red squares symbolize the detections from the Radar algorithm and the cyan square corresponds to the mean value of the ensemble formed by these red squares. On the other hand, the detections of the MD targets are represented by purple triangles. An explanation of the cyan squares is the fact that they are detected as road signals, since these scatterers present a lower speed than the half of the maximum allowed by the implemented highway (<60 km/h).

5.2.1. 1MD&1SD

The first scenario is the furthest case for one MD and SD evaluated previously in the Radar algorithm with a single detection. The green rectangle represents the observation window to determine the Doppler frequency as well as the speed of the target.

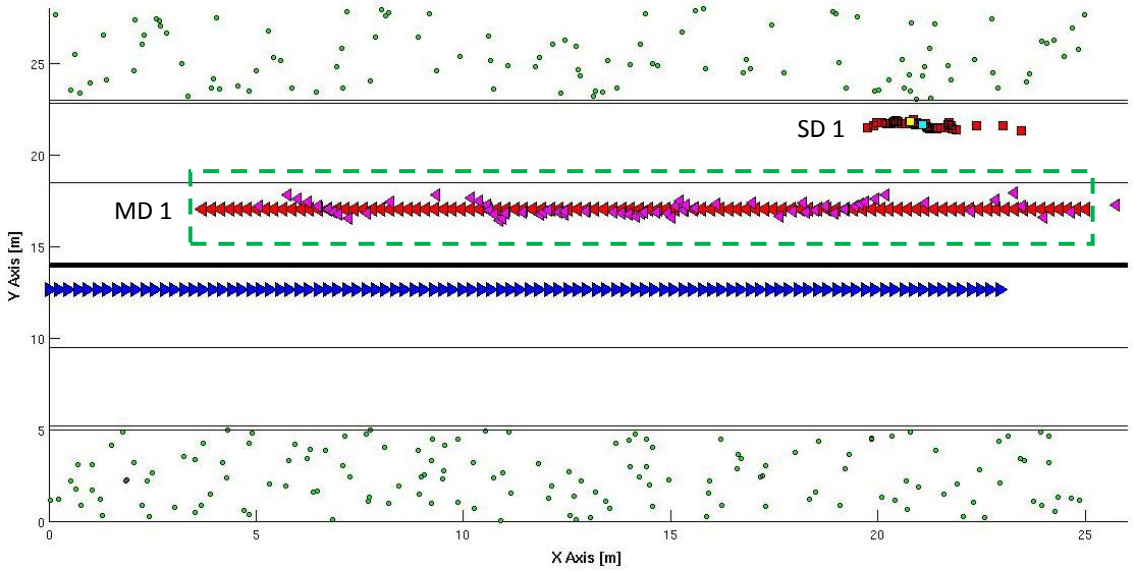

Figure 5.8 *Tracking of the 1MD&1SD scenario for an OFDM frame of 1000 OFDM symbols.*

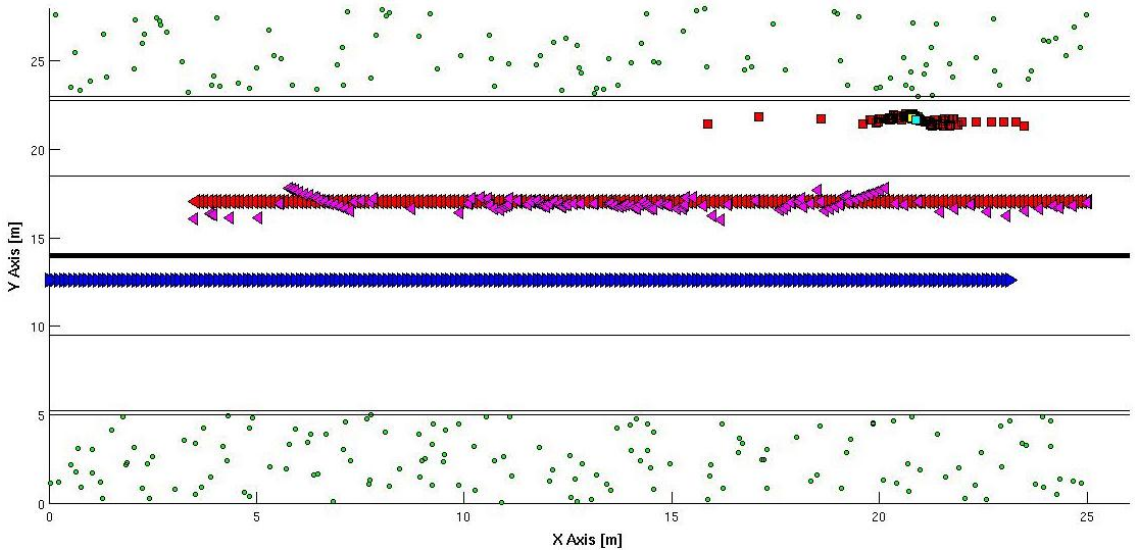

Figure 5.9 *Tracking of the 1MD&1SD scenario for an OFDM frame of 500 OFDM symbols.*

The **Figure 5.10** shows the raw detections before the filter process and without being averaged.

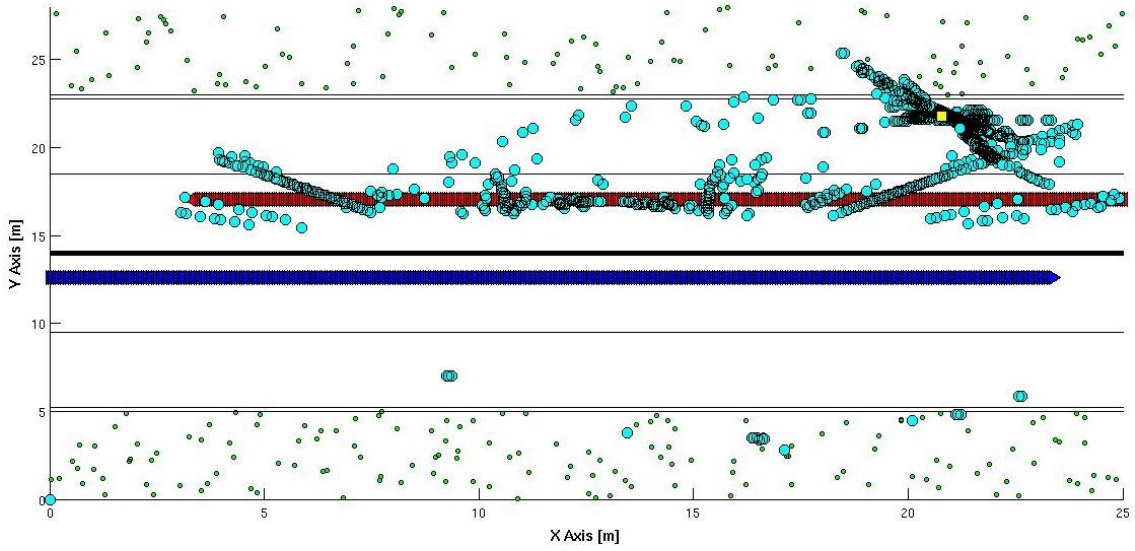

Figure 5.10 *Tracking of the 1MD&1SD scenario for an OFDM frame of 250 OFDM symbols before the filter and without average the samples.*

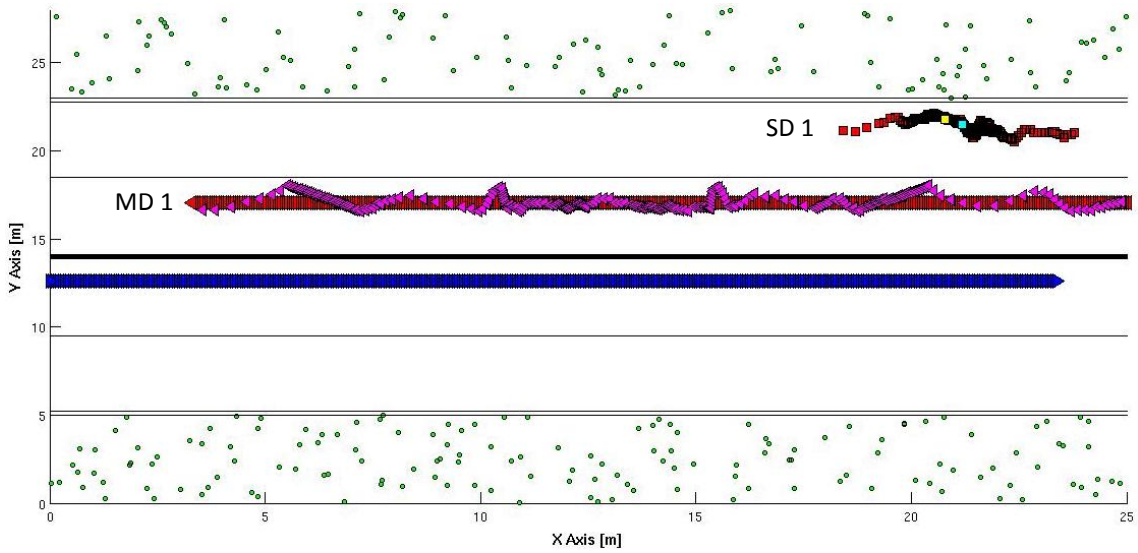

Figure 5.11 *Tracking of the 1MD&1SD scenario for an OFDM frame of 250 OFDM symbols after the filter.*

As can be observed, this scenario does not entail a high complexity to the Radar algorithm to detect and locate the targets. Indeed, the probability of detection presents good values for the different OFDM frames, around the 90% (see **Figure 5.18**). The estimated speeds are quite close to the theoretical with the help of the average process that can compress the positioning of the detected targets. On the other hand, the Doppler frequency has a values for an opposite direction situation as presented in the channel characterization.

Table 5.1 *Speed and Doppler frequency calculation for the 1MD&1SD scenario.*

Scenario 1 MD & 1SD				
Symbols/Speed&Doppler	Radar Speed	Real Target Speed	Estimated Target Speed	Doppler freq.
1000	28.8437 m/s	26.7774 m/s	25.9887 m/s	2.156 KHz
500			26.1974 m/s	2.1649 KHz
250			26.2989 m/s	2.1689 KHz

5.2.2. 3MD&2SD

The same simulations as the 1MD&1Sd have been performed for the 3MD&2SD.

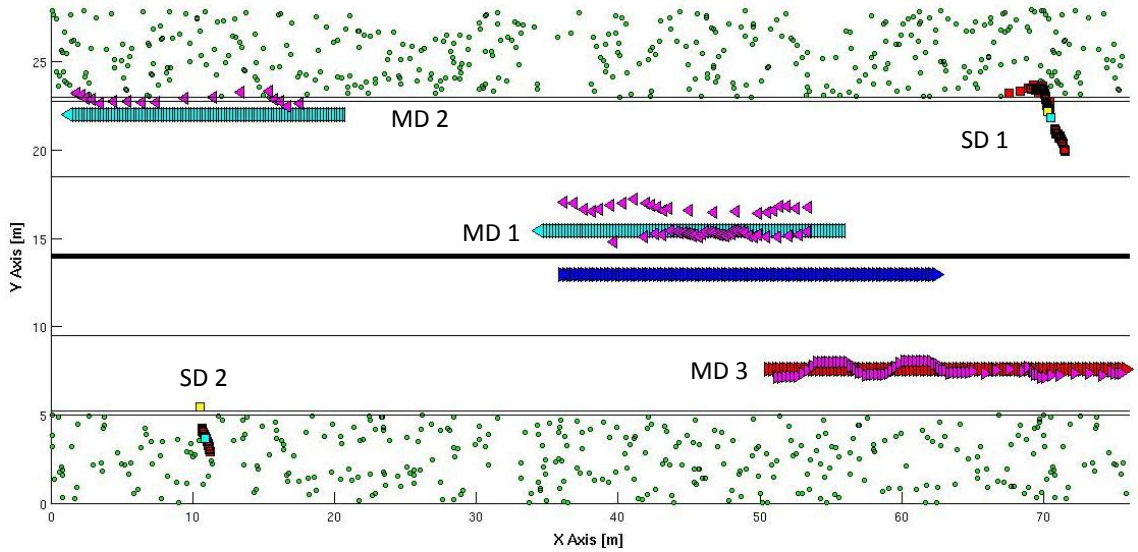

Figure 5.12 *Tracking of the 3MD&2SD scenario for an OFDM frame of 1000 OFDM symbols.*

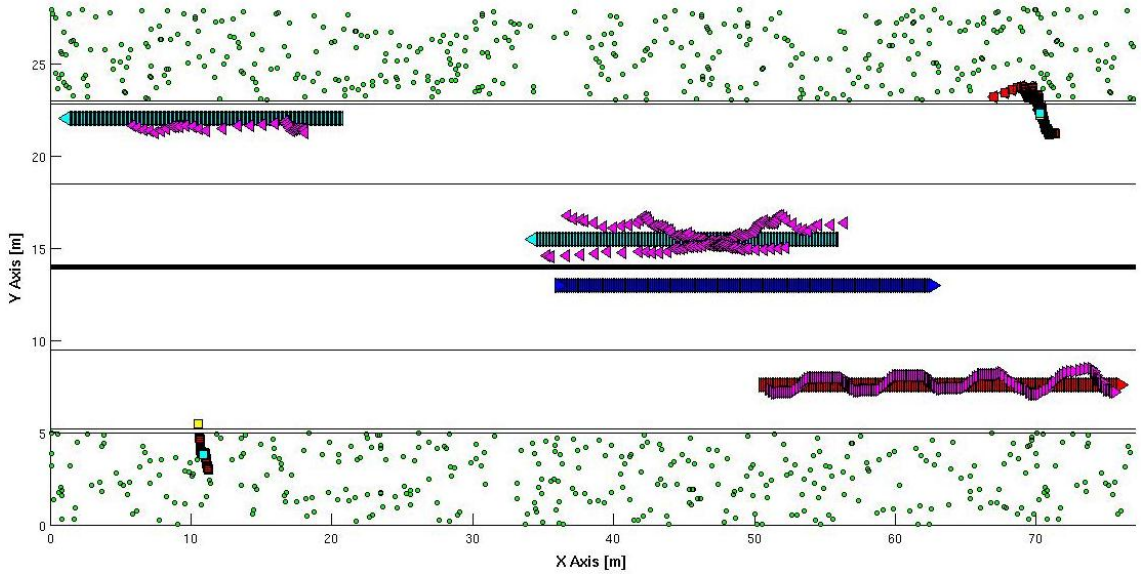

Figure 5.13 *Tracking of the 3MD&2SD scenario for an OFDM frame of 500 OFDM symbols.*

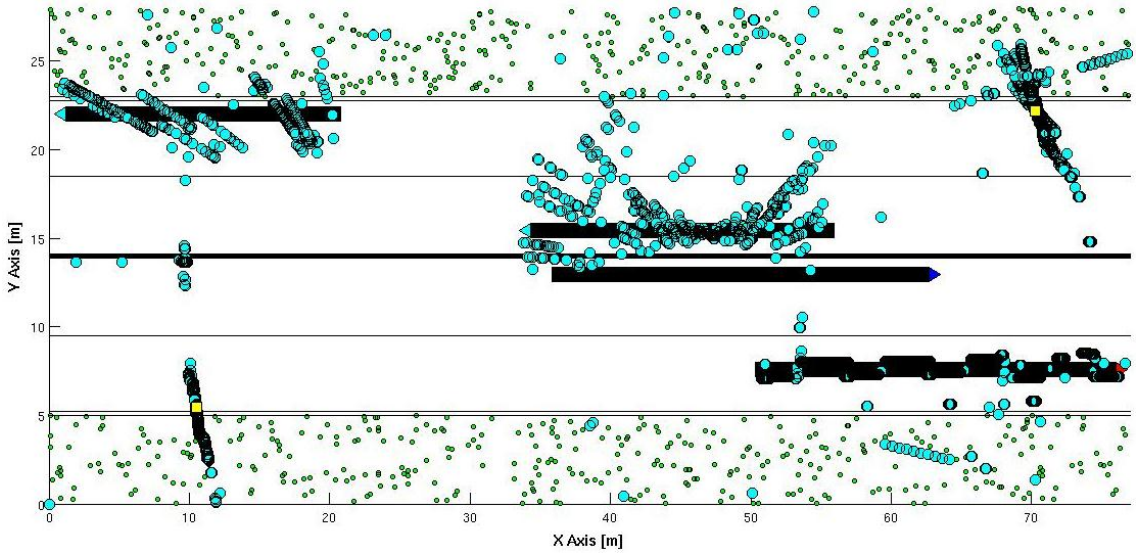

Figure 5.14 *Tracking of the 3MD&2SD scenario for an OFDM frame of 250 OFDM symbols before the filter and without average the samples.*

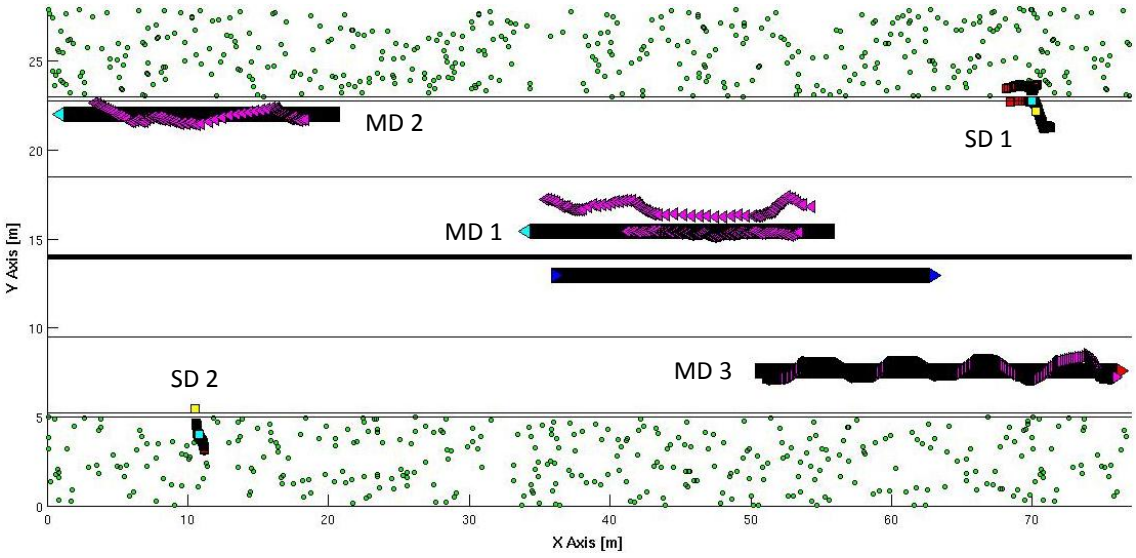

Figure 5.15 *Tracking of the 3MD&2SD scenario for an OFDM frame of 250 OFDM symbols after the filter.*

The inconvenience of this scenario according to the tracking algorithm is the detection of the MD2; it presents the lowest probability of detection under 50% for an OFDM frame of 250 symbols. The proximity of the MD2 to the diffuse area can be the main reason of these location errors. On the other hand, the SDs are more or less correctly detected as the rest of MDs. It is important to highlight that the MD1 is detected as two cars in parallel due to the vehicles are considered as points and its width is not taken into account. However, both sets of samples have been considered to belong to the same car.

The **Table 5.2**, **Table 5.3** and **Table 5.4** contain the calculated speeds and Doppler frequency of each MD for an observation widow equal to the theoretical displacement of the targets. The situations of the same and opposite direction are clearly identifiable.

Table 5.2 *Speed and Doppler frequency calculation for the target MD1 in the 3MD&2SD scenario.*

[TARGET MD1]				
Symbols/Speed&Doppler	Radar Speed	Real Target Speed	Estimated Target Speed	Doppler freq.
1000	33.15 m/s	26.73 m/s	21.68 m/s	2.157 KHz
500			26.24 m/s	2.336 KHz
250			23.32 m/s	2.221 KHz

Table 5.3 *Speed and Doppler frequency calculation for the target MD2 in the 3MD&2SD scenario.*

[TARGET MD2]				
Symbols/Speed&Doppler	Radar Speed	Real Target Speed	Estimated Target Speed	Doppler freq.
1000	33.15 m/s	24.12 m/s	19.77 m/s	2.082 KHz
500			15.26 m/s	1.904 KHz
250			18.42 m/s	2.029 KHz

Table 5.4 *Speed and Doppler frequency calculation for the target MD3 in the 3MD&2SD scenario.*

[TARGET MD3]				
Symbols/Speed&Doppler	Radar Speed	Real Target Speed	Estimated Target Speed	Doppler freq.
1000	33.15 m/s	31.65 m/s	30.46 m/s	105.7 Hz
500			30.67 m/s	96.89 Hz
250			30.74 m/s	94.81 Hz

5.2.3. 4MD&1SD

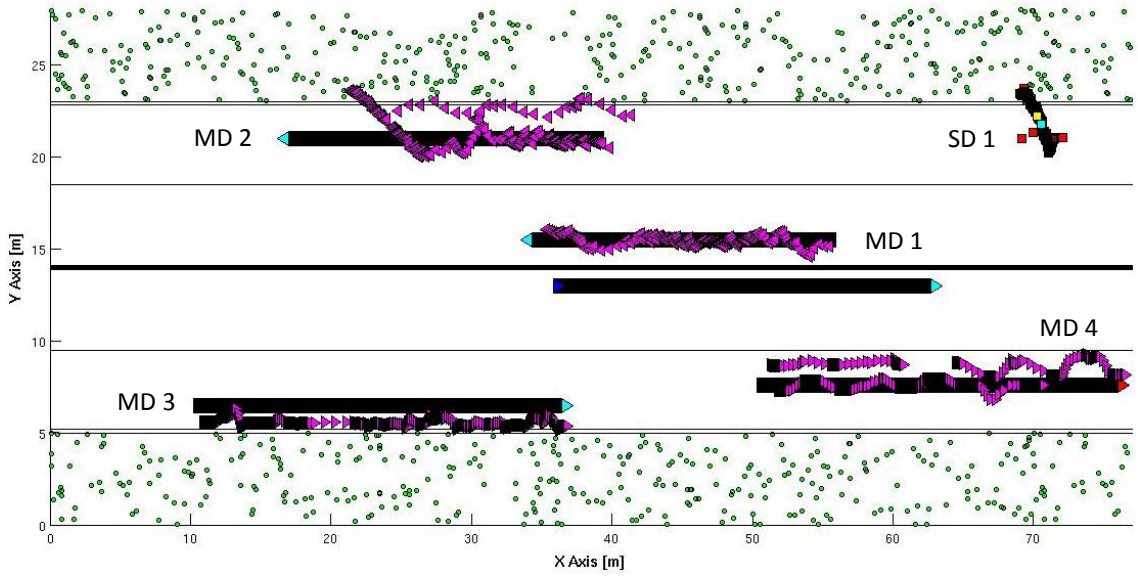

Figure 5.16 *Tracking of the 4MD&1SD scenario for an OFDM frame of 250 OFDM symbols.*

The detection problems of this scenario lie basically in the MD2 that coincides with the lowest probability of detection. The proximity to the diffuse area seems to be again the same problematic, despite of the MD3 is closer than the MD2. However, MD3 is closer to the Radar Car than MD2 and it maintains the distance on the contrary that MD2.

Table 5.5 *Speed and Doppler frequency calculation for the 4MD&1SD scenario using OFDM frames of 250 OFDM symbols.*

Scenario 4MD & 1SD				
Target id./Speed&Doppler	Radar Speed	Real Target Speed	Estimated Target Speed	Doppler freq.
MD1	33.15 m/s	26.73 m/s	24.84 m/s	2.256 KHz
MD2		27.63 m/s	22.69 m/s	2.172 KHz
MD3		32.34 m/s	31.91 m/s	24.78 Hz
MD4		31.65 m/s	31.14 m/s	54.54 Hz

5.2.4. 5MD&2SD

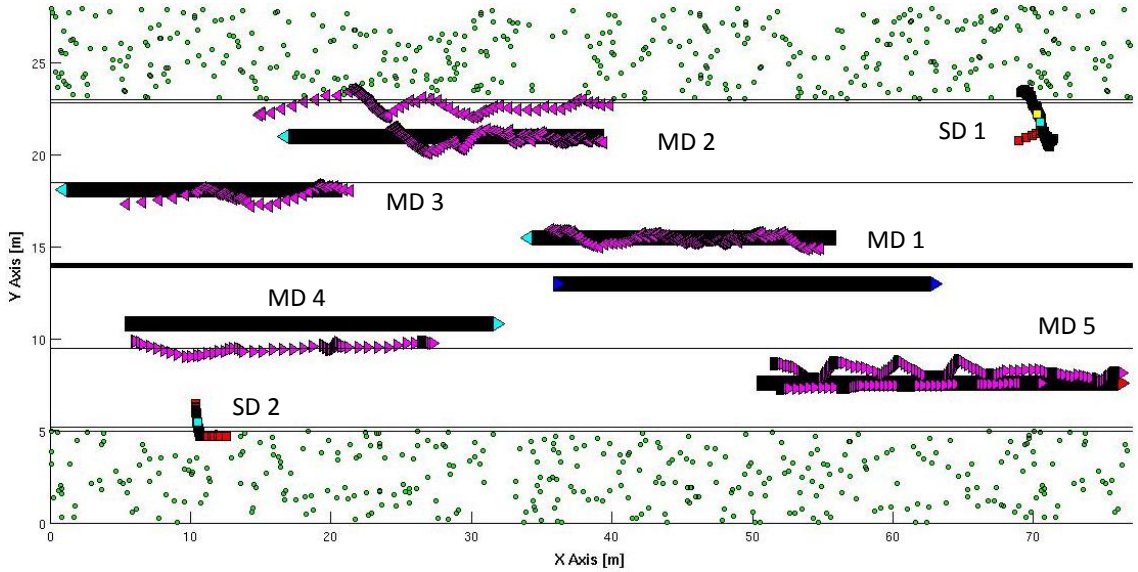

Figure 5.17 *Tracking of the 5MD&2SD scenario for an OFDM frame of 250 OFDM symbols after the filter.*

In this case, there are some problems to locate the targets identified as MD2, MD3 and MD4. The Radar algorithm is experiencing confusing the MD2 with the MD3 for their proximity and at the same MD2 is very near to the diffuse area. On the other hand, the MD4 presents the lowest probability, although the represented tracking suits more or less the theoretical trajectory. The Radar is confusing the MD4 with the SD2 as its probability detection indicates; however, the filter has removed these wrong results.

Table 5.6 *Speed and Doppler frequency calculation for the 5MD&2SD scenario using OFDM frames of 250 OFDM symbols.*

Scenario 5MD & 2SD				
Target id./Speed&Doppler	Radar Speed	Real Target Speed	Estimated Target Speed	Doppler freq.
MD1	33.15 m/s	26.73 m/s	23.69 m/s	2.190 KHz
MD2		27.63 m/s	35.54 m/s	2.656 KHz
MD3		24.12 m/s	19.66 m/s	2.032 Hz
MD4		32.34 m/s	26.21 m/s	227.6 Hz
MD5		31.65 m/s	30.68 m/s	51.64 Hz

5.2.5. PROBABILITY OF DETECTION

The **Figure 5.18** contains the probability of detection of the tracking performed for the previous scenarios, using a SNR equal to 20 dB, a frame formed by 250 OFDM symbols and for a threshold of 3 meters. Besides, these probabilities are obtained before the filtering and the average process (raw detections).

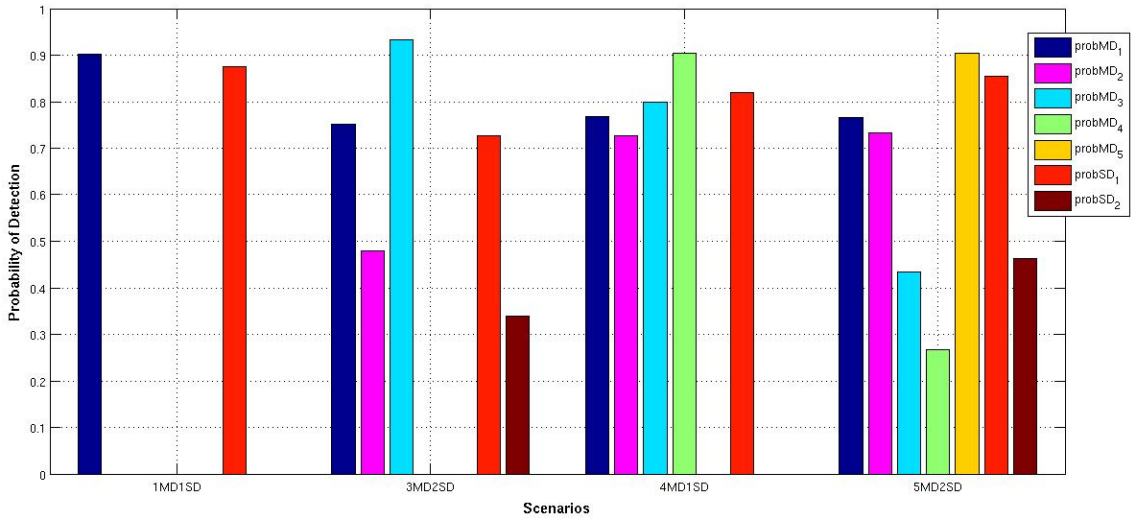

Figure 5.18 *Probability of detection for all the MDs and SDs of the different scenarios presented previously.*

5.3. CONCLUSIONS

The important points that can be highlighted from the results obtained in these simulations are that the probability of detection is proportionally related with the SNR, the slow fading and path loss exponent have an important role in the quality of the Radar decisions as well as the great importance of the diffuse scatterers, whose reflected power can hide the targets to locate.

The proposed scheme to mount the antennas on the car's roof (see **Figure 4.8**) entails some errors according to the locations of the targets, as the **Figure 5.6** presents for the vehicle number 5 or the example illustrated in the **Figure 4.9**. It could be solved adding more antennas or shortening the sampling time in the receiver, despite of the performed sampling time -within the range of nanoseconds or GHz in frequency- is supposed to be unfeasible nowadays. An increment of the distance between the antennas could be other possible solution, but the car dimensions dismiss this option.

A certain probability of detection has to be ensured for a correct tracking of the targets. In scenarios with low rates of good decisions, short OFDM frames are recommended in order to achieve higher update rates of the tracking system. Thus, the probabilities to locate the targets could be improved. On the other hand, the size of the window to determine the Doppler effect must be obtained empirically according to the type of via. This method to obtain the Doppler frequency is not optimal and can be proposed as a future work.

Finally, the Radar coverage is other important parameter to determine that depends of the type of car route. For crowded roads the coverage has to be smaller than in the opposite case, since the uncertainty is higher due to a large number of rays that belongs to the same sample of the channel impulse response. In other words, the rays have similar delay such that the integrator block sum together these rays, which implies that the Radar is not able to distinguish this set of possible targets and are interpreted as only one scatterer. A method to delimitate these areas could be by reducing the

transmitted power that affects the V2V communications. Other technique could be to use a splitter to duplicate the transmitted wave and attenuate the wave corresponding to the Radar application to reduce the coverage area; thus, both waves have to be distinguished by changing their polarization, for instance. To increase the sampling frequency is other possible solution but it is unfeasible as commented previously.

CONCLUSIONS

With the aim to improve the traffic safety system, this thesis has been focused on the viability study of a radar application in a V2V scenario. Consequently, a complete V2V communication system has been implemented so as to determine its features and design a possible radar algorithm regarding the inconvenience of such system. The simulated scenario is based on a 4x4 MIMO structure formed by omni-directional antennas, OFDM combined with PSK as the modulation scheme and a real V2V propagation channel, which respects the NWSSUS behavior of such channels. In order to keep the simulation scenario as close to reality as possible, the IEEE 802.11p standard is considered.

The main constraint that this system presents concerning the reliability of the communication application is the NWSSUS feature of the propagation channel, which contributes to the non stationary characteristic of the channel impulse response according to the time and frequency. Thus, the channel experiences noticeable changes during the transmission of an OFDM frame; it restricts the channel estimation method, which has to determine the channel and its variations during the time. Therefore, from the conclusions drawn in the Subsection 3.5.5, the MLE is not a suitable technique for this kind of channels. This estimation method uses the training sequence to obtain an approach of the propagation channel, but the NWSSUS feature is disregarded. It is important to highlight that for frame lengths in which the V2V channel can be considered constant, the MLE can be implemented with high performance; however, just like the channel experiences significant changes, the MLE presents a low efficiency. Some investigations have tried to solve this issue using the pilots included in the OFDM frame for estimating these variations [26]; nonetheless this topic is out of the scope of this thesis.

The proposed radar algorithm is based on the channel estimation to detect and locate the targets, which are distinguished as the power peaks of the channel impulse response. The ranging process is based on the respective delay times of these peaks, while the azimuth placement of the targets is performed trough the trilateriation method as the GPS system. In order to improve the probability of detection for the proposed radar method, a diversity technique using the phantom antenna concept has been implemented. It entails some errors, thus a filter process is required. With the purpose to determine the Doppler frequency a tracking system is essential, therefore, its implementation has been performed too. The Doppler estimations is carried out through a window mechanism, where the maximum and minimum distance of the desired target divided by the temporal duration of such window is determined to obtain its speed. And with the aid of the target placement, the relative speed can be calculated as well as the Doppler frequency. The duration of this window has to be determined as a multiple of the OFDM frame duration. The main reason to implement this method for determining the Doppler effect is due to unreliability estimation of the target phase, since the constructive or destructive rays summation modifies significantly the magnitude and phase of the channel coefficient that represents this target.

The tracking system can be considered as the radar algorithm applied for different time instants, although the historical of the recorded detections is employed to discard wrong decision from the radar application. The implemented filter is based on the previous knowledge of the dimension of the car route, since the detection and location system is supposed to be aided by a GPS system that can incorporated with the vehicle.

Concerning the radar application the limitations that arise from a V2V system are the required range resolution, which implies elevates sampling rates for the ADC used in the radar application, and the reflected power from the vehicles to detect that have to be higher than the rest of scatterers for their correct detection. The considered sampling frequency for the results presented in the Chapter 5 is within the range of GHz that leads to an unfeasible implementation, since there is not such commercial

ADC device nowadays. On the other hand, the SNR, the slow fading and the path loss exponent are the main factors that determine the reflected power of the desired targets. Besides, the diffuse scatterers influences is other responsible for the correct functioning of the radar algorithm. Therefore, if a certain reflected power from the interesting targets to locate is not assured, the radar application will present a low performance.

The final results obtained from the radar application present good performance according to the evaluated scenarios, OFDM frame lengths and SNRs used. The biggest scenario simulated consists of 5 cars to detect plus the radar vehicle and 2 road signals that contributes to the channel impulse response with a significant reflected power. For this situation, some mobile scatterers are difficulty detected as a consequence of their proximity to the diffuse zone or the proximity to other targets that affects the radar range resolution. It is important to highlight that this results cannot be directly extrapolated to other kind of car route, since the reflected power depends on the empirical gains obtained from the implemented GSCM. Thus, the results in other type of scenario can suppose an improvement or a worsening of the radar efficiency.

Finally, as a setup suggestion for the V2V applications is to use short OFDM frame lengths that present a good performance in terms of BER for the implemented estimation method. Furthermore, the radar application also takes advantage due to a higher detection rate of the targets.

FUTURE RESEARCH

The proposed future work mainly lies in the research of possible solutions to the most important problems of this radar application for a V2V environment. They can be summarized in these few points:

- The fact of using a high sampling frequency in the order of GHz is the main constraint for a practical implementation of the proposed method to detect and locate targets. Therefore, an investigation to perform an ADC with such sampling time could be a valuable investigation for this thesis.

- The azimuth detection of the targets have been solved by the trilateration technique, however, the best method to perform in a MIMO structure is to use the Digital Beam-Forming (DBF). It can be designed to take into account the interest region to detect targets, track them or establish a more reliable communication. The complexity and computational cost will increase but it is presented as a future solution to solve problems as the radar range resolution that is related with the sampling time for this thesis. Therefore, the problems regarding the sampling frequency could be also solved with the implementation of the DBF technique in this implemented system.

- A study about the type of antennas to use in a V2V scenario and the best location to place them regarding the car, inside or outside, is an indispensable requirement for all the V2V applications. Nowadays, few campaigns have been performed to solve this issue, whose interest is increasing day by day.

- In this thesis the positioning of the antennas on the car's roof has been performed for a 4x4 MIMO system and using the concept of the phantom antennas. Other field that can be investigated is to determine the optimal number of antennas to place on the car's roof and their best location, in a rectangle, circle, star, mesh and other possible geometric figures.

- An implementation of a V2V network could be used to improve the probability of detection of the proposed radar algorithm, since the information from other cars can be contrasted in order to distinguish the wrong from the correct decisions. It supposes a diversity gain obtained from all the vehicles with the same raging and locating system.

- The estimation method is not suitable for a NWSSUS scenario, therefore, other techniques have to be designed to overcome this problem.

- The method to estimate the Doppler frequency for specified scenarios is considered as a non-optimal technique. Thus, other kind of technique could be implemented to reduce the error.

REFERENCES

[1] World Health Organization (WHO),*World report on road traffic injury prevention*, Geneva, 2004.

[2] ETSI TR 102 698 V1.1.1 (2009-06), “Intelligent Transport Systems (ITS), Vehicular Communications; C2C-CC Demonstrator; Use Cases and Technical Specification”.

[3] “IEEE P802.11p/D9.0: Part 11: Wireless LAN MediumAccess Control (MAC) and Physical Layer (PHY) Specifi-cations: Amendment: Wireless Access in Vehicular Envi-ronments (WAVE),” Draft 9.0, Sept. 2009.

[4] Donnet, B.J.; Longstaff, I.D.; , "Combining MIMO Radar with OFDM Communications," Radar Conference, 2006. EuRAD 2006. 3rd European , vol., no., pp.37-40, 13-15 Sept. 2006

[5] C. Sturm; T. Zwick; W. Wiesbeck; , “An OFDM System Concept for Joint Radar and Communications Operations,” IEEE 69th Vehicular Technology Conference, Barcelona, April 2009.

[6] K. Mizui, M. Uchida, M. Nakagawa, “Vehicle-to-Vehicle Communication and Ranging System Using Spread Spectrum Technique,“ in Proc. IEEE Vehicular Technology Conference, pp. 335-338, May 1993.

[7] A. Garmatyuk, J. Schuerger, Y. T. Morton, K. Binns, M. Durbin, J.Kimani, “Feasibility study of a multi-carrier dual-use imaging radar and communication system,” in Proc. 37th European Microwave Conference, pp. 1473 – 1476, Munich, Oct. 2007.

[8] Letzepis, N.; Grant, A.; Alexander, P.; Haley, D.; “Multipath Parameter Estimation from OFDM Signals in Mobile Channels”. Institute for Telecommunications Research, University of Australia. Cohda Wireless Pty. November 15, 2010. DRAFT

[9] Sturm, C., “Waveform Design and Signal Processing Aspects for a Complete System Integration of Wireless Communication and Radar Sensing”, Institute of Technology Karlsruhe, Germany. DRAFT.

[10] Levanon, N., "Multifrequency complementary phase-coded radar signal," Radar, Sonar and Navigation, IEE Proceedings - , vol.147, no.6, pp.276-284, Dec 2000.

[11] Molisch, A., Tufvesson, F., Karedal, J., Mecklenbrauker, C., "A survey on vehicle-to-vehicle propagation channels," Wireless Communications, IEEE , vol.16, no.6, pp.12-22, December 2009

[12] Matolak. David W.; Sen, Indranil; Xiong, Wenhui; , "Channel Modeling for V2V Communications," Mobile and Ubiquitous Systems: Networking & Services, 2006 Third Annual International Conference on, vol., no., pp.1-7, July 2006

[13] J. Karedal et al., “A Geometry-based Stochastic MIMO Model for Vehicle-to-Vehicle Communications,” IEEE Trans. Wireless Commun., vol. 8, no. 7, July 2009, pp.3646–57.

[14] A. Paier et al., “First Results from Car-to-Car and Car-to-Infrastructure Radio Channel Measurements at 5.2GHz,”Proc. IEEE Int’l. Symp. Personal, Indoor, Mobile RadioCommun., 2007, pp. 1–5.

[15] A. Paier et al., “Car-to-Car Radio Channel Measure-ments at 5 GHz: Pathloss, Power-Delay Profile, and Delay-Doppler Spectrum,” Proc. Int’l. Symp. Wireless Commun. Sys., 2007, pp. 224–28.

[16] Molnar, B.G.; Frigyes, I.; Bodnar, Z.; Herczku, Z.; , "The WSSUS channel model: comments and a generalisation," Global Telecommunications Conference, 1996. GLOBECOM '96. 'Communications: The Key to Global Prosperity , vol., no., pp.158-162, 18-22 Nov 1996

[17] P. A. Bello, "Characterization of Randomly Time-Variant Linear Channels," IEEE Trans. Commun., vol. 11, 1963, pp. 360–93.

[18] A. J. Van Dierendonck, "GPS Receivers," in Global Positioning System: Theory and Applications, B. W. Parkinson and J. J. Spilker Jr, Eds. Washington, DC: Amer. Inst. Aeronautics and Astronautics, 1996, vol. I, pp. 329–407.

[19] S. M. Kay, "Fundamentals of Statistical Signal Processing: Estimation Theory", Prentice-Hall, 1998,595.

[20] Langton, C., "Orthogonal Frequency Division Multiplexing", Intuitive guide to principles of communications (2004).

[21] IEEE Std 802.11a-1999, Part 11, "Wireless LAN Medium Access Control (MAC) and Physical Layer (PHY) Specifications High-speed Physical Layer in the 5 GHz Band". IEEE, 1999.

[22] John R. Barry, Edward A. Lee, David G. Messerschmitt, *Digital Communication*. 3^{rd} ed. Kluwer Academic Publishers, 2004.

[23] S. Boyd and L. Vandenberghe, Convex Optimization, Cambridge University Press, 2004.

[24] www.stelladoradus.com/5.9-5.7-5.4-5.2.omni-directional.antennas.php, Stella Doradus antennas.

[25] Kaul, S.; Ramachandran, K.; Shankar, P.; Oh, S.; Gruteser, M.; Seskar, I.; Nadeem, T.; , "Effect of Antenna Placement and Diversity on Vehicular Network Communications," Sensor, Mesh and Ad Hoc Communications and Networks, 2007. SECON '07. 4th Annual IEEE Communications Society Conference on , vol., no., pp.112-121, 18-21 June 2007.

[26] L. Bernado , N. Czink , T. Zemen , P. Belanovi ., "Physical Layer Simulation Results for IEEE 802.11p using Vehicular non-Stationary Channel Model" .

[27] M. Skolnik, *Introduction to Radar Systems*, McGraw-Hill, New York, 3rd edition, 2002.

[28] www.volvoclub.org.uk/tech/tech_spec_V50_Nov2003.pdf, Technical Specifications Volvo V50.

[29] B. Donnet and I. Longstaff, "MIMO radar techniques and opportunities," European Radar Conference, Proceedings of the 3rd, pp. 112–115, September 2006.

APPENDIX A

This appendix is assigned to the V2V propagation channel characterization for a rural scenario. The same and opposite direction (SDir. and ODir.) of the transmitter regarding the receiver have been simulated in order to obtain a more accurate characterization of such scenario.

In **Figure A.1** the rural scenario for the same direction is depicted, while **Figure A.2** represents the opposite direction.

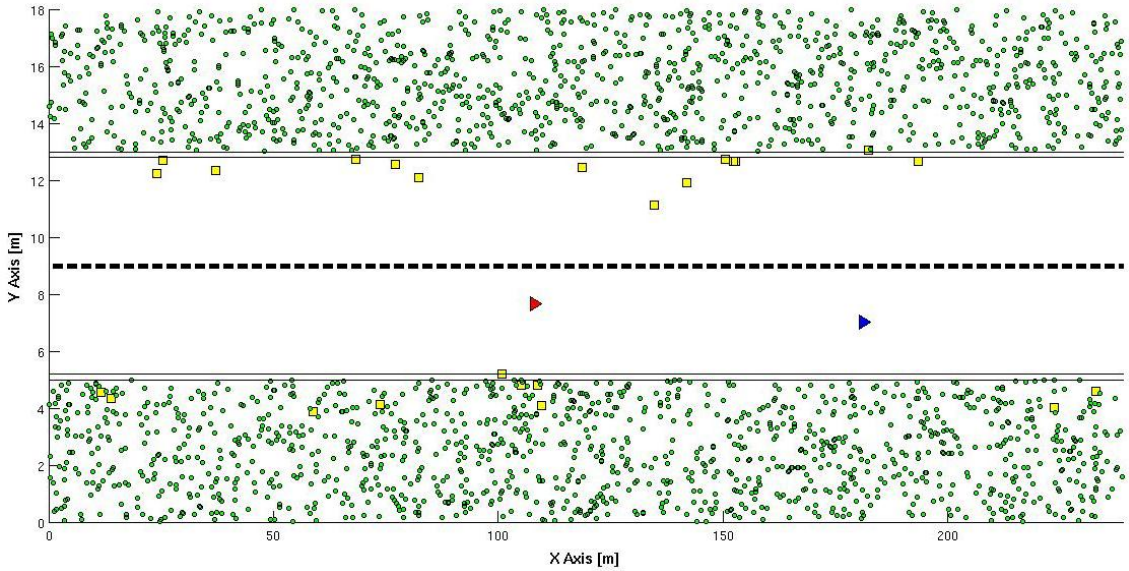

Figure A.1 *Same direction rural scenario.*

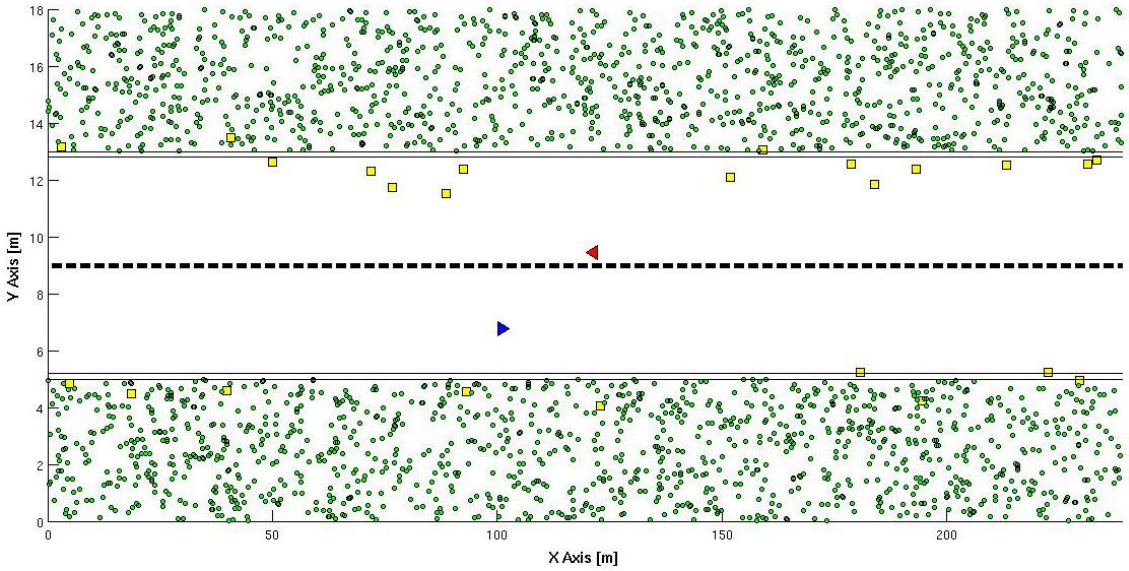

Figure A.2 *Opposite direction rural scenario.*

Figure A.3 and A.4 illustrate the module of the channel impulse response for the same and opposite direction, respectively. As can be observed, the delay for the LOS is longer for the same direction situations than the opposite direction. The reason is the higher distance between the transmitter and receiver for the SDir. than the ODir. scenario.

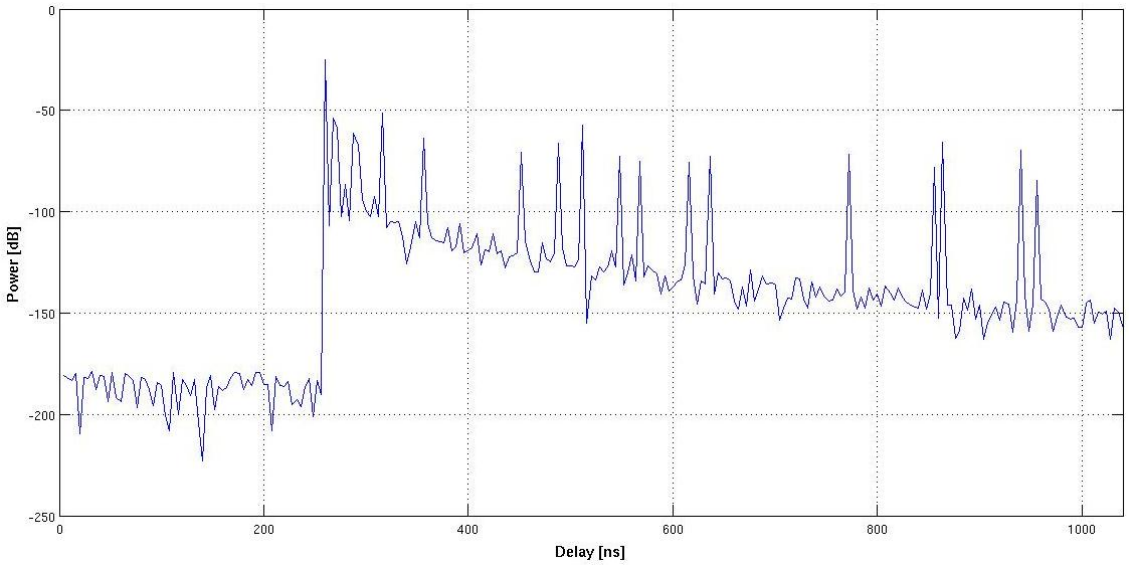

Figure A.3 *Module of the channel impulse response for the rural scenario with same direction.*

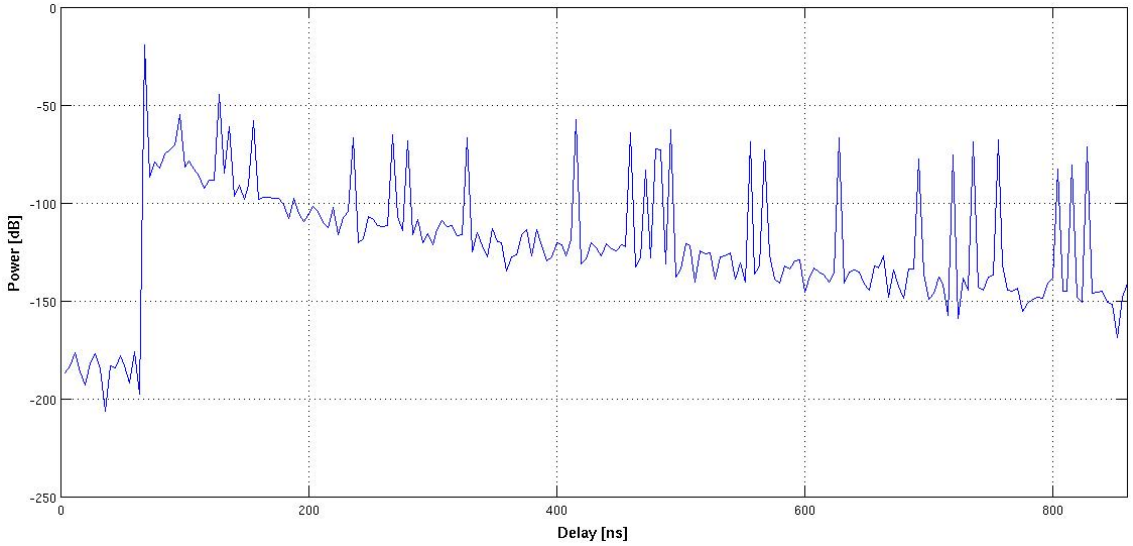

Figure A.4 *Module of the channel impulse response for the rural scenario with opposite direction.*

Doppler frequency in the rural scenarios is lower than in the highway as a consequence of the allowed speeds in such types of roads. In **Figure A.5** the LOS presents a lower Doppler frequency close to 0Hz, since the relative speed is not significant as a consequence of the same direction of the transmitter and receiver vehicles. The most interesting results is for the ODir. situation, where the LOS presents the higher Doppler frequency, roughly 850 Hz, and the rest of scatterers have low values, around +/- 150 Hz. There are other scatterers whose respective Doppler frequencies are between the maximum and minimum values. They correspond to the scatterers placed between the transmitter and receiver regarding the x axis. Thus, they see the transmitter and receiver approaching to them, which entails a high relative speed.

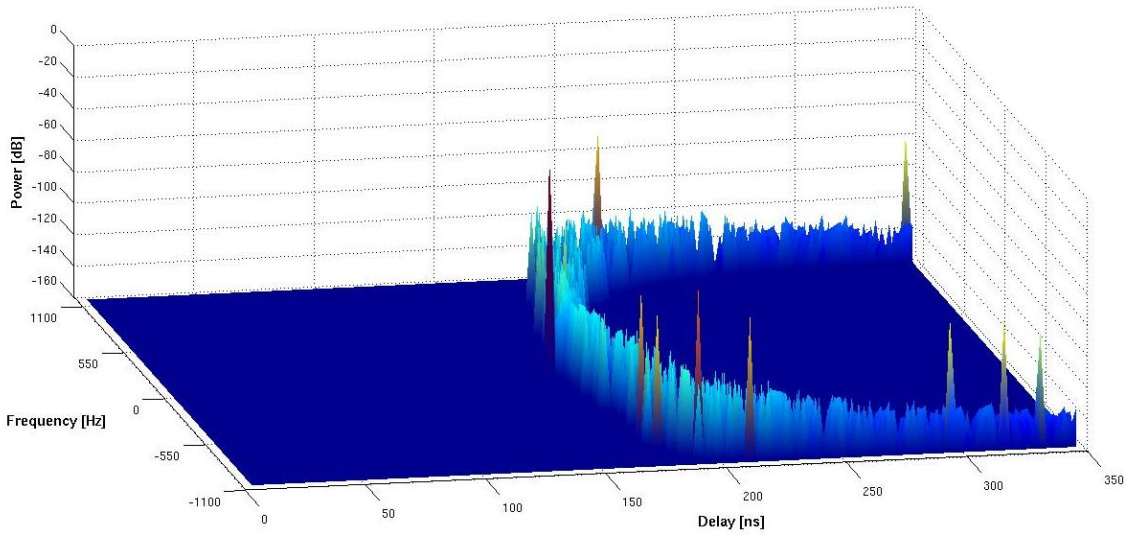

Figure A.5 *Doppler frequency for the rural scenario with opposite direction.*

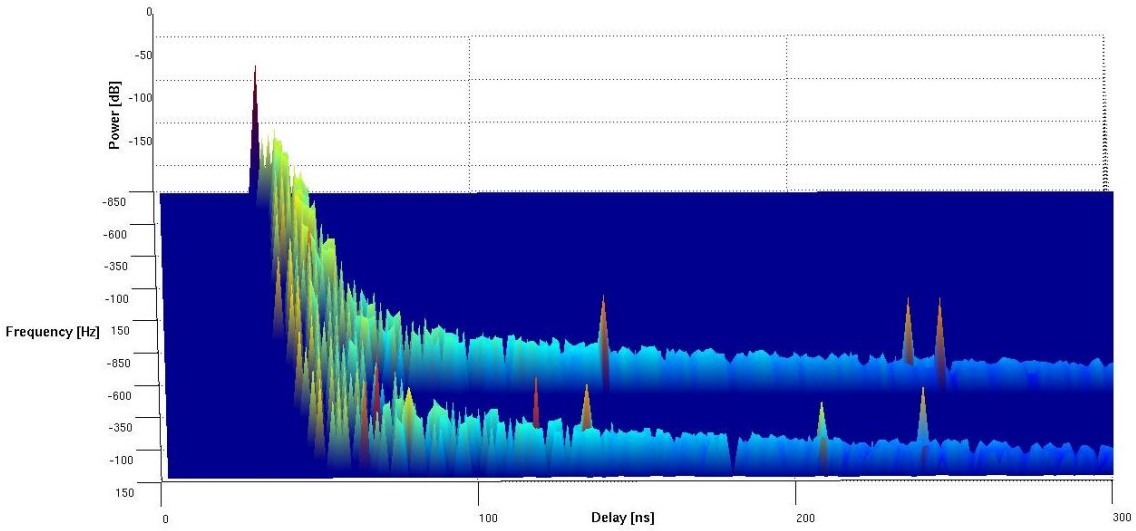

Figure A.6 *Doppler frequency for the rural scenario with same direction.*

In **Figure A.7 and A.8** the power delay profiles of both scenarios for a duration of 2 seconds are depicted. For the SDir. situation the LOS maintain the same delay during the measurement, since the distance between transmitter and receiver is not shortened. However, there are some scatterers that are approaching to the transmitter or receiver, represented as straight lines with positive slopes, while other scatterers are moving away from LOS. **Figure A.8** has a behavior similar as the explained in the Chapter 3 for the highway scenario.

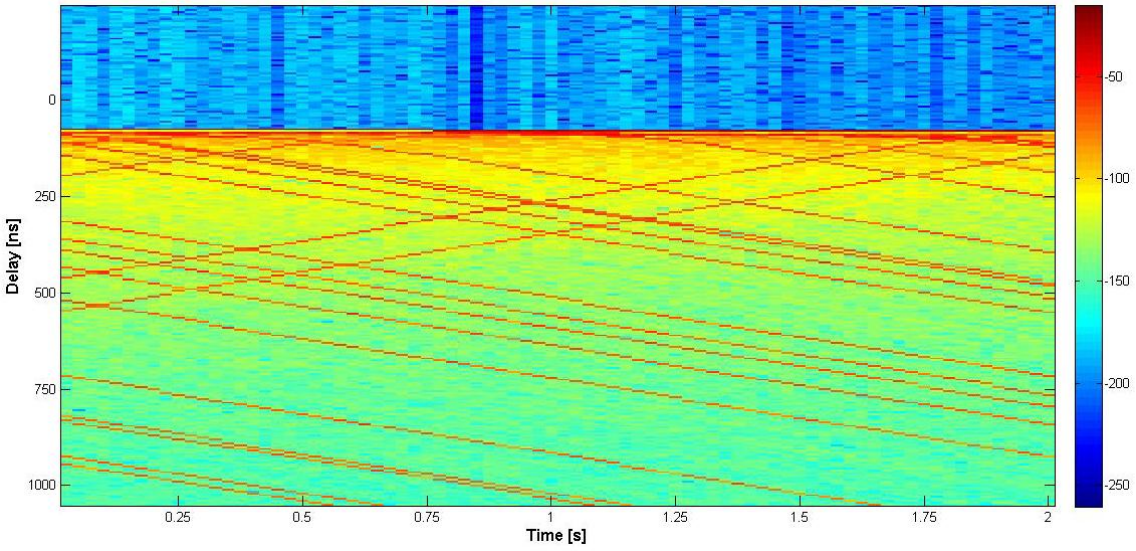

Figure A.7 *Power Delay Profile for the rural scenario with same direction.*

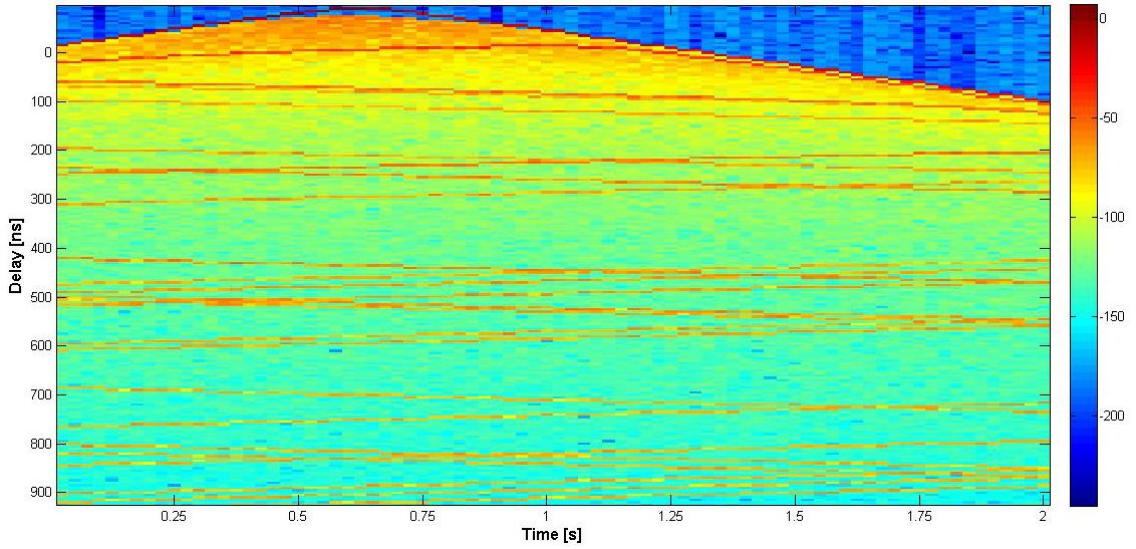

Figure A.8 *Power Delay Profile for the rural scenario with opposite direction.*

APPENDIX B

In this appendix the convolutional block codes proposed by the standard 802.11a are evaluated over the OFDM implemented system, where different SNR values and types of channels have been used. Furthermore, the behavior comparison of the channels performed has been studied.

The **Figure B.1** contains the results of the simulations for an OFDM frame length of 1000 symbols and channel rate variation equal to 125 channels per second. These parameters only affect the V2V channel (GSCM), since the Rayleigh and Gaussian channels are supposed to be constant in time and frequency during the transmission of the entire OFDM frame.

The channel rate chosen in the V2V channel is the lowest of the performed rates, which presents the best BER values. However, the GSCM channel is still worse than the Rayleigh and Gaussian channel.

On the other hand, the correct functioning of the convolutional block codes is clearly highlighted, since all the curves with coding present an improvement for SNR higher than 8 dB. One feature of this type of coding is the bad performance obtained for low SNR as can be observed from the **Figure B.1**, where the curves with coding present worse BER values than without it.

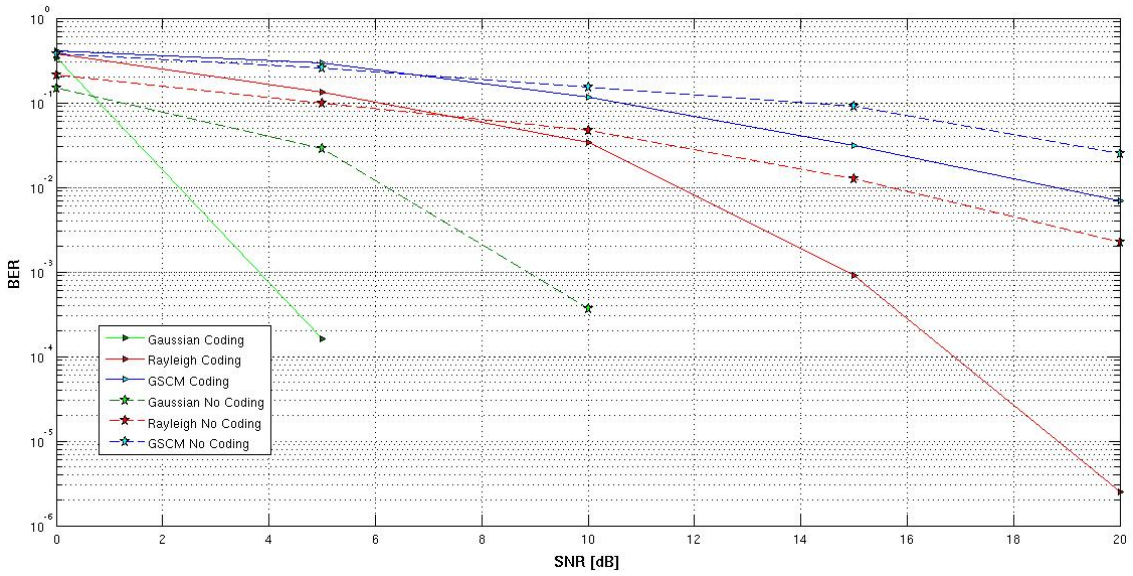

Figure B.1 *Comparison of a Gaussian, Rayleigh and GSCM channel behavior in the implemented system for different SNR values and with or without coding.*